Analysis of burnt scar using optical and radar satellite data

STELLA CHELANGAT MUTAI

February, 2019

SUPERVISORS:
Dr. V.A. Tolpekin
Dr. L. Chang

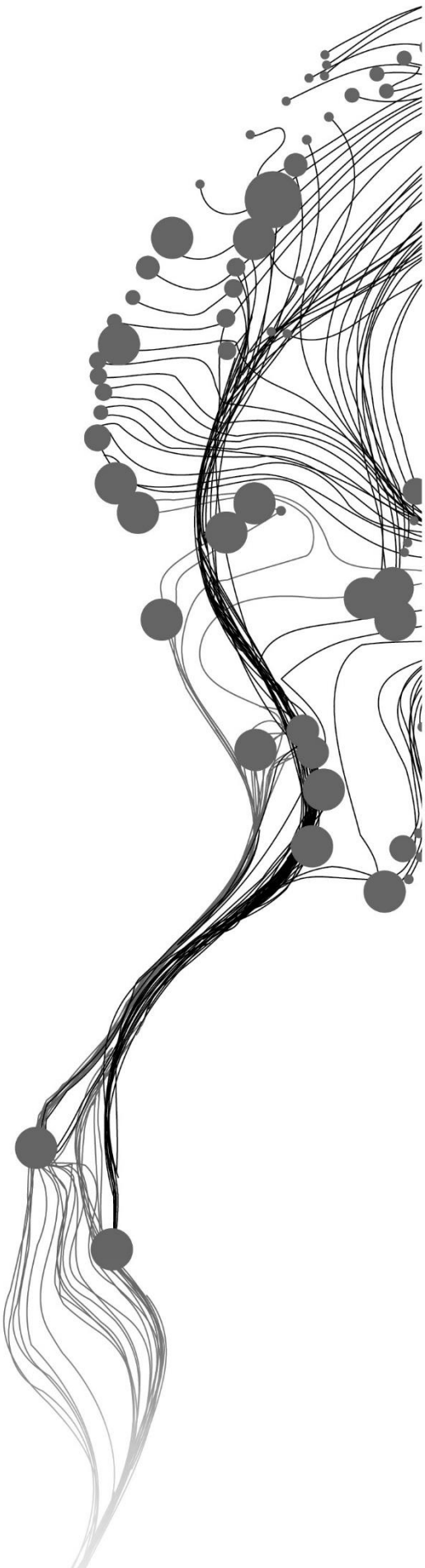

Analysis of burnt scar using optical and radar satellite data

STELLA CHELANGAT MUTAI
Enschede, The Netherlands, February, 2019

Thesis submitted to the Faculty of Geo-Information Science and Earth Observation of the University of Twente in partial fulfillment of the requirements for the degree of Master of Science in Geo-information Science and Earth Observation.
Specialization: Geo-information Science and Earth Observation Geoinformatics GFM.

SUPERVISORS:
Dr.V.A.Tolpekin
Dr.L.Chang
Advisor: drs. J.P.G. Bakx, Course Director

THESIS ASSESSMENT BOARD:
Prof. Dr. Ir. A. Stein (Chair)
Dr. N. Ghasemi (External Examiner, Wageningen University & Research, Wageningen Environmental Research (WENR))

ABSTRACT

This study compares the use of Sentinel 1 (S1) SAR sensor alongside with Sentinel 2 (S2) optical sensor in detection and mapping of burnt and unburnt scars occurring after a bushfire in Victoria, Australia, and Spain. The bushfires had recently occurred in the period of 2017-2018. The C-band dual polarized S1 data have been investigated to assess the backscatter intensity together with polarimetric decomposition component to determine forest burn severity over the two sites. The backscatter coefficient was also used in deriving texture measures from local statistics, using grey level co-occurrence matrix (GLCM). This was because of its sensitivity in the identification of textural variation of burnt and unburnt scars. While for S2 the difference normalized burnt ratio (dNBR) was utilized to determine the magnitude of burnt severity levels present in both areas. Its analysis was explored using a contextual classifier Support Vector Machine and Markov Random Field classifier (SVM-MRF). This is because of its integration of spectral information and spatial context through the optimal smoothing parameter without degrading image quality. The training and test set datasets consisting of burned and unburned pixels were created from S2 scenes used as reference data. The experimental results showed that a strong correlation exists in both spectral sensitivity and polarimetric sensitivity of the two defined classes after classification. The performance of the algorithm was evaluated using the kappa coefficient and f-score measurement. All fire zones yielded an accuracy of (0.80) except for S1 data in Spain. Also, the performance in users and producers accuracy provided the highest accuracies in both S1 and S2. The entropy alpha decomposition helped to classify the target based on their physical properties as presented by the H-α plane. The entropy and alpha values decreased and formed a pattern after the fire. The sensitivity analysis to the GLCM features showed that homogeneity, contrast and entropy were the key statistical features that showed clear separation of burnt and unburnt scars using backscatter intensity. This was after the key parameters such as number of quantization levels, window size, pixel pair sampling distance which was one and the orientation were optimized. The use of S1 in discrimination of burnt and unburnt scars was highly dependent on local incidence angle, acquisition geometry and environmental conditions. In hilly areas, the low incidence angles showed high discrimination of burnt from unburnt areas compared to high incidence angles. Also, topography was of high influence as areas facing slopes in hilly areas showed high discrimination of unburnt areas from burnt compared to areas facing backslopes. The Spain dataset did not foreshow any changes in vegetation structure after the fire as compared to Australia using S1. This led to the conclusion that also the intensity of the fire and its effect to vegetation structure is of great influence to the sensitivity of SAR sensor in the analysis of changes in forest structure after a bushfire. Also optical data in such cases can be used as a substitute as it showed strong spectral sensitivity to changes in Spain fire irrespective of the intensity of the fire. Nevertheless, results in both areas verify the use of satellite SAR sensor and optical in forestry application and their sensitivity highly depends on vegetation structure, geographical nature of the area of study and fire intensity.

Keywords: Burnt, Unburnt, Backscatter intensity, polarimetric decomposition, Texture, Bushfires.

ACKNOWLEDGMENTS

I would like to express my sincere gratitude to my supervisors Dr. Valentyn A. Tolpekin for your great support and inspiration and great effort in explaining things clearly and critically to me. You have inspired me and enabled my dream to come into fulfillment and shown be the ability of how far I can achieve in my research offered through your great advice and correction. I would also like to extend my appreciation to my second supervisor Dr. Ling Chang for your positive criticism and correction which broadened my perspective in the research.

I would like to thank my GFM 2017 colleagues for their love, friendship and support over the past 18 months of our academic journey. In particular, I would wish to thank my study mates Robert Ohuru and Andy Baptist for great support both academically, emotionally and prayers and being like a family to me.

I would like to thank my entire family my parents whom I dedicate this research to, my cousin Philemon Kipkemoi who is my inspiration and mentor and also to my twin sister and brother who have journeyed with me through the academic life I am forever grateful.

I would also wish to express my sincere gratitude to the Dutch government for granting me the opportunity to develop and sharpen my skills in Geoinformatics through funding by Nuffic scholarship programme.

Above all, I would like to express my sincere gratitude to the Almighty God for His divine grace, favor and sustenance that has enabled me to successfully accomplish my studies. All this has been your strength and doing thankyou Lord.

TABLE OF CONTENTS

LIST OF FIGURES

LIST OF TABLES

LIST OF ACRONYMS

AVHRR Advanced Very High-Resolution Radiometer
DEM Digital Elevation Model
dNBR Difference Normalized Burn Ratio
ESA European Space Agency
EU European Union
EOS Earth Observation Science
GLCM Grey Level Co-occurrence Matrix
JRC Joint Research Commission
MAP Maximum A Posteriori
MSI Multispectral Instrument
MRF Markov Random Field
NBR Normalized Burn Ratio
OA Overall Accuracy
PA Producers Accuracy
RBF Radial Basis Fuction
RDTC Range-Doppler Terrain Correction
SAR Synthetic Aperture Radar
S1 Sentinel 1
S2 Sentinel 2
SNAP Sentinels Application Platforms
SLC Single Look Complex
SVM Support Vector Machine
SRTM Shuttle Radar Topographic Mission
UA Users Accuracy
UTM Universal Transverse Mercator
VV Vertical send, Vertical receive
VH Vertical send, Horizontal receive

1. INTRODUCTION

This chapter mainly describes the history of wildfires, its effect over time and gaps present in mitigating the fires. Section 1.1 presents the motivation of the research together with the problem statement. Section 1.2 defines the main objective of the research, its sub-objectives followed by the research questions to be handled. Section 1.3 defines the innovation of the research and finally, Section 1.4 describes the structure that is followed in the write-up.

1.1. Motivation and Problem statement

Forest is a key component of ecology and sustainable development and at the same time a dynamic resource. It is mainly affected by coexisting ecological processes, direct management interventions, and forest fires. Forest fires are generally referred to as wildfires due to their frequency and intensity (Westerling et al., 2006). Over the past years, the effect of wildfires in the forest as a result of the natural or human-induced phenomenon has attracted recognition both locally and globally. The implications associated with wildfires still continue even after it is contained as it leads to loss of vegetation cover, leaving exposed ground vulnerable to erosion and release of greenhouse gases in the atmosphere (Forshed et al., 2009). Different types of forest fires have been discussed in various literature. Key differences between wildfires and bushfires explored dependent on vegetation type. Wildfires being uncontrolled fires in a wildland area and characterized by its cause of ignition, weather and physical properties(USDA, 2003). Bushfires, on the other hand, are an uncontrolled fire in the woody or grassy or forested area especially occurring in Australia zones which is a sparsely-inhabited region (Lucas et al., 2007). The duration and intensity of bushfires determine not only the number of greenhouses and aerosols emitted but also the recovery process after the fire event (Akagi et al., 2011). Severe and frequent bushfires have caused significant changes in forest structure, species and biomass stocks (Xaud et al., 2013). Such severe changes over extensive areas are clearly assessed best using remote sensing (Chuvieco et al., 2002).

Satellite remote sensing has been used for detection, mapping, managing fire-prone areas and estimating the severity and intensity of bushfires (Chuvieco, 1999). It has been seen as a good and time-saving method in monitoring and quantifying amount of change that has resulted after fire (Stroppiana et al., 2003). In particular optical satellite data has been extensively used and has proved useful data in the mapping of burned areas (Koutsias et al., 2000; Roy et al., 2002; Mitri & Gitas, 2004; Stroppiana et al., 2015). However, the optical data has a disadvantage of being hindered by cloud cover or smoke during fire instance and errors due to spectral overlap (Kuenzer & Dech, 2013; Allison et al., 2016). Cloud cover reduces the observation rate in the visible/infrared bands which when depicting low fire severity and fast vegetation regrowth after fire may cause low spectral separability between burnt and unburned zones (Tansey et al., 2004). Thus this reduces the fire mapping capability of optical data sets. In contrast, the use of synthetic aperture radar (SAR) has the ability to penetrate clouds and fire smoke providing information

on burnt severity extent (Hoekman et al., 2010). Its weather independency also is an advantage compared to optical sensors. SAR has widely been used for biomass estimation, vegetation mapping and also ecological monitoring and growth (Kumar et al., 2017).

It utilizes microwave energy in both quantitative and qualitative analysis of the target surface by measuring the difference in scattering mechanism based on surface roughness (Polychronaki et al., 2013). SAR sensor emits an electromagnetic signal and receives the signal echo called backscatter, which allows detection of nature and position of material in accordance to the travel time of received pulse (Richards & Jia, 2006). It measures the variation in dielectric constant of target objects and determines the backscatter intensity of the microwave energy received and emitted in the resulting SAR product (kasischke, 1997). It also directly relates to forest structure in relation to its wavelength, polarization and local incidence angle resulting in information on the change in forest structure due to fire severity.

In recent studies, SAR has been used in the mapping of burned areas depicting sensitivity of backscatter signal to vegetation structure and biomass (Kasischke et al., 2000). The removal of leaves and branches after fire alters the scattering mechanism which results in temporal variations of backscatter intensity. The effects of fires on the backscatter coefficient have been exploited in several fire-related studies. This includes identification of fires scars in boreal forestry by exploiting the C-band backscatter of burned areas (Kasischke et al., 2010). The research on boreal forest depicted stronger return of backscatter intensity from burned scares as compared the unburned as a result of changes in moisture content (Bourgeau-Chavez et al., 1996). Similar observations were made also in tropical rain forest environment but discovered under dry weather decrease in backscatter compared to wet conditions however the discrimination of burnt and unburnt areas was difficult (Huang & Siegert, 2004). Some studies also reported the use of SAR in the mapping of burnt scars in the Mediterranean and the influence on rainfall in backscatter coefficient (Menges et al., 2004). The potential of SAR in the estimation of burnt severity after the fire has also been reported (Bourgeau-Chavez et al., 1996). However, most of the reported studies have focused on the detection and mapping of fire severity using SAR.

A major issue when utilizing SAR images in fire burn scars monitoring is the retrieval of biophysical parameters with great impact from local topography. This causes an influence in the backscattering coefficient especially due to the tilt of terrain which changes the scattering mechanism (Luckman, 1998; Sivasankar et al., 2015). Few studies have been done on the effect of geographical aspect of an area, its influence on local topography which directly affects backscatter intensity in the retrieval of burnt and unburnt areas after a bushfire. This research aims to analyze the use of backscatter intensity in the retrieval of burnt and unburnt areas in relation to the geographical aspect of the study area. In this research, we shall compare the effect of bushfire on hilly-mountainous areas to flat-terrain areas in two study areas, Australia and Spain. The focus being comparing the use of satellite SAR and optical imagery in the identification of burnt and unburnt patches within fire perimeter zones.

1.2. Research Objective

1.2.1. General Objective

This study is aiming to analyze the use of satellite SAR data and its comparison to optical imagery for identification and classification of burnt and unburnt patches after a forest fire.

1.2.2. Specific Objectives

1. To develop a forest fire burnt severity map that compares the size and extent of change on pre and post-fire instances.
2. To explore the sensitivity of polarimetric decomposition and backscatter intensity in the identification of burnt and unburnt areas.
3. To determine the degree of spectral contrast between burnt and unburnt areas.
4. To evaluate the contrast in texture analysis of unburnt areas and unburnt areas.

1.2.3. Research Questions

1. What is the suitable measure of burnt severity levels existing after the forest fire?
2. Is there a difference of target decomposition and backscatter intensity in the analysis of burnt and unburnt areas?
3. What are the effects of utilizing radar backscatter in retrieving the spectral and polarimetric aspect of the burnt and unburnt areas?
4. What are the effects of utilizing radar backscatter in retrieving the GLCM textural variation of the burnt and unburnt areas?

1.3. The innovation of the study

The proposed attempt for this study is in the identification and classification of the burnt and unburnt patches comparing the ability of satellite SAR and optical dataset obtained after a fire in separating the two. The novelty will be specifically looking at the geographical aspect of two study areas (Australia and Spain), the influence it has on topography and how they affect both the backscatter coefficient and spectral analysis. This will take into consideration the fire severity and vegetation cover in both areas that are within fire perimeter zones. The effect of topography influence on the two parameters will act as a guiding factor in decision making and understanding its impact on the rate of spread of fire, impact on land cover changes and mitigation of fire events prior to occurrence by fire management.

1.4. Thesis structure

This research has been documented in six main chapters. Chapter 1 is an introduction which contains motivation of research, problem statement, research objectives, and research questions, innovation of the study and summary of thesis structure. Chapter 2 is a literature review. Chapter 3 describes the methods used to achieve the objectives. Chapter 4 describes the study area and materials used in the research. Chapter 5 shows the results that are relating to the research objective and were obtained after the implementation of the methodology. Chapter 6 presents the evaluation and discussion of results. Finally, the conclusions and recommendations are in chapter 7.

2. LITERATURE REVIEW

This chapter is divided into two sections: First, the related work in Section 2.1 which describes past researches that have been done in line with our research, their achievements and gaps left in the studies. Secondly is the theoretical background in Section 2.2. In this section, we describe in Section 2.2.1 the concept of SAR remote sensing, Section 2.2.2. the concept and formulation of polarimetric signatures. Section 2.2.3 relates polarimetric signatures to polarimetric decompositions and its interpretation in fire monitoring. Finally, Section 2.3 describes the textural component in relation to the backscatter coefficient using SAR imagery and its interpretation in fire scar mapping.

2.1. Related work

Fire scars have been detected and monitored using remote sensing on surface reflectance characteristics (Vallejo, 1999). Since early 1980,s remote sensing (RS) has proved an accurate tool in the estimation of bunt severity levels of fire affected areas both at regional and local scales (Chu & Guo, 2013; Lentile et al., 2006). Space and airborne sensors have been used for assessing environmental conditions before and after the fire to detect the post-fire spectral changes and examine the vegetation influence (Lentile et al., 2006). The optical sensors that have been used in examining and evaluating burnt areas include Moderate Resolution Imaging Spectrometer (MODIS) (Boschetti et al., 2015). Landsat imagery (Salvador et al., 2000; Boschetti et al., 2015). Advanced Very High-Resolution Radiometer (AVHRR) (Remmel & Perera, 2001). Systeme Pour observation de la Terre Vegetation (SPOT-VEGETATION) (Pereira et al., 2002) and recently Sentinel 2- Multispectral Instrument (MSI) (Fernández-Manso et al., 2016). The above mentioned optical sensors have been widely used due to their high quality in terms of spectral and temporal resolution. Also, the need for moderate to high spatial resolution (10 m to 30 m) for mapping of burned areas was advocated by fire management for its analysis in the greenhouse effect, particles and aerosols (Mouillot et al., 2014; Randerson et al., 2012). This information is used for post-fire remedy and for an environmental management strategy.

Majority of the burned area mapping have attempted to detect the spectral changes caused after the fire which alters the vegetation (Roy et al., 2005; Giglio et al., 2006). These changes have been observed using the optical wavelength bands although they showed variation in space and time of the fire. Postfire characteristics of forest fires can be divided into two signals; the formation and deposition of charcoal or alteration of vegetation structure (scar) and plant canopies (Gitas et al., 2012). Previous studies have shown that burned areas generally tend to have lower reflectance and relatively dark in the visible spectral range (Almeida-Filho & Shimabukuro, 2004; Anderson et al., 2007; Masek et al., 2006). According to (Arnalds, 2015), the mapping of burned areas using the visible spectral region does not give accurate results due to the landcover types such as water bodies, wetlands, and soil. The spectral region appears darker making it difficult to discriminate burnt and unburnt areas. Bastarrika et al., (2014) has shown that

the near-infrared (NIR) in the spectral region where the signal for burned areas is highly sensitive is considered to be the most used region for mapping forest fire. Schroeder et al. (2016) explained that pre-fire images of forest usually depicts high reflectance in the NIR region while there is a decrease in reflectance at the postfire occurrence.

Various methods for burnt area analysis include the manual interpretation and detection of burnt areas (Silva et al., 2005), use of decision tree classification (Kontoes et al., 2009) whereby the method was efficient and offered high spatial and thematic accuracy results but unstable when data changes. Maeda et al. (2009) used the artificial neural network (ANN) using MODIS sensor to detect high-risk zones of fire in Amazon Brazil. He identified it as a fast and precise method for forest fire mapping however difficulties in model interpretation was experienced. Koutsias et al. (2013) applied a thresholding method used on analysis of pre and post-fire images in analyzing the extreme of fire severity. However, most studies have employed spectral differences between pre and post-fire images for burned area mapping and fire severity studies. The spectral indices such as normalized burnt ratio, burnt area index (BAI), mid-infrared burn index (MIRBI) and global environmental monitoring index (GEMI) have commonly been used to observe such differences (Chuvieco et al., 2002; Bastarrika et al., 2011(Bastarrika et al., 2011); Schepers et al., 2014).

However, these approaches are limited due to cloud contamination it's difficult to obtain suitable pre- and post-fire images for clear analysis. Secondly burned areas demonstrate spatial and spectral diversity due to fire severity, the time difference in image acquisition dates and fire dates and existing vegetation types (Stroppiana et al., 2012). Lastly cloud, shadows and water bodies foreshow similar spectral response to burned areas leading confusion in determining the coverage of unburnt patches (Boschetti et al., 2015). Change detection method between pre- and post-fire images have been mostly used to achieve good results however better approach for burned area detection and mapping is needed that will overcome the limitations mentioned.

2.2. Theoretical Background of SAR

2.2.1. Concept of SAR

Basically, SAR is a side-looking radar system that takes multiple images along an orbital path and transmits the electromagnetic signals that resulted after interaction with the target surface and records the backscattered echoes (Moreira et al., 2013). The specific properties of the SAR sensor being used determine the amount of backscatter coefficient that returns from the target surface to sensor (Koo & Chan, 2008). The properties include object roughness, dielectric properties of the surface, local incidence angles, polarization and wavelength, biomass and moisture content of vegetation. The SAR sensor has the ability to produce high-resolution images. The images are formed through the formation of virtual aperture and wavelength that's longer than the physical antenna length utilizing the Doppler effect of the echoes (Koo & Chan, 2008). However, SAR also experiences shortcomings with vegetation, speckle

effect, and shadows that hinder its visual and classification interpretation difficult (Sinha et al., 2015). The SAR wavelength runs from short wavelength to longer wavelength in the order of X, C, S, L, and P band and have distinctive properties that differ on various surfaces (Richards & Jia, 2006).
The use and application of SAR in various studies has grown over time from 1950,s. Since then several studies have been implemented that has contributed to the technological development of both airborne and spaceborne SAR missions. SAR has been widely used in the monitoring of landcover surfaces, natural phenomena such as forest, waterbodies. This is due to its capability in penetration of earth surface materials, all weather and usability during the night (Moreira et al., 2013). However, availability of data varies in all sensors, most of them requiring a special request and only a few are accessible to public dependent on special request.

2.2.2. Polarization Signatures

Polarization signatures provide a wealth of information about various properties of a surface as radiation with different polarizations scatter in different ways depends on the target surface (Richards & Jia, 2006). There exist four polarimetric channels consisting of both horizontal and vertical polarizations which are HV, VH, HH, and VV. HH means that the wave is transmitted and received horizontally. Similarly for VV that the wave is transmitted and received vertically and for VH the wave is transmitted vertically and received horizontally. Finally, for HV the wave is transmitted horizontally and received vertically. The HH and VV are referred to as co-polarized transmit and receive polarizations in the same direction. The HV and VH are called cross-polarized transmit and receive polarizations in the orthogonal direction (Aponte et al., 2014). The single polarized system is a system that transmits and receives either VV or HH polarized wave. The dual polarized system is a system that transmits and receives waves in two combinations of polarizations HH or VV and HV or VV and VH that transmits and receives waves in all combinations of polarizations (Massonnet & Souyris, 2008). In forestry analysis, the channels of polarization are significant in modeling forest burn severity. For the X and C band L bands co and cross-polarized were tested for burnt severity (Tanase et al., 2014) and for the co-polarization, the backscatter increased with burnt severity while for cross-polarized it decreased with burn severity. For wavelengths in X and C band, the polarization was dominant at the upper part of tree crown canopy while for L bands penetrate the canopy to higher extent interacting unburnt scars (Toan et al, 1992; Shoshany & Sternberg, 2001). A study by Ruecker & Siegert (2000) confirmed there is a decrease in VH polarization under dry weather conditions while during wet conditions the backscatter increased thus discrimination from unburned surroundings becoming difficult for C-band. Menges et al. (2004) also analyzed the effect of co and cross-polarized after a bushfire and discovered for both C and L- bands showed low values for burned areas and high for the unburned forest in relation to cross-polarized wave, however, for L- band depicted higher values compared to C- band. Finally, for Mediterranean forests (Gimeno et al., 2004) identified that for the C- band co-polarized backscattering increased independently with an increase in

precipitation. Tanase et al. (2010) mentioned that the scenes characterized by wet conditions presented higher levels of backscatter compared to ones obtained during dry conditions although both showed potential in the estimation of burnt severity after a forest fire.

2.2.3. Polarimetric Target Decomposition

The polarimetric decomposition theorem is used to analyze and understand the scattering mechanism of ground targets (Lee, 2009). It was first introduced by (Huynen, 1957), and has its founding roots by on light-based scattering by smaller anisotropic particles (Stretton, 2016). Many targets in radar remote sensing require a statistical description due to a combination of coherent speckle noise random vector scatter effect from target surface and volume. The development of a dominant scattering, mechanism which is invariant to changes in wave polarization is used for purpose of classification or inversion of scattering data. This is through expressing the average scatter mechanism as the sum of independent elements to associate physical mechanism with each component. There are two main types of target decomposition Coherent and Incoherent target decomposition (Veci, 2015). First is the coherent target decomposition characterizes completely polarized scattered waves whose polarimetric information is contained in a scattering matrix and only used for pure targets. Examples are the Pauli, Kroger, and Cameron decomposition (Alberga et al., 2004; Gaglione et al., 2014; Cameron e al., 1996). The Kroger decomposition can be represented as a combination of sphere, plane, and helix.

The second is Incoherent target decomposition which takes into consideration distributed scatterers (natural targets) by using the coherency covariance matrix which is a second-order statistics which represent Hermitian average covariance and coherency matrices (Zhang et al., 2008). The incoherent decomposition is a combination of second order statistics 3×3 coherency matrix or equivalent to 4×4 Mueller matrix that corresponds to the complex objects enabling an easier physical interpretation (Cloude & Pettier, 1996).

The polarization of the electromagnetic wave is represented by a modified Stokes vector their relation given by the Muller matrix (or Stokes matrix). A three-component scattering mechanism was proposed by (Freeman & Durden, 1998). H-alpha target decomposition theorem by (Cloude & Pettier, 1996). An imaging radar polarimetric data for unsupervised classification of scattering behavior by comparing polarization properties of each pixel in an image to simple classes of scattering such as even number, an odd number, and diffuse scattering by (van Zyl, 1989). Freeman and Durben considered three scattering mechanism volume scattering, double bounce, and single scattering. The volume scattering is from randomly oriented dipoles, double bounce from a different orientation of wave hitting the orthogonal surface with different dielectric constants and surface scatter from a rough surface (Freeman & Durden, 1998). The model contains an equal number of input and output model parameters and was being applied to C-, L- and P- band AIRSAR images of different terrains. The above target decompositions are used to analyze fully polarimetric SAR data, not much research exists on dually polarized decomposition.

However, the Cloud – Pottier decomposition can be used to analyze both the full and dual polarized data. The decomposition is used in the analysis of eigenvalue of a coherency matrix and is decomposed into eigenvalues and eigenvectors (Cloude & Pettier, 1996). In this research, the eigenvector-based decompositions are used to generate a diagonal form of coherency matrix which can be used for physical interpretation. Cloude & Pettier, (1996) considered such a decomposition as on an algorithm that identifies the dominant scattering mechanism via the extraction of the largest eigenvalue (Cloude et al., 2008). It consists of three parameters that are the entropy, anisotropy and alpha angle defined as a function of decomposition of eigenvalues and eigenvectors from the scatter matrix (Cloude & Pottier, 1997). The entropy indicates the randomness of the scattering mechanism (H~0= mechanism of unique scattering; H~1= multiple scattering mechanisms). The H values are usually high indicating large variation due to a variety of species distribution. Anisotropy A offers complementary discrimination of information at high entropy and the alpha provides information on the main scattering mechanism (Baxter et al., 2008). The alpha denotes the scattering dominating the target, where α=0 (isotropic surface), α=45 (horizontal dipole) and α=90 (isotropic dihedral scatter) respectively (Cloude et al., 2008). The alpha angle is independent of roughness and increases with angle of incidence and with a dielectric constant of the surface. The association of entropy (H) and alpha (α) is one of the key ways of understanding forest targets. The H/α plane is segmented into important zones according to its scatter behavior. Vertically three classes are distinguishable include surface, volume, and multiple scattering and horizontally the three classes are the low, medium and high entropy as defined by Cloude and Pottier (1997). The class boundaries relate to boundaries between physical models of the scattering behavior. It results into nine distinct classes however the high entropy surface scatters is excluded as a feasible region due to its inability to classify scattering types with increasing entropy thus we obtain eight useful classes.

2.3. Texture Feature Extraction

Texture is defined as the measure of the quality of an object while texture analysis is the process of analyzing the qualities of textures i.e. smooth or rough and many others in relation to its spatial variation of intensity values (Pathak & Barooah, 2013). There exist three main descriptors in texture analysis these includes texture classification or discrimination, texture description and boundary establishment between different texture elements (Beyerer et al., 2015). Texture depicts spatial information or pixel neighborhood position of elements in an image according to (Ojala et al., 1996). Haralick et al. (1973) define texture as spatial relationship of tonal elements often very small to be distinguished as individual elements such as trees, leaves and leaf shadows that can be segmented in an image. This forms a definition of image characteristics either rough or smooth, irregular or regular and random or linear providing visual appearance of image features (Ojala et al., 1996). The spatial distribution of grey values as a statistical approach is one of the features of texture description and various literature present it as one of the most employed methods in texture analysis (Rao et al., 2002). Texture computation is seen as a non-

deterministic spatial distribution of grey level values that result from the computation of local mean, variance and standard deviation (Pietikinen, 2004). The statistical method was defined in first, second and higher order representing one to more pixels on the feature. According to (Haralick et al., 1973) the statistical description of image texture characterization formed fourteen features. The initial features described optical transformation, autocorrelation functions, and digital transformations which resulted in eight groups. The other five groups describe structural elements, spatial grey tone co-occurrence probabilities, autoregressive models, textural edges and grey tone run lengths (Pathak & Barooah, 2013).

This research aims in looking at burnt and unburnt areas comparing pre/post-fire images analysis by use of H_alpha dual polarimetric target decomposition. The results obtained will be compared to the optical vegetation index obtained. The backscatter intensity values will be used in evaluating the textural component.

3. METHODS

This chapter describes the methods adopted for detection and characterizing of burnt and unburnt areas resulting from forest fires and analyzed using Sentinel 1 and Sentinel 2 datasets covering Victoria, Australia, and Spain. The methods include initial preprocessing, generating covariance matrix, polarimetric decomposition of Sentinel 1, contextual classification and texture analysis. An overview of the methodology followed for this research is depicted in Figure 1.

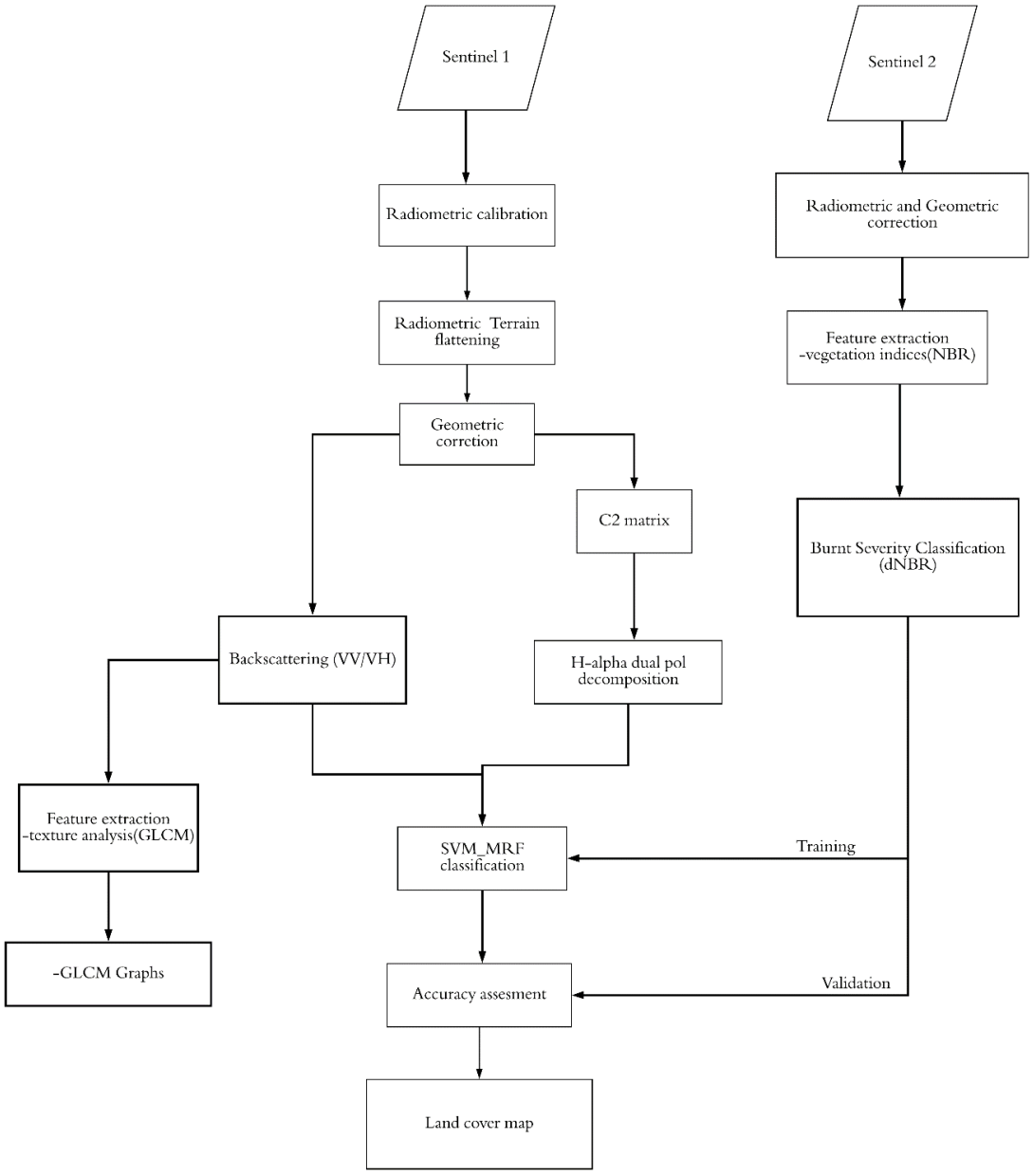

Figure 1: Methodological Flow Diagram

3.1. Generation of Scattering matrix [C2]

SNAP software was used to generate the scattering matrix of the dual-polarimetric. The 2×2 coherent matrix $[S]$ contains information about the single co- and cross polarization (VH and VV) (Cloude & Pettier, 1996). This establishes the existing relationship between the transmitted and scattered electromagnetic wave from a cell resolution by describing the backscatter information of the target for both polarizations (Jin & Xu, 2013).

$$[S]=\begin{vmatrix} S_{HH} & S_{HV} \\ S_{VH} & S_{VV} \end{vmatrix} \quad (3.1)$$

The scattering matrix measures the phase and amplitude of each element represented in complex form. The diagonal and off-diagonal elements representing the co and cross-polarized elements respectively.

3.2. Polarimetric Decomposition

The target decomposition theorem is used to evaluate the difference in backscatter intensity before and after fire events. The backscatter intensities which include dual (VV/VH) and the second will be polarimetric target decomposition. The eigenvector decomposition of the target covariance matrix will be implemented as described by (Cloude & Pottier, 1997). The main advantage of using this decomposition technique is that it provides a clear description between signal processing theory and estimation of noise from the covariance matrix (Cloude & Pettier, 1996).

Incoherent decomposition called the H-alpha dual decomposition is implemented. The created coherency matrix $[C2]$ in S1 is used as input for the Entropy/Alpha dual polarization decomposition. It is used to discriminate three scatters which include isotropic surface, horizontal dipole and isotropic dihedral. According to Cloude & Pottier (1997) there are three parameters extracted from eigenvalues ratio which include Entropy H which measures the randomness of scattering. Anisotropy A provides complementary information of entropy and facilitates interpretation of scatterer process. Alpha provides main scattering mechanism ranging from surface scattering ($0^{\circ} \leq \alpha \leq 30^{\circ}$), dipole scattering ($40^{\circ} \leq \alpha \leq 50^{\circ}$) and dihedral scattering mechanism ($60^{\circ} \leq \alpha \leq 90^{\circ}$). The entropy H and alpha α are separated into nine different regions of different scattering behavior (Ji & Wu, 2015) as shown in Figure 2:

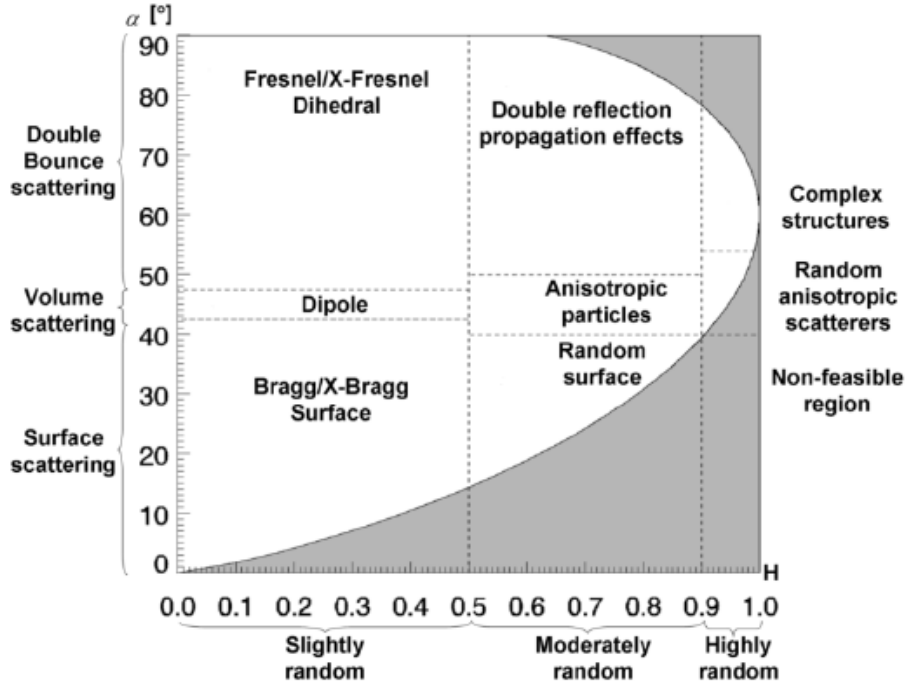

Figure 2: Segmentation of the H-alpha plane. Source: (Jagdhuber et al., 2014)

The H-α plane discriminates between surface reflection, volume diffusion and double bounce reflection along the x-axis and low, medium and high degree of randomness along entropy axis (Lee & Pottier, 2009). The surface scattering characterizes agriculture fields, bare soils, flat surface and water, volume scattering appears mainly in vegetated and forested areas and double bounce typical of forested and urban buildings. Visual interpretation is a key step in detecting and collecting relevant information about fire affected areas and other land cover features. Earlier the results of decomposition of S1 were used to identify burnt and unburnt areas by displaying them in red, green, blue RGB composite then the properties of burnt areas were collected for analysis and classification process.

3.3. Support Vector Machine (SVM)

The support vector machines are non-parametric classifiers used mostly for classification and regression and its concept introduced by (Cortes & Vapnik, 1995). It is a statistical learning algorithm that finds an optimal hyperplane and maximizes the margin between two defined classes using fewer training samples (Vapnik, 2006). SVM tends to maximize the margin between the hyperplane and the training samples while minimizing the empirical error caused by the training samples. The learning is an iterative process of finding a decision boundary that separates the training patterns (Zhu & Blumberg, 2002). The influence of inseparable samples is done using the regularisation parameter C. A detailed description of SVM working is described by (Richards & Jia, 2006).

A set of L training samples with pairs $(x_i y_i)$ where $i = 1,2 \ldots l$ whereby the existing class label is $y_i \in 1, -1$ and $x_i \in R^s$. The separating hyperplane is described as $f(x)$ tries to find the maximum separation between two closest vectors and is denoted equation 3.2 where x represents a point on hyperplane, b represents the marginal distance from origin to the point on hyperplane. The w represents the norm vector $w \in R^s$ which is also perpendicular a point in a two-dimensional vector.

$$f(x) = w.x + b \tag{3.2}$$

The aim of SVM is to maximize margin between two defined classes which is represented as two parallel hyperplanes along the main separating hyperplane passing through the closest training sample represented in Equation 3.3 and 3.4. The best point is one which $\| w \|$ weight vector is least.

$$w.x + b = +1 \tag{3.3}$$

$$w.x + b = -1 \tag{3.1}$$

However, in seeking to maximize the margin between the hyperplane and nearest samples a constraint is experienced represented in Equation 3.5

$$\min \frac{1}{2} \| w \|^2 + C \sum_{i=1}^{l} \xi_i \tag{3.5}$$

Whereby ξ_i is the degree of slackness that allows some misclassification error and C regularisation parameter controls the rate of misclassification in our sample. Thus linear SVM is extended to non-linear SVM by introducing the kernel basis function which operates in high dimension feature by use of Lagrange multipliers shown in Equation 3.6 and problem denoted Equation 3.7 (Richards & Jia, 2006).

$$f(x) = \sum_{i\varepsilon} \lambda_i y_i K(x.x_i) + b \tag{3.6}$$

$$max_\alpha \sum_{i=1}^{l} \lambda_i - \frac{1}{2} \sum_{i=1}^{l} y_i y_i K(x_i.x_i) \tag{3.7}$$

Whereby $C \geq \lambda_i \geq 0$ and $\sum_{i=1}^{l} y_i y_i = 0$ and $i = 1,2 \ldots . l$. The $\alpha_i \alpha_j$ are considered as Lagrange multipliers while λ_i is between regularisation parameter C and kernel function K. The most common used kernel is the radial basis kernel (RBF). It is selected as the optimal kernel in its parameter adjustments according to classifier performances and a one-against-one (OAO) strategy is used to handle multi-class problems (Kavzoglu & Colkesen, 2009). The RBF contains two parameters namely parameter (C) and the gamma parameter (y).

3.4. Markov Random Field (MRF)

Markov Random Field (MRF) is a widely considered technique in the in-depth understanding of contextual information (Richards & Jia, 2006). Contextual information refers to a relationship of feature in

relation to its neighboring pixels. The main application of MRF has been on remote sensing image analysis to improve image classification accuracy, textural analysis, edge detection algorithm and (Li, 2010; Jackson et al., 2002). MRF and its formulation are described in (Mather & Tso, 2013).

Let $d = d_1, d_2 \ldots . d_m$ represents a set of random variables which is defined on the set of S containing m number of pixels with each random variable taking a label L while d represents a set of digital number (DN) values known as random fia eld. The label L is highly dependent of on user defined possible classes which include forest, agriculture, water, bare land etc. A random field is considered to relate to a neighbourhood system and therefore called a Markov Random Field if only its probability density function satisfies the following conditions;

I. **Positivity**: $P(w) > 0$, it means there does not exist any label configurations which isn't possible.
II. **Markovianity**: $P(w_r|w_{s-r}) = P(w_r|w_{Nr})$ it means the membership of the label of pixel is highly dependent on its neighbourhood.
III. **Homogeneity**: $P(w_r/w_{Nr})$ it means that probability is the same for all pixels r regardless of pixels location.

An additional condition is Isotropy which denotes dependence variation of pixels with its neighborhood as a function of direction.

3.5. Neighbourhood System

In our thesis research were mainly interested in the spatial contextual classification of our images. MRF mainly deals with local neighborhood while Gibbs Random Field (GRF) deals with the global neighborhood (Mather & Tso, 2013). Its represented by the probability density function is shown in Equation 3.8.

$$\mathrm{P(w)} = \frac{1}{\mathrm{Z}}\exp[-\frac{\big(U(w)\big)}{\mathrm{T}}] \tag{3.8}$$

Whereby $P(w)$ represents the probability of w , Z is called the partitioning function and is a sum of all possible combinations of w represented in equation 3.9. $\cup\,(w)$ represents the Energy function and lastly is T which is a constant called temperature.

$$Z = \sum exp - \frac{(u(w))}{\mathrm{T}} \tag{3.9}$$

Maximizing of $P(w)$ is equivalent to minimization of the energy function $\cup\,(w)$ shown in Equation 3.10

$$U(w) = \sum_{c\varepsilon C} V_c\,(w) \tag{3.10}$$

The $\mathrm{C} = \mathrm{C}_1 \cup \mathrm{C}_2 \cup \mathrm{C}_3 \cup \ldots .$, it is a collection of all possible cliques which are a representation of a part of a neighborhood. The C is denoted as a single pair, a pair of neighboring sites or triple neighboring sites

in a neighborhood system respectively. In this study C_2 has been used as a second order neighborhood system.

3.6. Maximum A Posterior Solution (MAP)

A Maximum A Posterior (MAP) is obtained by minimization of global posterior energy. This helps in pixel labeling problems. Posterior energy is as a result of the combination of prior energy and conditional energy. MAP solution is formed according to the Bayesian formula as shown in Equation 3.11 (Bassett & Deride, 2018).

$$P(\theta|d) = \frac{(P(d|\theta)P(\theta))}{(P(d))} \quad (3.11)$$

Where θ is the membership value and d is a dataset. The formula can also be expressed as shown in equation 3.12 whereby $P(\frac{\theta}{d})$ is the posterior energy function.

$$P\left(\frac{\theta}{d}\right) = arg\ max\left\{P\frac{\theta}{d}\right\} \quad (3.12)$$

For the minimization of the global energy function, it is expressed in equation 3.13.

$$P\left(\frac{\theta}{d}\right) = P\left(\frac{\theta}{d}\right) + P(\theta) \quad (3.13)$$

Where $P(\theta/d)$ is the conditional energy and $P(\theta)$ is the prior energy function. To create a balance between two energy functions an additional parameter denoted as λ is added into the Equation 3.14.

$$P\left(\frac{\theta}{d}\right) = (1-\lambda)P\left(\frac{\theta}{d}\right) + P(\theta) \quad (3.14)$$

The λ ranges from 0-1 and results to smoothness in output. Therefore, to obtain MRF-MAP estimate minimization of global posterior energy is needed. However, the use of Simulated Annealing (SA) algorithm has been often used in global minimal energy and shown greater strength compared to other algorithms such as Iterative Conditional Modes (ICM) and Maximiser of Posterior Marginals (Mather & Tso, 2013).

3.7. Simulated Annealing (SA)

Simulated Annealing (SA) is an iterative relaxation algorithm that was first proposed by Metropolis et al., (1953) for behavior simulation. It is preferred as it reaches a global minimum with the least computational time. SA is implemented in minimizing energy function to approximate MRF-MAP estimate. The algorithm begins at a high temperature T_0, at equilibrium, it tends to converge the slowly decreases according to a scheduled time frame. The process is an iterative one and at the convergence point $T_0 \rightarrow 0$ no more updates are yielded, and a solution is found. The optimal solution is determined by two main parameters initial temperature T_0 and update temperature T_{upd} (Mather & Tso, 2013).

3.8. Validation

The spectral index normalized burn ratio (NBR) will be used as a reference to detect burnt and unburnt areas on S2-A images, for better analysis and verification and provide burnt and unburnt patches (Escuin et al., 2008). The NBR is used in the identification of burnt zones occurring after forest fires and calculated as shown in equation 3.15. Its formula relates similarly to the normalized difference vegetation index (NDVI). However, it differs slightly as it uses near-infrared (NIR) which covers 750-900 nm and short-wave infrared (SWIR) which covers 2080-2350 nm portion of the electromagnetic spectrum (Allison et al., 2005). The NIR reflects strongly in vegetation while SWIR is lower but after the fire, the SWIR reflects stronger than the NIR.

$$NBR = \frac{(NIR-SWIR)}{(NIR+SWIR)} \tag{3.15}$$

From the result of NBR the ratio between pre- and post-fire images as it measures forest regeneration with time aspect.

$$dNBR = preNBR - postNBR \tag{3.16}$$

After that difference between the image before and after the fire as shown in Equation 3.16 the result is used to develop the burnt severity levels which will include five major classes (1) unburned areas (2) lightly burned areas (3) medium burned areas and (4) deeply burned areas and (5) post-fire regrowth (Allison et al., 2005). Validation is an essential part of any classification as it assesses the accuracy of results and we can tell the correctly and not correctly classified pixels in the image. The validation sets are chosen with reference to the vegetation index (dNBR) which is used in the detection of burnt and unburnt areas by computing the difference of two images (pre/post) fire images as shown in Equation 3.16. They are segmented to extract burnt and unburnt areas. According to Madoffe et al. (2000) defines unburned areas as having the forest fire not burning forest floor, lightly burnt areas are partially burned and scorched trees and burn is Scottish. They further described that moderately burned area are whereby most vegetation is burned to ground level and most forest floor coverage is burnt while deeply or highly burned areas and the forest floor is consumed by combustion and skeletons of vegetations are left as remnants. A random feature selection of training and test sets shall be used to reduce data redundancy.

Validation dataset is used to test the ability of the SVM_MRF classifier to classify new pixels in new datasets. Finally, the results obtained are validated using training and test sets to produce overall accuracy. The classification results are evaluated by accuracy assessment accuracy takes into consideration the overall accuracy (OA), users' accuracy (UA), producers' accuracy (PA) and kappa coefficient (Kc) which uses the error matrix incorrectly classified pixels. According to Powers (2007) for us to be able to ascertain the relevance of our SVM classification system the precision and recall evaluation metrics will also be analyzed. Precision (P) is defined as a measure of classifiers exactness calculated by the number of true positives over the number of true positives Tp plus the number of false positives Fp.

$$P = \frac{Tp}{Tp+Fp} \tag{3.17}$$

Recall (R) is defined as a measure of classifiers completeness and calculated by of true positives over the number of true positives Tp plus the number of false negatives Fn.

$$R = \frac{Tp}{Tp + Fn} \tag{3.18}$$

The F1 score conveys the balance between precision and recall and calculated as;

$$F1 = 2 \times [\frac{(P \times R)}{(P+R)}] \tag{3.19}$$

3.9. Spatial Texture Analysis

After the pre-processing steps, texture analysis is performed on each backscatter (VV and VH).
Texture analysis is vital in ground object recognition as it represents the spatial relationship of grey-levels in an image (Dinstein et al, 1973). It improves the accuracy of interpretation in classification in many remote sensing applications (Dekker, 2003). This provides vital information about SAR imagery (Dubois et al., 2008). The GLCM texture analysis is the most commonly used landcover monitoring applied in numerous studies (Franklin, 2001; Clausi & Yu, 2004). In this study, GLCM is implemented to obtain statistical texture features.

The grey level co-occurrence matrix (GLCM) is a second ordered statistical texture analysis approach often used in texture classification and texture segmentation (Arivazhagan & Ganesan, 2003). It describes the spatial distribution of intensities that occur in an image. GLCM requires images to be quantized to a certain number of grey levels. The texture measures depict the spatial distribution of grey level value and its homogeneity to each in relation to a specific lag distance at (x, y) and orientation (0°,45°,90° and 135°). At origin 14 texture features were extracted from the GLCM features however seven of them are most relevant in remote sensing image analysis. The features are as follows as shown in Figure 3. The commonly used texture features include angular second moment (ASM), contrast, variance, homogeneity, correlation, and entropy as they are considered to obtain optimal results (Rao et al., 2002; Soh et al., 1999). In the study, thirteen textural features were experimented at all directional invariant texture angles (0°,45°,90° and 135°), a lag distance of 1, a window size of 9×9 and 256 level quantization was used because of efficiency and sufficiency in its performance on separation of burnt and unburnt patches in S1.

$$\text{Angular Second Moment} = \sum_i \sum_j \{P(i,j)\}^2 \tag{3.20}$$

$$\text{Contrast} = \sum_{i,j=1}^{N} (i-j)^2 P(i,j) \tag{3.21}$$

$$\text{Entropy } = -\sum_{i,j=1}^{N} P(i,j) log P(i,j) \quad (3.22)$$

$$\text{Homogeneity} = \sum_{i,j=1}^{N} \frac{1}{1+(i-j)^2} P(i,j) \quad (3.23)$$

$$\text{Variance} = \sum_i \sum_j (i-u_i)^2 P(i,j) \quad (3.24)$$

$$\text{Correlation} = \sum_i \sum_j \left(\frac{(ij)P(i,j)-u_x u_y}{\sigma_x \sigma_y}\right. \quad (3.25)$$

4. STUDY AREA AND MATERIALS

This chapter gives an overview of the study area and materials utilized during the research. Section 4.1 describes the influence of the choice of the study area. Section 4.2 describes the dataset and time zones. Section 4.3 describes the software used and its packages. Section 4.4 describes the pre-processing steps involved in utilizing both sentinel 1 and Section 4.5 for Sentinel 2 data. Finally, Section 4.5 describes the method used in the selection of validation and training sets.

4.1. Description of choice of study area

The two case study areas selected for our research were Victoria, Australia, and Spain respectively. The choice of our study areas was influenced by the following factors, firstly they experience severe wildfires occasionally that have caused massive impact on human lives and economic and environmental degradation. Thus, it would be key to look into the causes of fire and the measures to be undertaken to mitigate future fires and also for sustainability of the forest ecology. Secondly, they have a forest structure that influences the spread of fire rapidly. Thirdly they have varying geographical phenomena that would be of interest in our research in understanding how each area responds to fire occurrences. Fourthly the have recent forest fire occurrences that could be of interest in our research. Lastly due to the recent fire occurrences the availability of recent launched satellite missions S1 and S2 time frame the datasets would be suitable and available for study areas.

The selection of the fire zones in the two areas was mainly influenced by their geographical position which varied from hilly areas in Australia to flat areas in Spain and variation in vegetation cover. The level of fire severity especially in Victoria, Australia as there were many bushfires. Their time of occurrence which had to be recent in the period of 2017 and 2018 which would reflect how timely and important our research is to specific stakeholders involved in forest fire management. Finally, the availability of data from respective forest database which had the area of the fires and the fire perimeter zones showing the extent of the fires which is a guiding factor during analysis of our thesis.

For Victoria, Australia the Victoria bushfire database was used, which contained bushfires registered and updated from 1939 to 2018 (Victoria, 2018). The database contained information in vector shapefile format of all the burns and bushfires in the area, their date of occurrence, the level of severity, location of the fire, fire type, season, area coverage and method of obtaining the fire perimeters together with accuracy in the resolution of the method used. From the dataset three bushfires were extracted between 2017 and 2018 using a criterion that they were bushfires, their occurrence date was recent (2017/2018) and their burnt severity level was the highest in the database.

Fire zone	Database name (FIRE_NO)	Date of fire	Area coverage(HA)	Fire type
Fire 1	S34	26/11/2017	1054.81	Bushfire
Fire 2	M35	12/03/2017	1249.75	Bushfire
Fire 3	2BNN0030	11/03/2017	218.96	Bushfire

Table 1: Description of fire zones in Victoria, Australia.

In Spain, the data was provided by César Vicente Fernández and Francisco Senra Rivero (PAU, 2018). From the authors, we obtained two fire zones located in the southwestern part of Spain. The data contained fire perimeter zones of the two areas, also the description of the direction of fire, the landcover and the terrain of the areas. The fires recently occurred in 2017/2018 also as described in Table 2.

Fire zone	Database name (fire name)	Date of fire	Area coverage(HA)	Fire type
Fire 4	Hu_Nerva	02/08/2018	1749.79	Forest fire
Fire 5	Hu_ Moguer	24/06/2017	1033.34	Forest fire

Table 2: Description of fire zones in Spain

4.1.1. Australia study area

Victoria is located in the southeastern corner of Australia. It covers an area of about 240,451 km^2. It has diverse climatic areas, ranging from semi-arid and hot in the northwest to cool temperatures along the coastal region (Attiwill & Adams, 2013). It is located 34° 20' N and 39° 00' S and between longitudes 141° E and 150° E .Bushfires in Victoria Australia occur frequently and are due to the naturally occurring phenomenon in the Australian environment. This is because of its hot and dry climate during summer. Most of the bushfire has destroyed a greater number of homes, human lives, and properties. The devastating bushfires have occurred and range through the dense eucalypts forest which contains flammable oils in the leaves regenerates faster after the fire and are present in all of the varying continents climate zones (Fairman et al., 2016). In southern Australia, there exists two distinctive eucalyptus forest species, those species that are of high-severity nature and those that mostly survive the fire levels highly had a longer tree life span (Jenkins et al., 2016). The eucalyptus class types consist of low open woodlands to tall closed forestry and consist mostly of woodland trees of medium-height (Martin & Topp, 2018). Increased temperatures and extended droughts mostly increase the frequency of fire intensity and highly depends on fuel loads, wind patterns and topography which varies highly in Victoria (Clarke et al., 2013). About 2.60 million ha of forest was severely damaged by three major bushfires in 2003,2006-2007 and

2009 (Whittaker & Mercer, 2004). It is estimated that about 50% of the 8.6 million hectares of forest area burned between 1962 and 2014 occurred mostly from 2003 (Fairman et al., 2016).

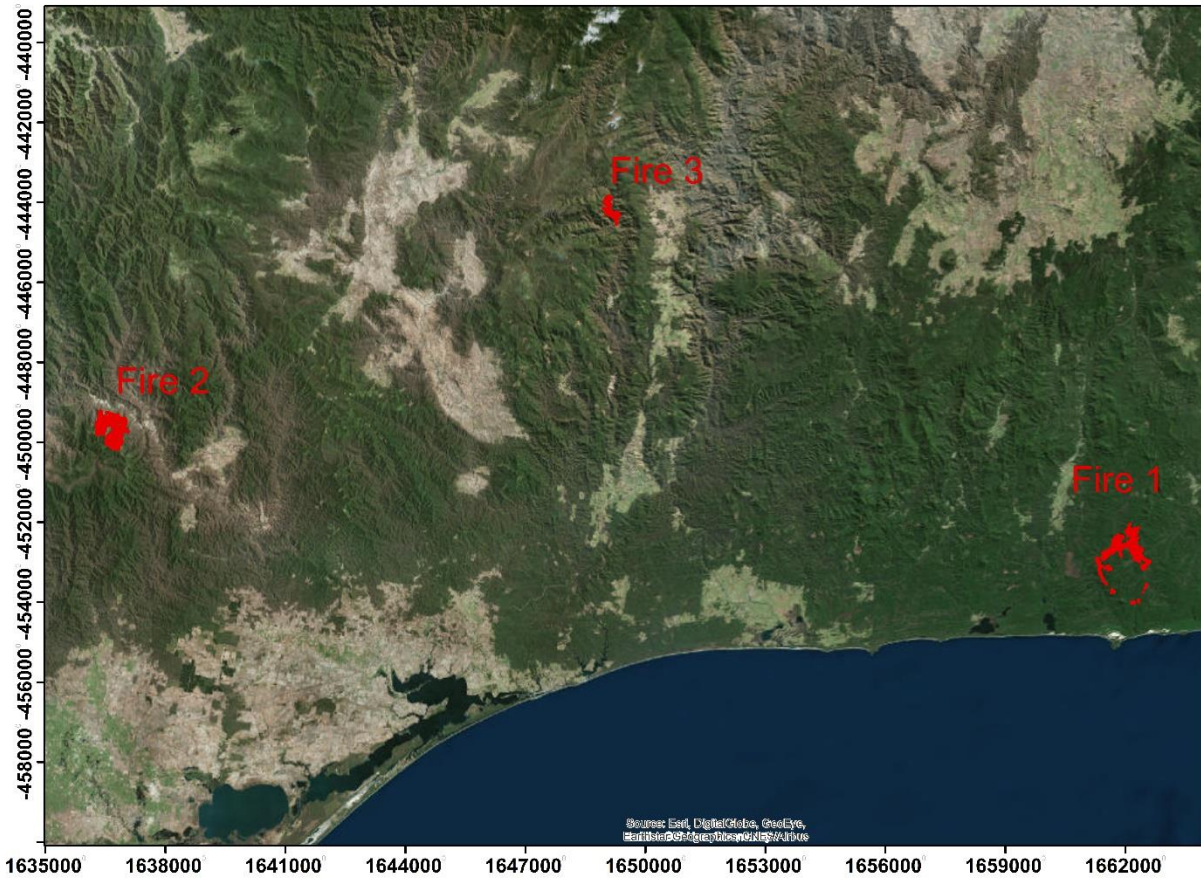

Figure 3: In red: Fires selected for this study from the Victoria bushfire database between 2017/2018. Map source: Esri, Digital globe, Geoeye, Earthstar Geographics, CNES/Airbus DS, USDA, USGS, AeroGRID, IGN, and the GIS User Community.

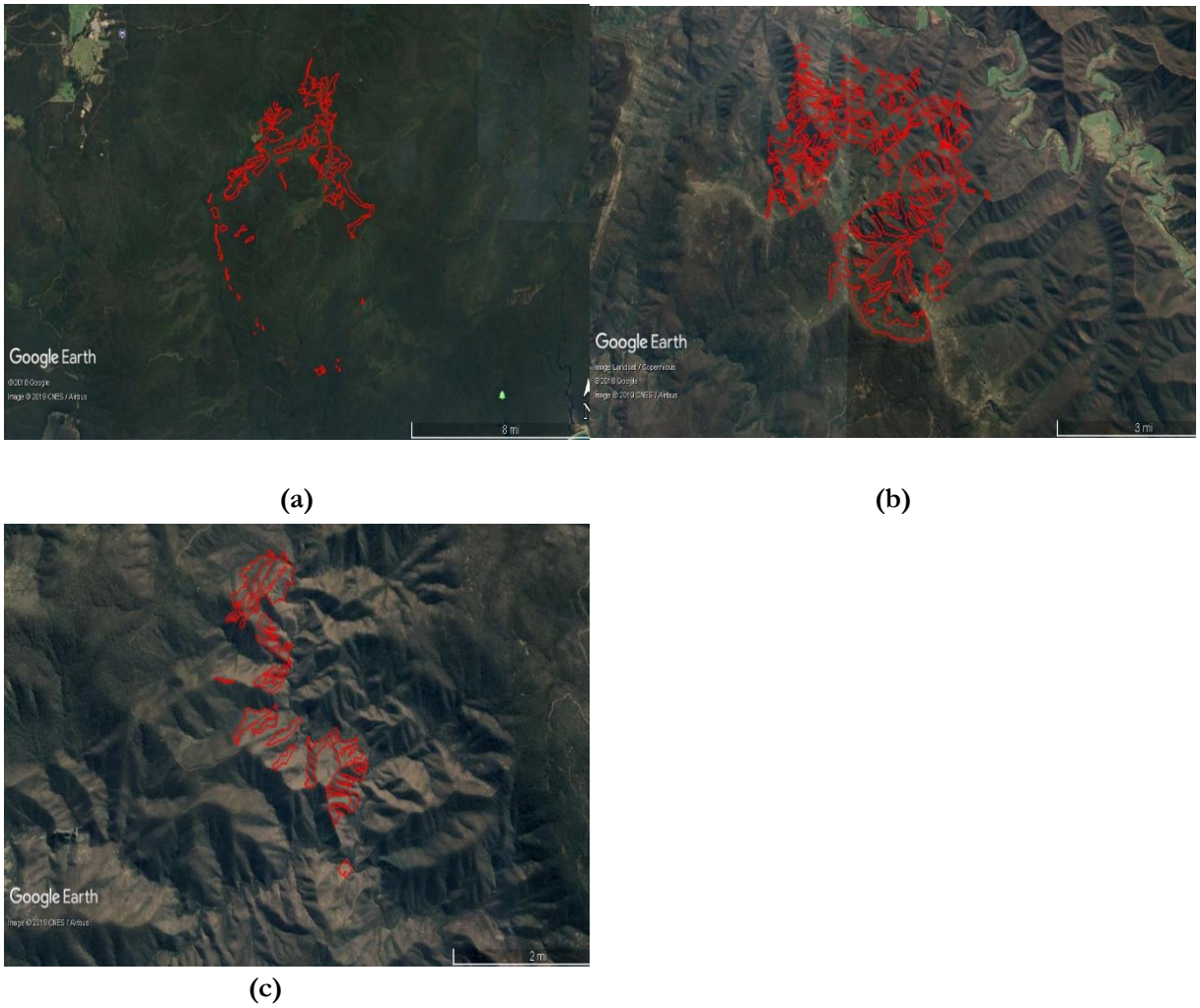

Figure 4: Selected bushfires from Victoria database a) fire 1, b) fire 2 and c) fire 3. The red lines indicate fire footprints with some holes within it. Map source 2018 Google earth © 2019 CNES/Airbus. Image Landsat/Copernicus.

4.1.2. Spain study area

Spain is a country situated along the Mediterranean basin in Southern Europe. It covers an area of about 505,370 km² around the Iberian Peninsula. The coastal regions are in the southern and eastern region, while the mountainous area in the northern sections. It is located between latitude 26° 47' N and 44° 01' N and between longitudes 19°00' E and 5° 36' W. Its climate is characterized by warm and hot and dry summers and also wet winters (Giannakopoulos et al., 2005). Due to the agricultural sector Spain experiences large and high variability in climate changes. The vegetation is also diverse with a special type of Mediterranean forests especially oak as well as pine forests replanted mostly after forest fires (Riera Mora, 2006).

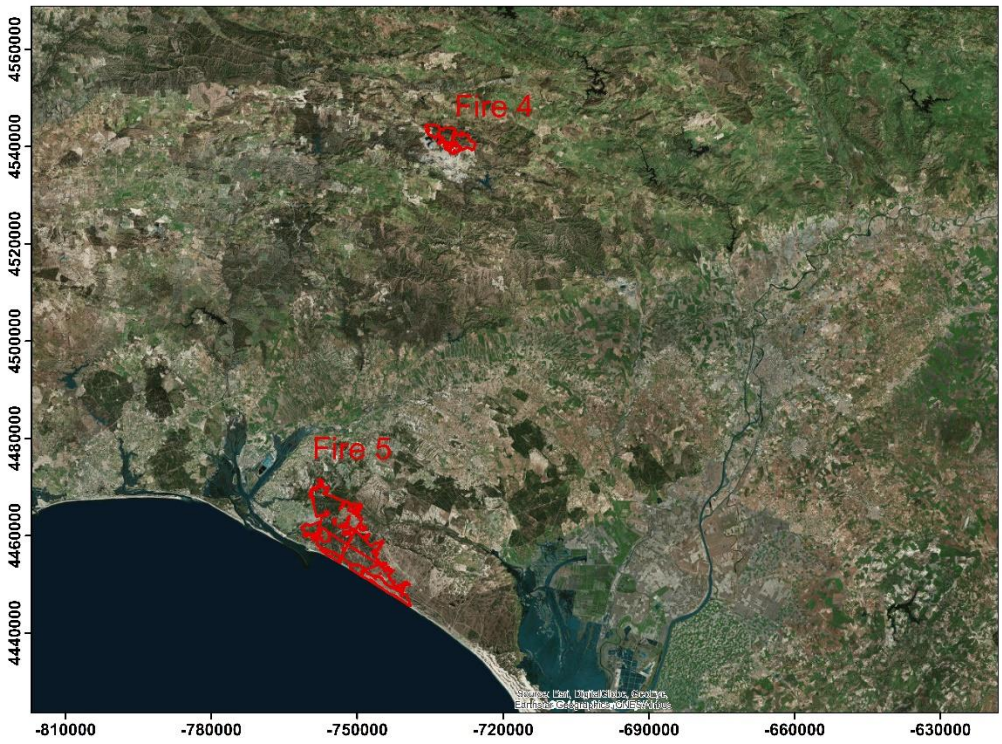

Figure 5: In red: Fires selected for this study from Spain between 2017/2018. Map source: Esri, Digital globe, Geoeye, Earthstar Geographics, CNES/Airbus DS, USDA, USGS, AeroGRID, IGN, and the GIS User Community.

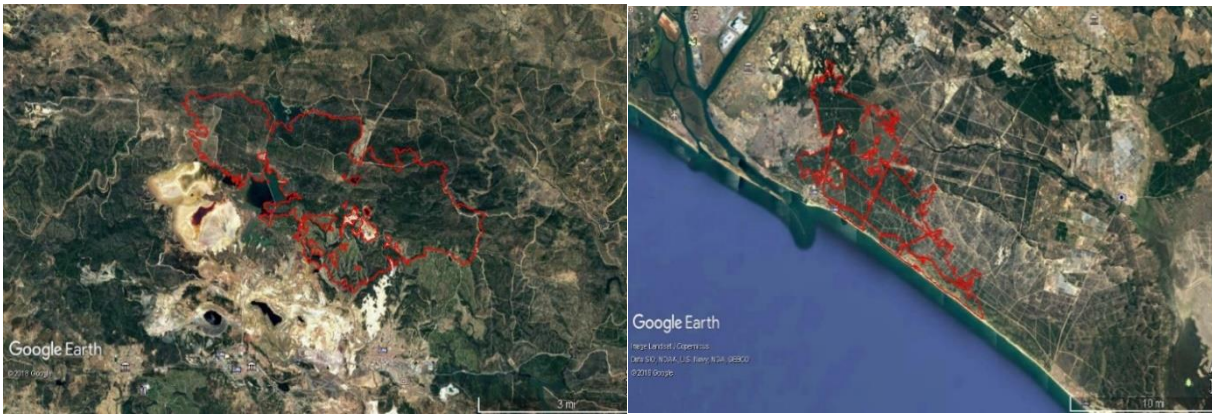

(a) **(a)**

Figure 6: Selected fires zones a) fire 4 and b) fire 5 respectively in Spain: the red lines indicate the fire extent area with holes within it. Map source: © 2018 Google. Image Landsat/Copernicus. Data SIO, NOAA, U.S. Navy, NGA, GEBCO.

4.2. Satellite Dataset

Data	Sentinel 1 (Fire 1)	Sentinel 1 (Fire 2)	Sentinel 1 (Fire 3)	Sentinel2 (Fire 1)	Sentinel2 (Fire 2)	Sentinel2 (Fire 3)
Fire date	26/11/2017	12/03/2017	11/03/2017	26/11/2017	12/03/2017	11/03/2017
Acquisition date (pre/post)	16/11/2017 27/01/2018	02/03/2017 07/04/2017	25/02/2017 08/05/2017	17/10/2017 14/02/2018	17/02/2017 18/04/2017	17/02/2017 18/04/2017
Product type	L1 SLC	L1 SLC	L1 SLC	S2MSI1C	S2MSI1C	S2MSI1C
resolution	4 × 20 m	4 × 20 m	4 × 20 m	10m	10m	10m
Instrument mode	IW	IW	IW	INS-NOBS	INS-NOBS	INS-NOBS
Polarization	VH/VV	VH/VV	VH/VV			
Orbit	Descending					

Table 3: List of radar and optical data used in Victoria, Australian study area respectively

Data	Sentinel 1 (Fire 4)	Sentinel 1 (Fire 5)	Sentinel 2 (Fire 4)	Sentinel 2 (Fire 5)
Fire date	02/08/2018	24/06/2017	02/08/2018	24/06/2017
Acquisition date (pre/post)	20/07/2018 14/08/2018	19/06/2017 20/07/2017	31/07/2018 05/08/2018	11/06/2017 21/07/2017
Product type	L1 SLC	L1 SLC	S2MSI1C	S2MSI1C
Resolution	4 × 20 m	4 × 20 m	10m	10m
Instrument mode	IW	IW	INS-NOBS	INS-NOBS
Polarization	VH/VV	VH/VV		
Orbit	Descending			

Table 4: List of radar and optical data used in Spain study area respectively

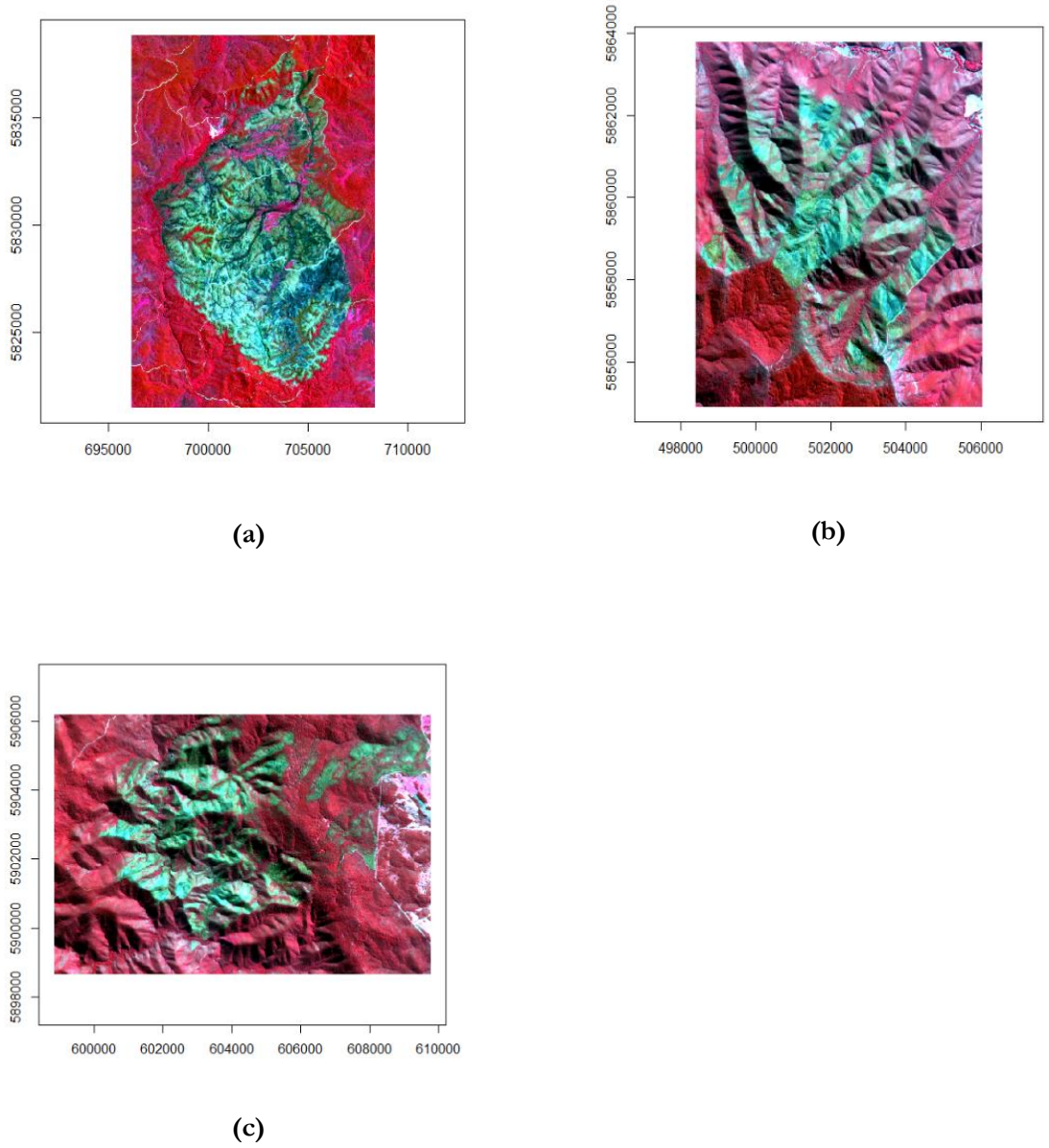

Figure 7: Sentinel 2 postfire images covering the area of bushfires from figure 4. (a) fire 1, (b) fire 2, (c) fire 3, respectively. Band combination is=8:4:3. Green representing burnt areas while red represents the unburnt areas in Victoria, Australia.

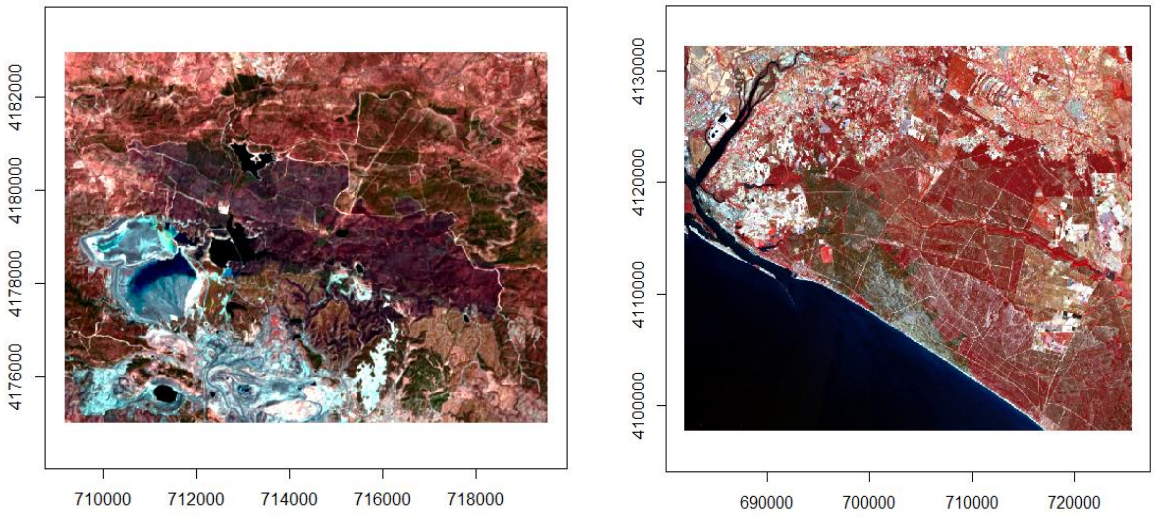

(a) **(b)**

Figure 8: Sentinel 2 postfire images covering the area of bushfires from figure 6. (a) fire 4, (b) fire 5, respectively of Spain. Band combination=8:4:3.

The RGB bands represent Band 8 is red is Near infrared(NIR) covers 842nm in electromagnetic spectrum. Band 4 is visible red or orange covers 665nm in electromagnetic spectrum. Band 3 is visible light green and covers 560nm in electromagnetic spectrum.

4.3. Software

All pre-processing of S1 was performed using freely available Sentinel Application Platform (SNAP) toolbox version 6.0 provided by European Space Agency (ESA). It was used for co-registration, calibration, debursting, radiometric and geometric correction, polarimetric decomposition of SAR. Erdas Imagine 2016 was used for vegetation index calculation (Geospatial, 2016). ArcMap version 10.6.1 developed by ESRI was used for producing map outputs on the standard processing work station. Sen2cor plugin was used for atmospheric correction for S2 images (GmbH, 2015). Most of classification and analysis were done using R and R studio (R Development Core Team, 2018). The libraries used for processing were Rgdal (Rowlingson, 2018) used to read the longitude/latitude description of an image, MASS (Ripley & Venables, 2002) supports statistical functions and computations , e1071 (Meyer et al., 2018) supports functions related to classifiers such as the support vector machines, mvtnorm (Alan et al., 2018) used in probability computations, quantiles and density plots, rgeos (Roger et al., 2018) used for topology and spatial operations on geometries, Rcpp (Eddelbuettel & François, 2011) used to write R functions in fast speed. The classification codes were developed by earth observation science (EOS)

department in ITC. They include SVM hyperspectral classification, SVM_MRF_VHR classification code, and GLCM textural analysis.

4.4. Pre-processing of Sentinel 1

The main pre-processing steps of dual polarized channel S1 was done in Sentinel Application Platform (SNAP) software obtained in single look complex product (SLC) containing phase information involve (Maître, 2008). The main pre-processing steps of the SLC image involve:

- Radiometric calibration provides correction of pixel values as an actual representation of radar backscatter of reflecting surface. This is to correct for instrument distortion which may cause an error in quantitative physical measurements of SAR data. An absolute calibration vector is included as an annotation in image product which allows conversion of image intensity values into Digital Number (DN) values (Rosich, 2004). The corrections are applied by the software automatically determining the input and output and the product is saved as complex output.
- Debursting: The S1 IW SLC image is composed of several bursts overlapping in azimuth time for each subwaths, separated by black lines and each sub-swaths has its own dimensions and geocoding (Sanders et al., 2016). The deburst operator generates a continuous image in reference to azimuth time, by removal of black separation lines as well as redundant lines between bursts (Sowter et al., 2016). The input is to the operator S1 TOPSAR-Deburst is the SLC IW image with multiple subwaths its intensity values of VV and VH polarization and output was deburst SLC image. After a deburst operator, the target product is usually one dimension for all bands and similar geocoding.
- Radiometric terrain flattening aids in correcting terrain that is rugged which results in misclassification during landcover classification. Terrain variations is a function of the relative orientation of surfaces in relation to the source of illumination and position of the sensor to the target (Small, 2011). Terrain variations not only affect the position of a point on earth surface but also the brightness of the radar return. The facet method proposed by Small et al. (1998) compensates the terrain variation effect by calculation for each image pixel a facet of digital elevation model (DEM) that corresponds to the scatter area. The parameters used are the source image whereby select the source bands or by default, all bands are selected. The second parameter is the DEM used in computing the local illuminated area and the Shuttle Radar Topographic Mission (SRTM) 3Sec (90m) was used. The DEM resampling method used in getting the elevation from DEM was bilinear resampling method. The process will run automatically after parameters are well defined.
- Geometric correction, which is a refining of pixel absolute location, using SRTM DEM. Geocoding of images is a key process as it will convert the slant range onto map coordinate system through the range-doppler terrain correction (RDTC) implements the range-doppler orthorectification method of SAR image (Schubert & Small, 2008). It uses the orbit state vector information in metadata, the radar timing annotations, slant to ground range conversion

parameters together with reference DEM to derive precise geolocation (Schubert et al., 2014). The parameters to be defined will be processed using SRTM 1Sec (30m) as inputs of DEM data which is automatically downloaded. Both the DEM and image resample will implement the bilinear interpolation method. A pixel spacing of 30m and map projection of universal transverse Mercator (UTM) and the datum, world geodetic system (WGS) 1984. The areas without elevation will be masked with reference to the DEM data.

4.5. Pre-processing of Sentinel 2

The Sentinel -2A Level 1C (L1C) MSI images used in this study were downloaded from ESA.
The images correspond to level 1C products that are not radiometrically and geometrically corrected Top-of-Atmosphere (TOA). The corrections done include orthorectification and spatial registration on global reference system (UTM/WGS84 projection) with subpixel accuracy. The atmospheric correction was done using Sen2cor which performs pre-processing of L1C Top-of-Atmosphere (TOA) images and applies scene classification with an atmospheric, terrain and cirrus correction. Then it converts to ortho image L2A Bottom-Of-Atmosphere (BOA) reflectance product (ESA, 2015). The L2A products spatial resolution varied from 10m to 60m depending on spectral bands however the images were resampled to 10 m resolution using nearest neighbor resampling. All the images were cloud free thus there was no need for cloud mask for the elimination of cloud pixels. The top of atmosphere reflectance images was converted to surface reflectance images. The surface reflectance images were subset to selected fire and NBR was computed for both pre and post-fire images followed by dNBR.

4.6. Selection of validation and training sets

Sampling sites for training are obtained through visual interpretation of images both before and after the fire and drawing of vector training sets using ArcMap. While the selection of validation sets is from the vegetation indices difference normalized burnt ratio (dNBR) as there was no ground truth data thus interpretation of S2 images will act as a reference dataset. Also, the RGB post-fire images shown in figure 7 & 8 is utilized. The performance is measured according to the accurate assessment of unsupervised classification. This ensures the correct identification of a land cover pattern. The training and test sets are separated using a random sampling procedure. Training sets contain two-thirds of the total data and the test set one third. Cross-validation will allow testing of the data using a full training set by means of the k-fold-cross-validation which uses repeated sampling to avoid biases from the initial sampling (Gütlein et al., 2013). The S1 is used to map burnt and unburnt areas, access the characteristics of unburnt patches and its spectral properties. This is because it contains backscatter information that is sensitive to forest structural parameter. According to different reflectance property and spatial distribution, it shows accurate and reliable information on position and extent of unburnt patches, and the vegetation or other land cover contained in the unburnt patches (Antropov et al., 2016).

Fire Zones	Number of training samples	Number of test samples
Fire 1	50	40
Fire 2	60	50
Fire 3	40	35
Fire 4	21	24
Fire 5	33	22

Table 5: Number of training and test samples for each fire zones (1-3) Victoria, Australia and (4-5) Spain respectively.

5. RESULTS

This chapter shows achieved results obtained from the implementation of our defined method in chapter 3 and its interpretation in relation to our research objectives. The method adopted was for detection and characterizing of burnt and unburnt areas resulting from severe forest fires in both Victoria, Australia and Spain captured by Sentinel 1 and Sentinel 2 datasets. The results include optical based spectral indices, S1 data analysis on polarimetric decomposition and backscatter coefficient, comparison of contextual classification of both S1 and S2 and finally texture analysis of S1 using backscatter coefficient.

5.1. Optical-based spectral indices (dNBR)

The Victoria bushfire database provided bushfire shapefiles that showed the perimeter of the fires as well as the distribution of the severity levels inside it facilitating the decision making the process faster as shown in Figure 4. Spain also provided shapefiles that showed the fire perimeter extent of the fire shown in Figure 6. In both Australian and Spain fire zones, the S1 and S2 images were acquired a month before the fire and a month after the fire. The preferred time zone of image acquisition was potential because of the need to obtain immediate changes after the fire has distinguished off to determine its severity. Also, images acquired immediately after the fire may not be appropriate as the fire could still be burning while images acquired two or three months after fire could not exhibit the damage caused by the fire as forest regeneration would have occurred fastly. Additionally, the high spatial resolution (10m) of the images, enabled analysis of fire heterogeneity exhibiting great potential in analyzing fire severity scale. This enabled the understanding of spatial variability of fire and its extent.

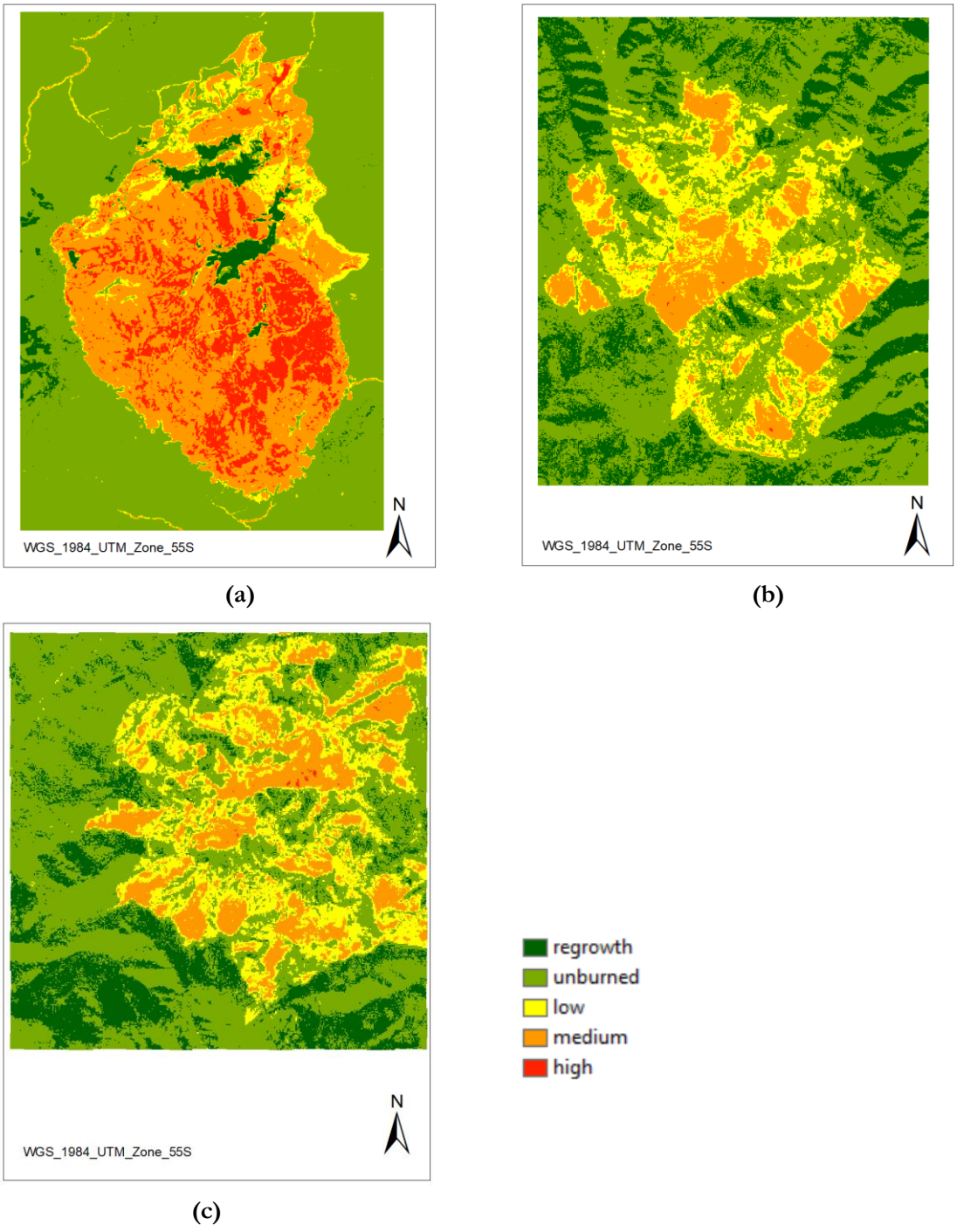

Figure 9: Difference normalized burnt ratio (dNBR) from S2 of fire zones a) fire 1, b) fire 2 and c) fire 3 respectively of Victoria, Australia. Calculated from the difference between pre- and post-fire images depicting changes covering the area of bushfires.

Fire scar differentiation using optically based indices was attainable in analyzing Australian bushfire and also Spain data. Australian bushfire burnt severity estimation was accurate for highly burned sites and medium burned sites however for low and unburned sites there was a classification error. The threshold-

based classification of dNBR was used as a methodological reference to obtain burnt severity maps for both Australia and Spain. The burnt severity using S2 data was developed by comparing pre and post-fire satellite images as this showed the capability of different spectral bands in burned area detection. The burnt ratio index was found to be sensitive to regenerating vegetation and also showed forest regeneration is slower especially in areas where the degree of burnt severity was high.

The results obtained from dNBR show that the unburned pixels depict very low optimal values that are close to zero. In regard to burned pixels, the optimal values of dNBR are considerably high reaching a mean value of 0.66. The categories used in the index were classified into five classes as shown in Table 6. A bigger proportion of the bushfire 9(a) lied between medium to highly burnt areas while for bushfire 9 (b) and (c) lied between medium to low burnt severity areas as shown in Figure 9. However, it was noted that the burnt severity levels consisted of some classification error especially between the high and medium burned areas were difficult to separate two classes and also between the unburned and low burned areas.

ΔdNBR Values	**Burn Severity**
<-0.1	Post-fire regrowth
-0.1 to 0.1	Unburned
0.1 to 0.27	Low severity burn
0.27 to 0.66	Moderate to high severity burn
>0.66	High severity burn

Table 6: dNBR burn severity category

Source: (Benson, 2005)

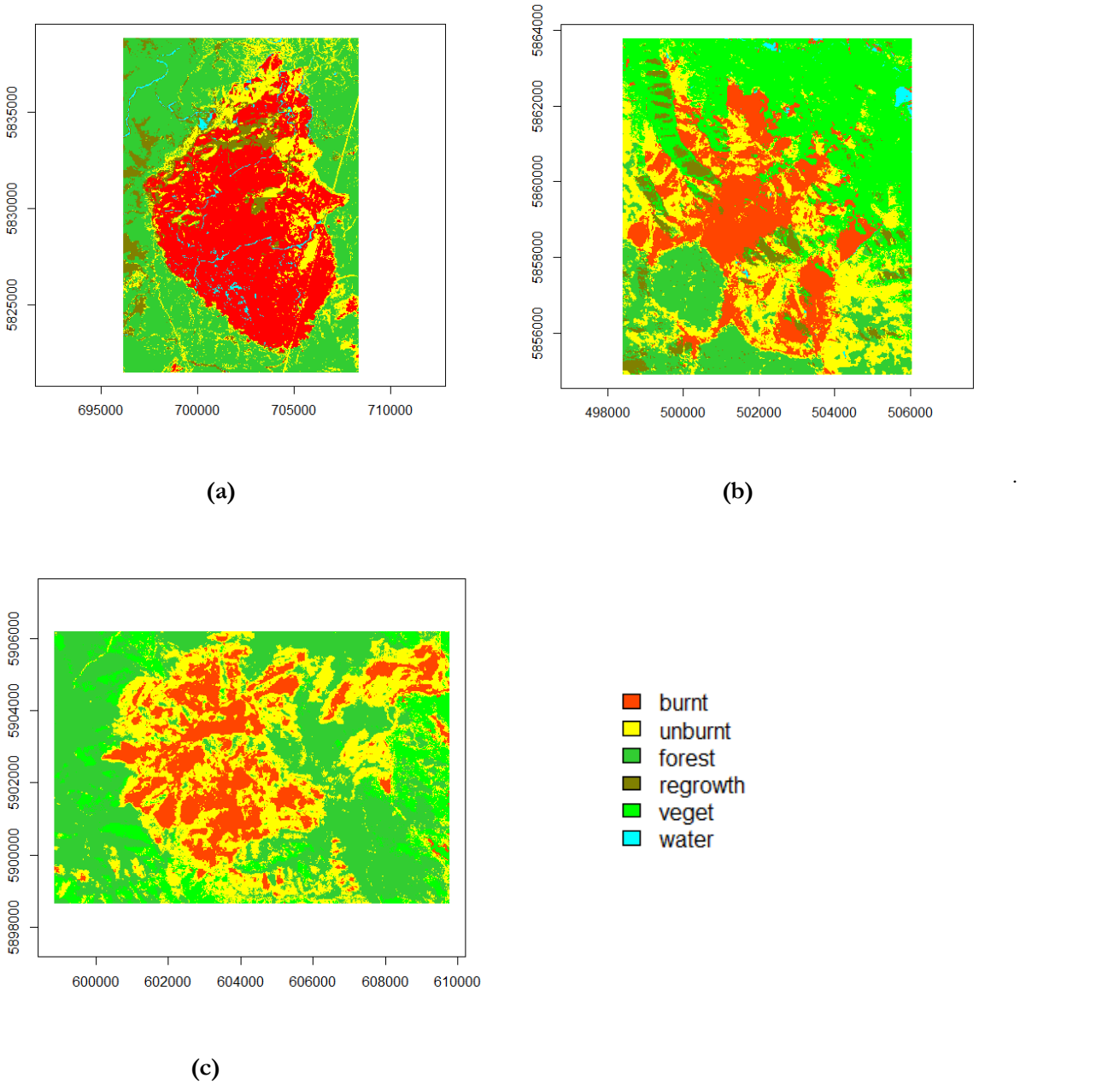

Figure 10: SVM classification of the bushfire zones from S2 of fire zones a) fire 1, b) fire 2 and c) fire 3 respectively of Victoria, Australia. The bushfires show the land cover present in the area generated from the burnt ratio index in figure 9.

The results obtained from vegetation indices aided in the identification of land cover classes present in each of the fire zones identified using the nonlinear SVM classification. The optical data were classified into classes defined in Figure 10 which were later recorded to two classes to compare the ability of optical and SAR in differentiating the burnt and unburnt patches.

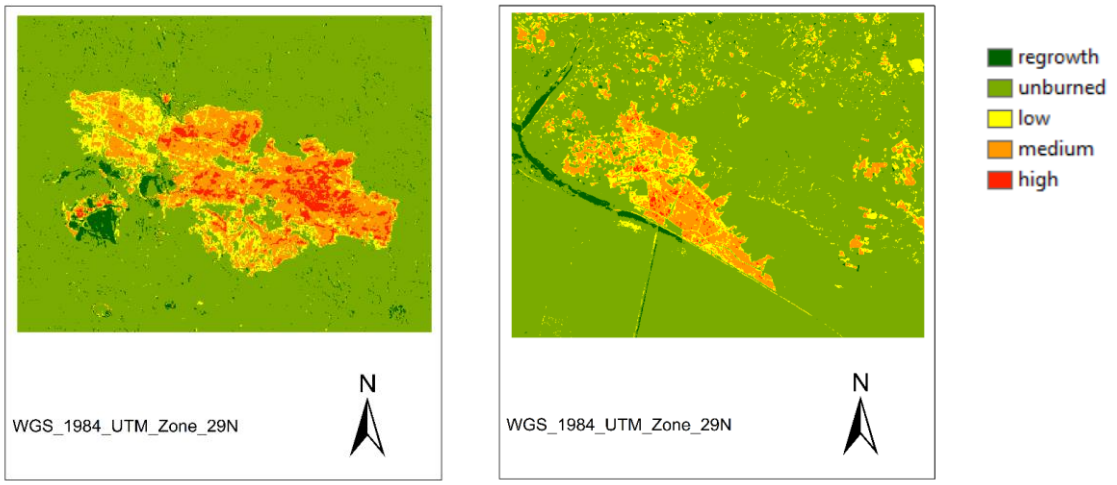

(a) **(b)**

Figure 11: Difference normalized burnt ratio (dNBR) from S2 of fire zones (a) fire 4 and (b) fire 5 respectively of Spain. Calculated from the difference between pre- and post-fire images depicting changes covering the area of bushfires.

The Spain data changes between pre- and post-fire images were also analyzed using similar burnt ratio index as shown in Table 6. The two fire zones shown in Figure 11 depicted five severity burnt levels similarly to Australian bushfire zones shown in Figure 9. It was noted that in both the Australian and Spain data there was visual contrast within the burned zones indicating spatial patterns and variation of effects. The initial assessment of dNBR values of burned areas tended to portray high values as compared to unburned areas that showed very low values in Spain data. Good contrast was seen between the burnt and unburnt areas, however, there existed a high degree of complexity in the separation of intermediary severity level. In fire zone 11 (a) most burns occurred at high-to-medium severe burn areas while in fire zone 11 (b) most burns occurred between medium-to-low severity. Also, there was high misclassification between low severity levels and unburnt areas in both fire zones 11 (a) and (b) similar result was identified also in Australian bushfire.

5.2. Sentinel 1 (S1) data analysis

The polarimetric features used for classification were real and imaginary parts of $S_{VH}S_{VV}$. Two classes mainly identified for analysis were burnt and unburnt areas.

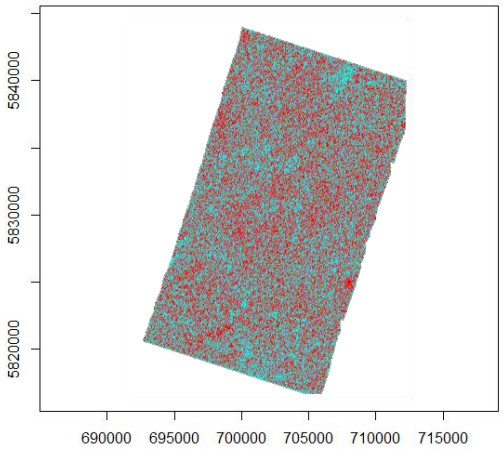

(a)

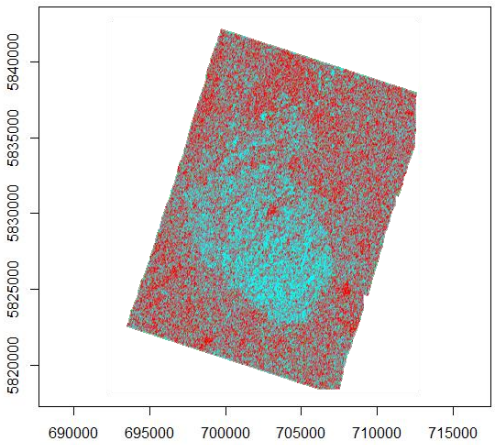

(b)

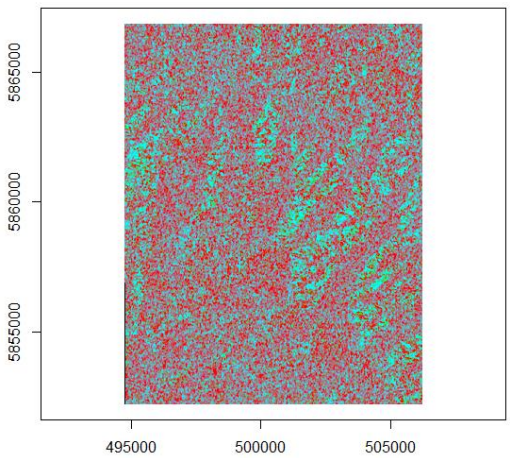

(c)

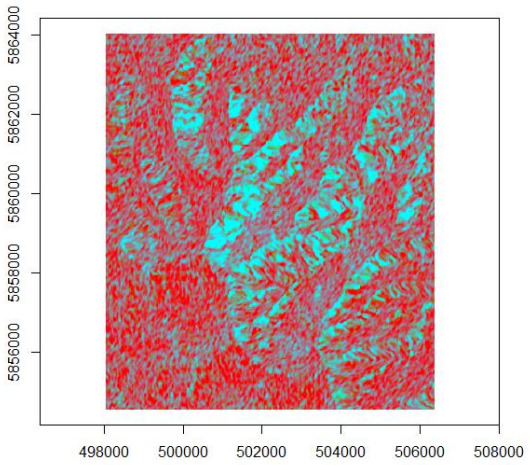

(d)

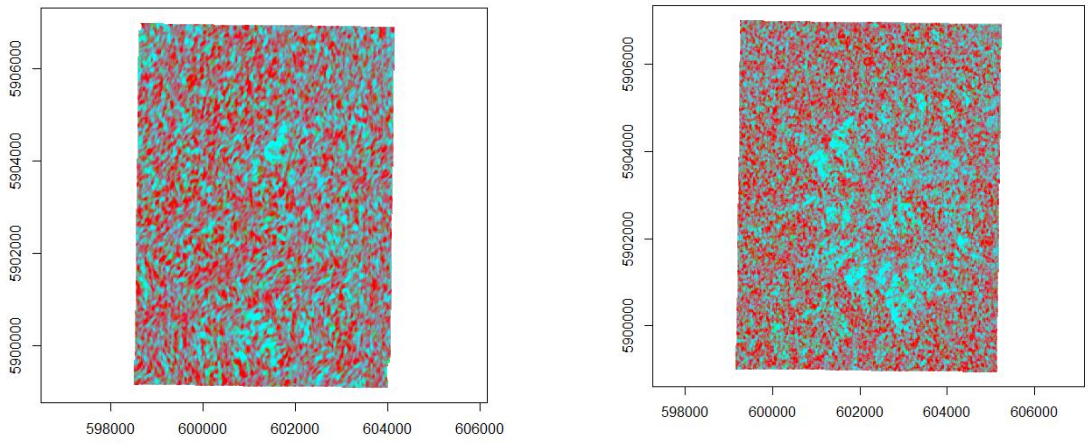

(e) **(f)**

Figure 12: Comparison of H-Alpha target decomposition covering the area of bushfires in Victoria, Australia from figure 4 (a-c) using S1 pre-images as (a, c, e) post-fire images (b, d, f) respectively. The red color represents entropy and blue color represents alpha.

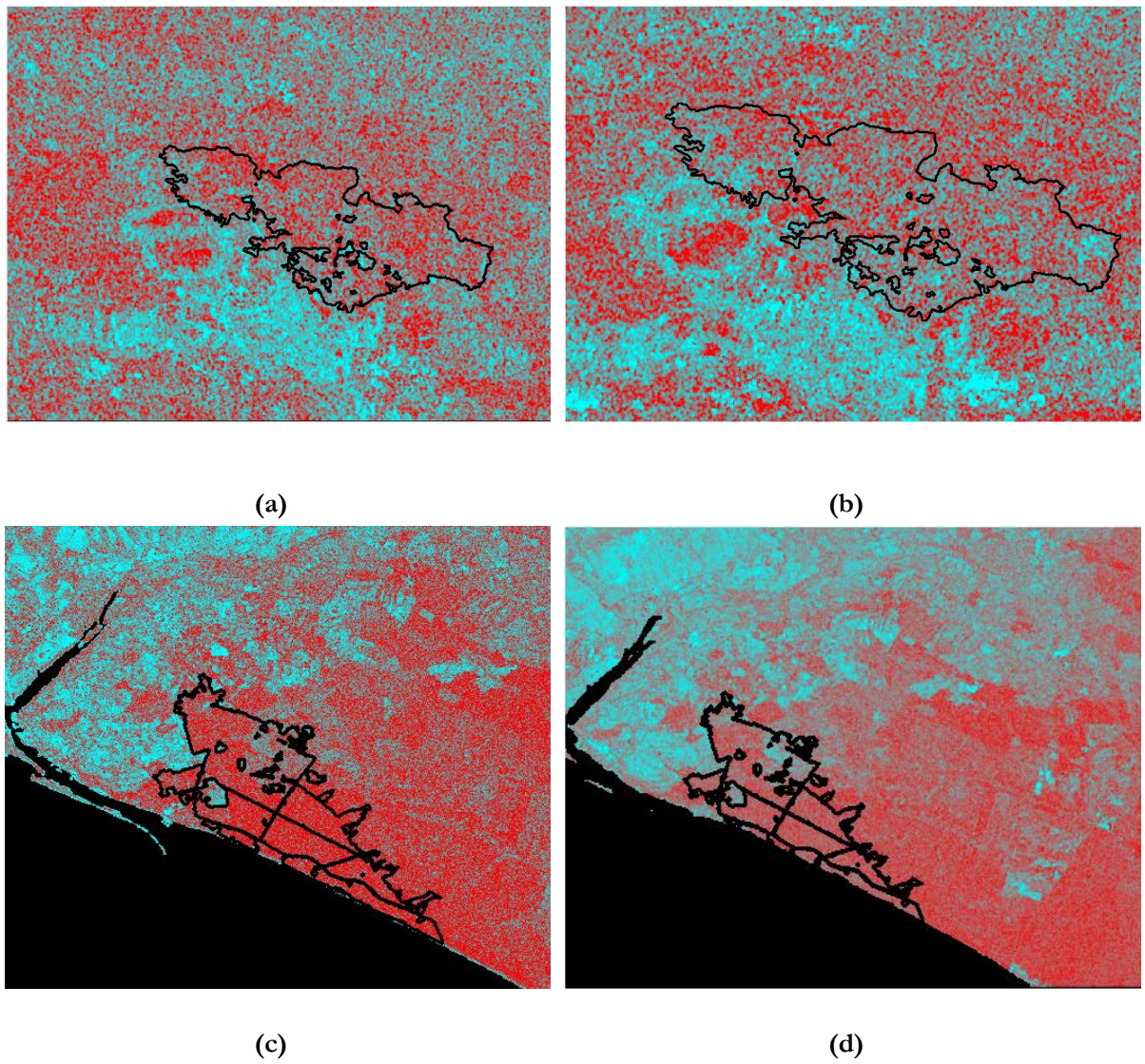

Figure 13: Comparison of H-Alpha target decomposition covering the area of bushfires in Spain from figure 6 (a and b) using S1 pre-images as (a, c) post-fire images (b, d) respectively. The red color represents entropy and blue color represents alpha. The black polygon indicating the fire extent boundary.

To visually ascertain burnt and unburnt patches in S1 the use of backscatter intensity for Victoria, Australian bushfire in fire 1 was possible but for fire 2 and fire 3 was not that distinguishable. A similar scenario was seen when discriminating burnt and unburnt patches also in Spain for fire 4 and fire 5. Thus, we settled to use RGB color composite H-Alpha decomposed images for all the fire zones. This resulted in some form of pattern comparing pre and post-fire images showing its sensitivity to forest structure changes. Red was assigned to entropy, green to anisotropy and blue to alpha values as shown in Figure 12 and Figure 13 representing Victoria, Australia, and Spain respectively.

As burnt severity increased the entropy and alpha values decreased this was due to decreased scattering randomness and increase in surface dominated scattering mechanism. The integration of backscatter and

polarimetric decomposition were sensitive to distinguishing the burnt and unburnt patches. The C-band S1 co-polarized backscatter (VV) increased with burnt severity while the cross-polarized (VH) backscatter decreased with burn severity. Low sensitivity to forest regrowth was observed for the C-band backscatter with most of it classified as burnt areas. This is because of burnt leaves, branches and tree trunks at some areas leaving bare soil area. Most of the unburnt forest and low severity were characterized by volumetric scattering (medium to high entropy and dominant dipole scattering) as foreshown in Figure 2.

A major issue in the use of S1 image was the influence of topography and local incidence angle on the backscatter coefficient during mapping of burned and unburned areas.

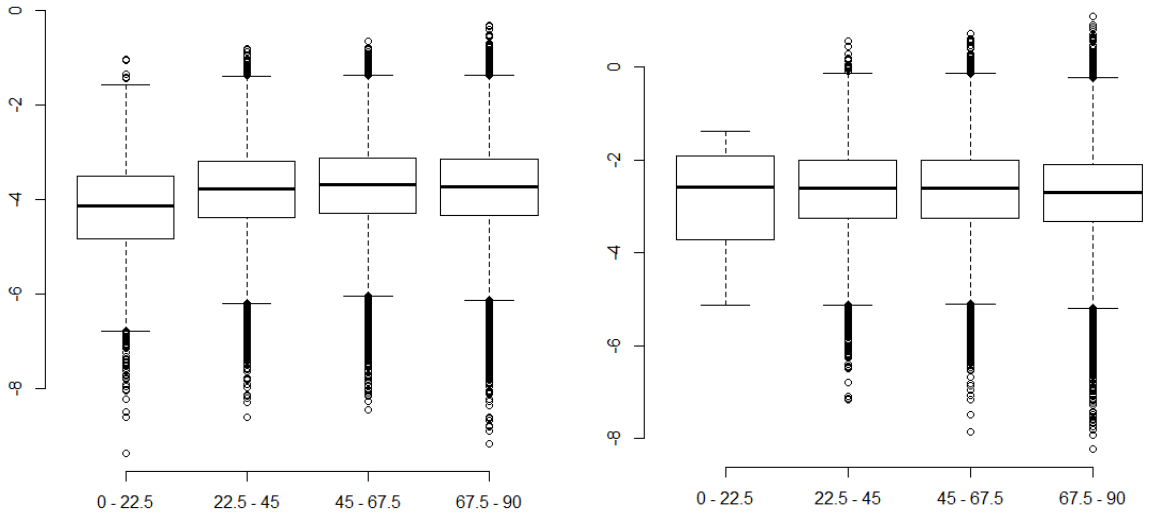

(a) **(b)**

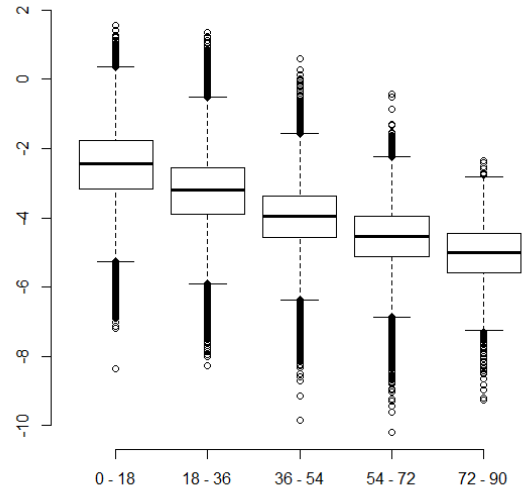

(c)

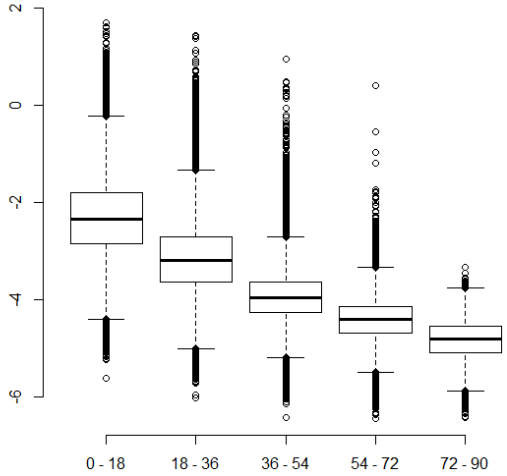

(d)

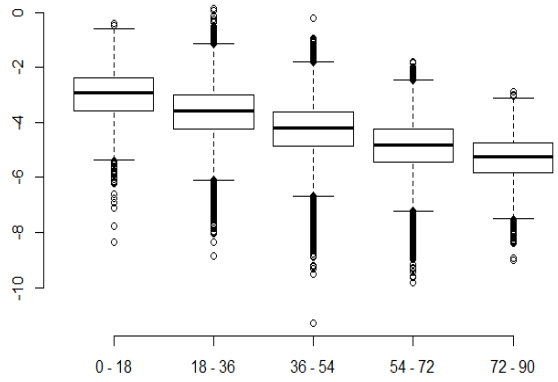

(e)

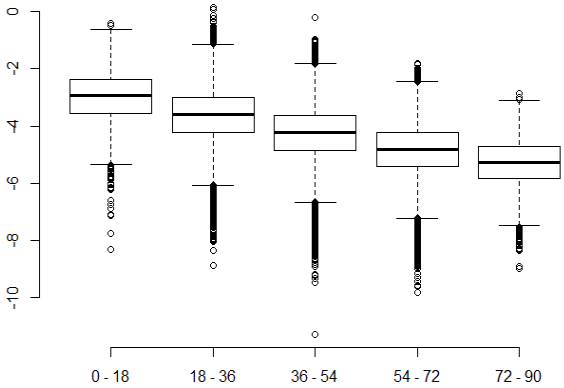

(f)

Figure 14: Boxplots showing backscatter intensity of VH coefficient projected against local incidence angle of bushfires in Victoria, Australia comparing images before and after the fire respectively.

The average backscatter of cross-polarized (VH) intensity was plotted against marginal interval of local incidence angles as shown in Figure 14. This is because VH intensity covers volume scatter thus is sensitive to the changes in vegetation. The dividing of incidence angle into five or four intervals was to enable us to understand the performance of backscatter analysis under different incidence angle margin. The output results of the boxplots foreshow at lower incidence angle there is better discrimination of burnt areas as one compares pre- and post-fire results. It is also noted in areas that remained unburnt the size of boxplots remained the same in both images. The backscatter values decreased slightly as one compares the pre- and post-fire plots however they all ranged -2 to -6 dB. In fire 2 and 3, the areas were

terrain thus steep slopes were experienced and incidence angle ranged from (0°-90°) shown in Figure 14 (c) and (e). Areas with lower incidence angles (0°-30°) and facing the radar sensor as shown in Figure 14 (d) and (f) of post-fire images shows a decrease in VH intensity and slight changes in boxplot size. This resulted from a brighter return of radar signal for areas with smaller incidence angles enabling discrimination of burnt and unburnt areas easier. However, due to the steepness of the areas shadows were experienced which were darker and portrayed similarly with areas facing away from the sensor which was also darker. Areas facing away from the sensor or with large incidence angle ranged (45°-90°) showed a high number of outliers this could be related to the presence of noise being greater in that range. This could have hindered discrimination of defined classes and resulting in high commission and omission errors. Lastly as one compares the ranges of smaller incidence angle in flat areas and steep areas we could see the flat areas ranges were high (0°-30°) as compared to steep areas (0°-18°) this showed clarity into why for flat areas the discrimination of burnt areas was easier as compared to steep areas. This was because of the higher return of backscatter signal to the sensor which increased its sensitivity to vegetation changes after the fire.

5.3. Burnt scar classification

Fire zone(MRF)	Lambda	Initial temperature	Updating factor
Fire 1	0.8	3.0	0.9
Fire 2	0.8	4.0	0.9
Fire 3	0.8	4.0	0.9
Fire 4	0.8	3.0	0.9
Fire 5	0.8	4.0	0.9

Table 7: Parameter tuning values obtained for MRF classifier for fire (a) fire 1 (b) fire 2 and (c) fire 3 bushfire zones of Victoria, Australia and (d) fire 4 and (b) fire 5 of Spain respectively.

After applying contextual classification and tuning the parameters of MRF classifiers i.e. the lambda, initial temperature, and updating factor for reducing the temperature for each fire zone is shown in Table 7. This was done through trial using a small subset of an image and different random values were tested and verifiedd according to their accuracy assessment the optimal one was selected.

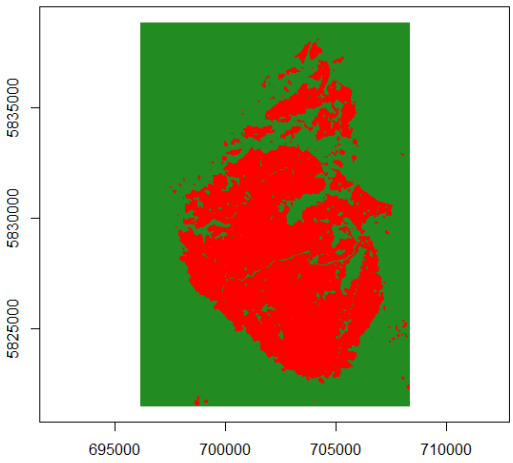
5835000
5830000
5825000
695000
700000
705000
710000

(a)

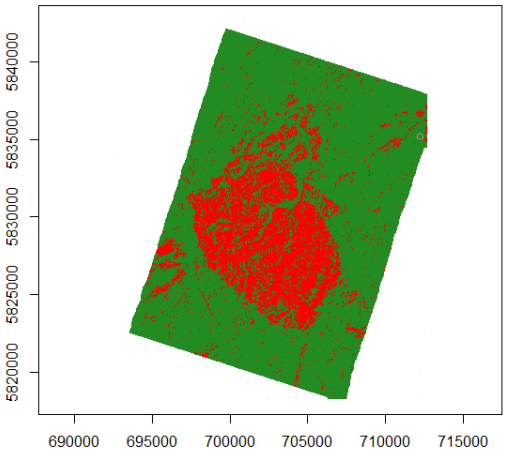
5840000
5835000
5830000
5825000
5820000
690000
695000
700000
705000
710000
715000

(b)

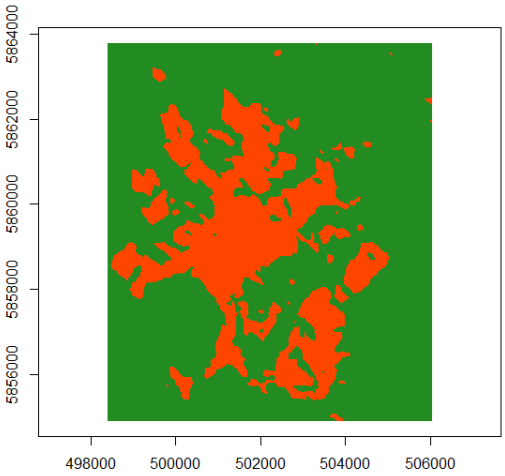
5864000
5862000
5860000
5858000
5856000
498000
500000
502000
504000
506000

(c)

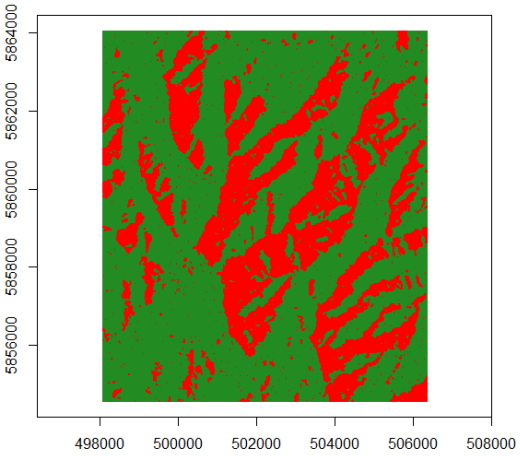
5864000
5862000
5860000
5858000
5856000
498000
500000
502000
504000
506000
508000

(d)

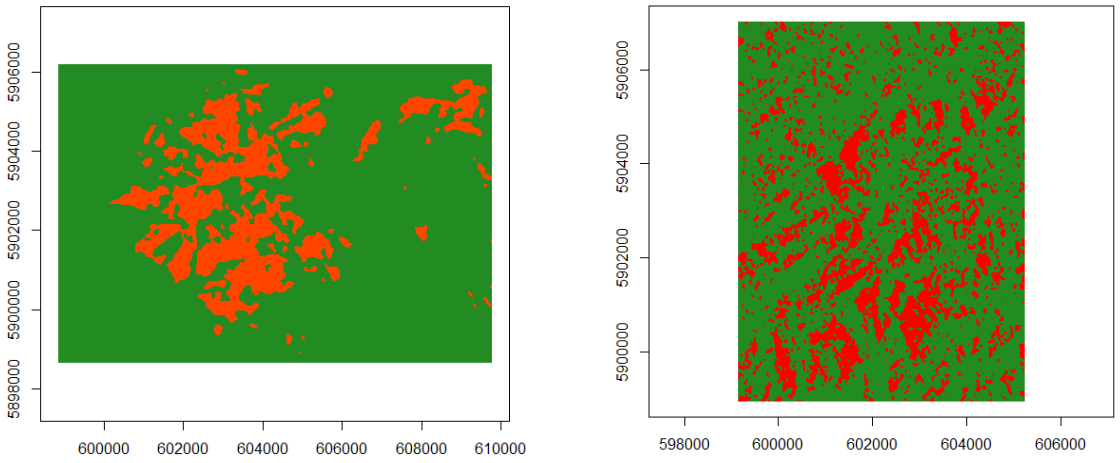

(e) **(f)**

Figure 15: Comparison of classification result of optical(S2) and radar(S1) respectively covering the area of bushfires in Victoria, Australia from figure 4 (a-c). Optical(S2) as (a,c,e) and radar(S1) (b,d,f) respectively. Red color representing burnt areas and green representing unburnt areas.

It was difficult to separate the burnt severity levels using the C-band S1 this is because of the transitional nature of the fire. All the burn severity levels largely overlap each other. However, we combined the backscatter intensity bands (VV and VH) together with H- alpha target decomposition bands (entropy, anisotropy, and alpha) and reclassified to two classes burnt and unburnt. This is shown in Figure 15 for Australian fire. In fire 2 & 3 had steep slopes which resulted in shadows making it difficult to determine whether the shadowed areas were burnt or unburnt areas this eventually affected the classification results. In Figure 15 (b),(d) and (f) S1 showed a stronger return of burnt and unburnt patches compared to optical dataset Figure 14 (a), (c) and (e) due to the high influence of geometry acquisition and captures terrain. S2 utilizes the spectral sensitivity of defined classes which take the measure of only the vegetation fill and crown closure while S1 utilizes the polarimetric sensitivity of removal of crown leaves, branches.

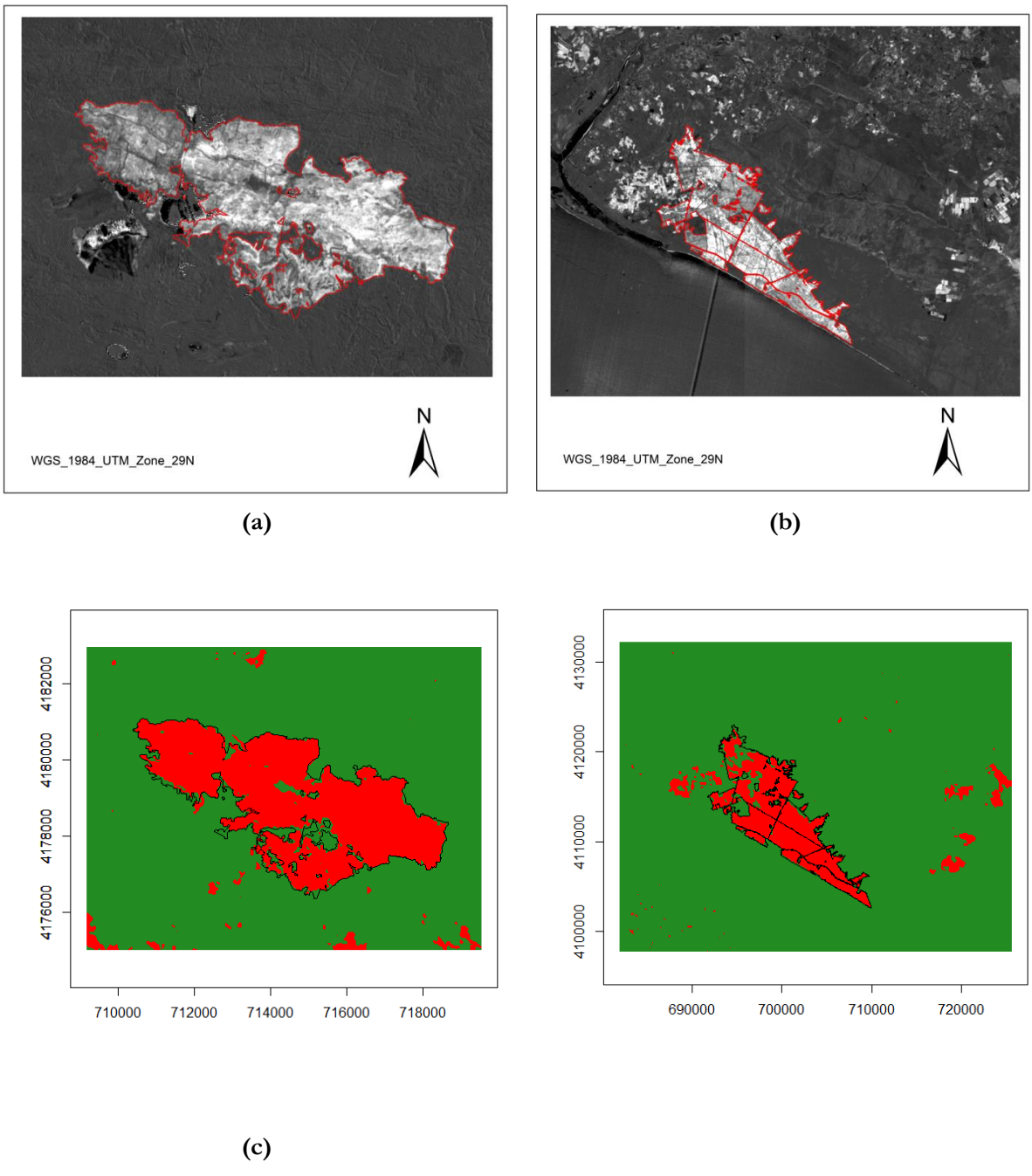

Figure 16: The dNBR showing grayscale indicating the magnitude of change in NBR, S2 on the upper side (a) and (b) overlaid with red polygon showing fire extent with brighter pixels within it indicating burnt areas and darker areas indicating unburnt areas. The lower side (c) and (d) is SVM_MRF classified image of the same area in Spain with a red color representing burnt areas and green representing unburnt areas.

However, it was also noted for the Spain fire zones 4 & 5 the optical dataset (S2) showed a stronger sensitivity to changes resulting after the fire compared to radar (S1) data. This is proved by the visual assessment of the H-alpha decomposition of S1 in Figure 13. The sensitivity to changes after the fire was not as severe in both fires as compared to Figure 14 as a similar approach was applied in both study areas.

The kappa coefficient also in table 8 (d) and (e) for both S1 and S2 differed greatly as compared to table 8 (a), (b) and (c) for Victoria, Australia as S2 had a higher kappa coefficient while S1 indicated extremely low value. Nevertheless, S2 classification resulted in a similar match with the fire extent of the polygon showing the spectral sensitivity of pixels to changes after the fire. Similarly, the result was matched to the burnt index as shown in Figure 16. There was misclassification of burnt pixels outside the defined fire extent as some the unburnt areas that appeared brighter in the dNBR Figure 16 (a) and (b) and were outside the boundary of the burnt area was classified as burnt areas as shown in Figure 16 (c) and (d). This resulted in a false high kappa coefficient shown in table 8 fire 4 & 5 for S2.

Fire	Sentinel 2_SVM	Sentinel 1_SVM	Sentinel 1_SVM_MRF
Fire 1	0.95	0.70	0.82
Fire 2	0.93	0.78	0.85
Fire 3	0.84	0.77	0.88
Fire 4	0.94	0.05	0.04
Fire 5	0.95	0.03	0.02

Table 8: Classification results for kappa coefficient for optical (S2) and radar (S1) for covering fire zones 1-3 Victoria, Australia, and 4-5 Spain respectively.

Fire	Kappa Sentinel 2	Producer accuracy	User accuracy	Number of training samples	Number of test samples
Fire 1	0.95	Burnt=84.35 % Unburnt=82.26%	Burnt=92.43% Unburnt=84.65%	50	40
Fire 2	0.93	Burnt=86.30% Unburnt=77.81%	Burnt=90.35% Unburnt=75.61%	60	50
Fire 3	0.92	Burnt=85.40% Unburnt=80.70%	Burnt=86.30% Unburnt=78.69%	34	40
Fire 4	0.94	Burnt=97.43 % Unburnt=94.54%	Burnt=94.56% Unburnt=95.78%	21	24
Fire 5	0.95	Burnt=88.64% Unburnt=91.35%	Burnt=95.65% Unburnt=95.67%	33	22

Table 9: Accuracy assessment results based on kappa statistics from SVM_MRF classification of S2 covering fire zones 1-3 Victoria, Australia, and 4-5 Spain respectively.

Fire	Kappa Sentinel1 (S1)	Producer accuracy	User accuracy	Number of training samples	Number of test samples
Fire 1	82%	Burnt=80.69% Unburnt=78.65%	Burnt=85.65% Unburnt=80.25%	50	42
Fire 2	85%	Burnt=88.9%3 Unburnt=78.66%	Burnt=87.43% Unburnt=82.11%	60	52
Fire 3	84%	Burnt=86.40% Unburnt=79.65%	Burnt=83.40% Unburnt=80.35%	34	31

Table 10: Accuracy assessment results based on kappa statistics from SVM_MRF classification of S1 covering fire 1-3 in Victoria, Australia.

To assess the certainty of our results in the separation of burnt and unburnt areas in both optical and SAR we used kappa coefficient and f-score measurement. Both the producer's accuracy and users accuracy were taken into consideration as shown in Table 9 and Table 10. The remote sensing indices that accessed burned versus unburned areas produced better overall accuracy, higher user and producer accuracy results as shown in table 8 through SVM_MRF classification of S1 and S2. This showed the capability of both the electromagnetic spectrum and SAR polarimetry in corresponding to changes in vegetation structure after a fire. Similarly, we obtained quite a good classification percentage accuracy and separation of burnt and unburnt areas within fire perimeter zones as shown by the use of precision and recall and f-score in Spain data assessment in Table 11.

Fire zone	SVM(%)	SVM_MRF(%)	Precision(%)	recall(%)	F-score(%)
Fire 4	91.60	94.20	0.94	0.91	0.92
Fire 5	90.20	93.60	0.92	0.89	0.90

Table 11: Accuracy assessment results based on F-score measurements from SVM_MRF classification of S2 covering fire 4& 5 of Spain.

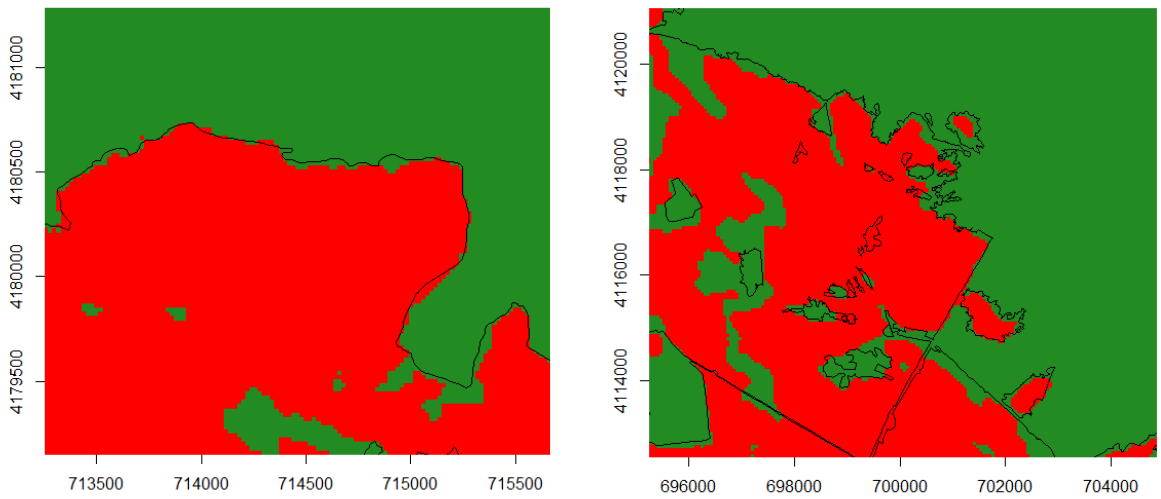

(a) **(b)**

Figure 17: Boundary classification from SVM_MRF output overlaid with fire perimeter zones in black representing Spain fire (a) fire 4 and (b) fire 5 respectively. Red signifies burnt area and green the unburnt area.

It was seen in particular after classification with SVM_MRF the vector shapefile that represents fire perimeter zone was not exactly fitting the boundary edges of the burnt zones depicted in classification results as shown in Figure 17 (a) and (b). This could have been attributed to the use of contextual classifiers SVM_MRF which cope up with the problem of intraclass spectral variation and spatial variability along the boundaries. Another problem could be related to the timing of digitization of vector fire perimeter which might have occurred at early stages of the while our spectral classification analysis was related to the post-fire analysis of the image. This may lead disparity of fire perimeter shapefile with the actual ground timing of fire timeout as shown in Figure 17. A similar result was noted in the polygons obtained from Victoria database as they reflected the start of the fire but did not execute the whole fire zone. Thus it was a limiting factor in determining whether a similar problem was experienced in Australia.

5.4. Texture Analysis

The result of texture analysis utilized backscatter intensity (VH to determine GLCM statistical measure in the retrieval of burnt and unburnt areas. The entropy, homogeneity and contrast statistics showed variation among the burnt and unburnt classes in Victoria, Australia bushfire shown in Figures 16-18.

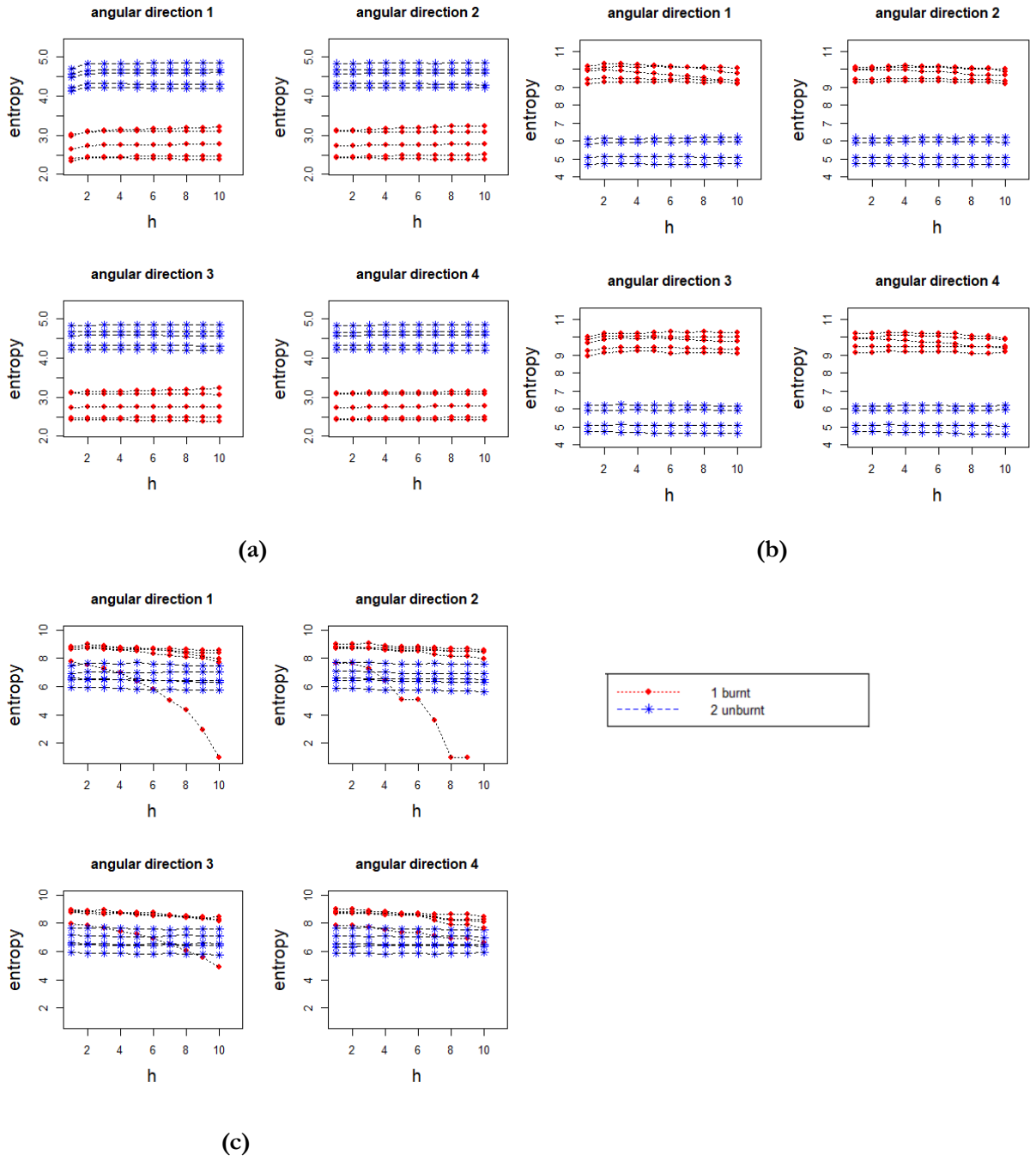

Figure 18: GLCM textural analysis showing the measure of entropy values using S1 VH backscatter intensity covering bushfire a) fire 1, b) fire 2 and c) fire 3 respectively in Victoria, Australia. Red color representing burnt areas and blue color representing unburnt areas.

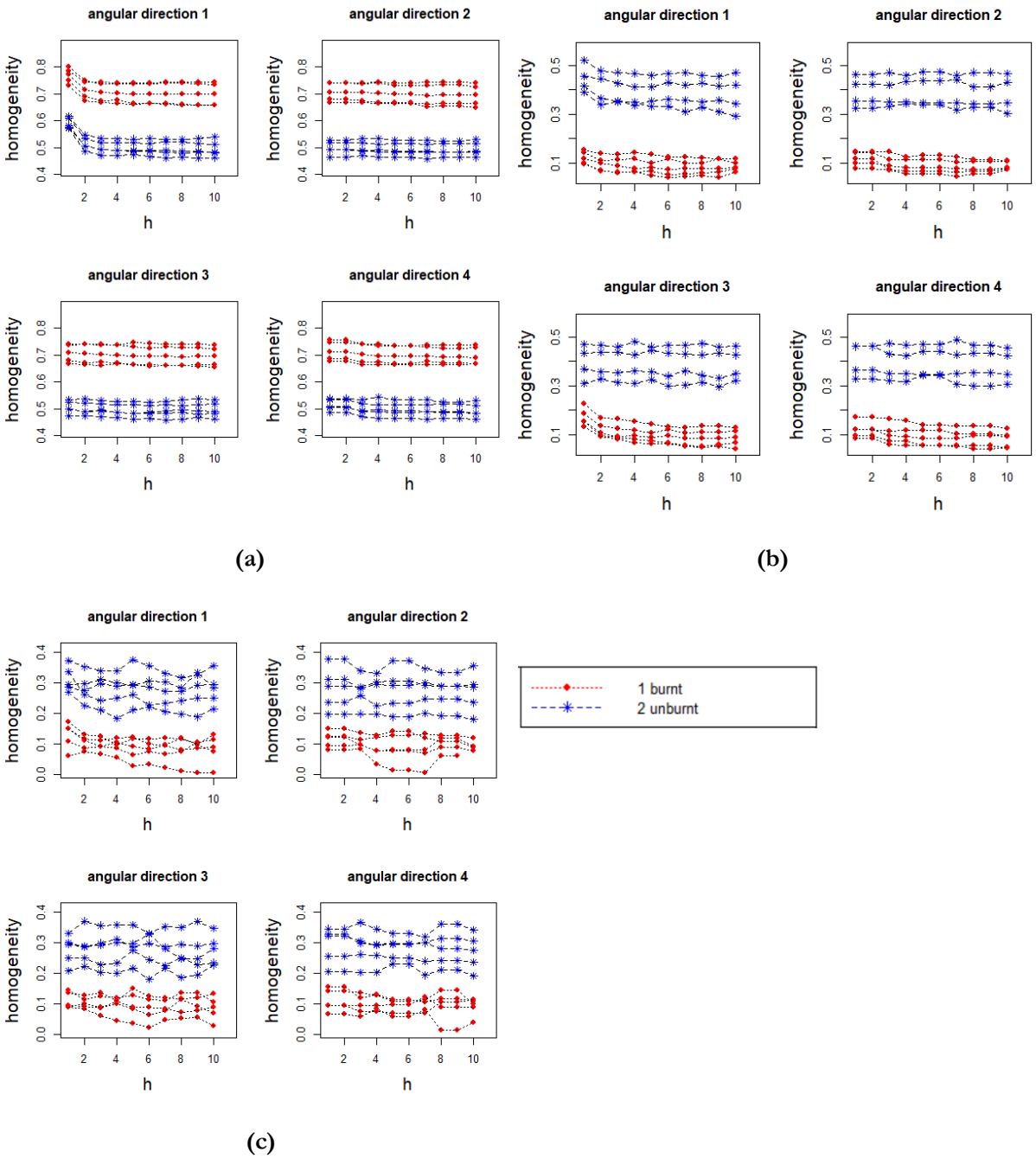

Figure 19: GLCM textural analysis showing the measure of homogeneity values S1 VH backscatter intensity covering bushfire a) fire 1, b) fire 2 and c) fire 3 respectively in Victoria, Australia. Red color representing burnt areas and blue color representing unburnt areas.

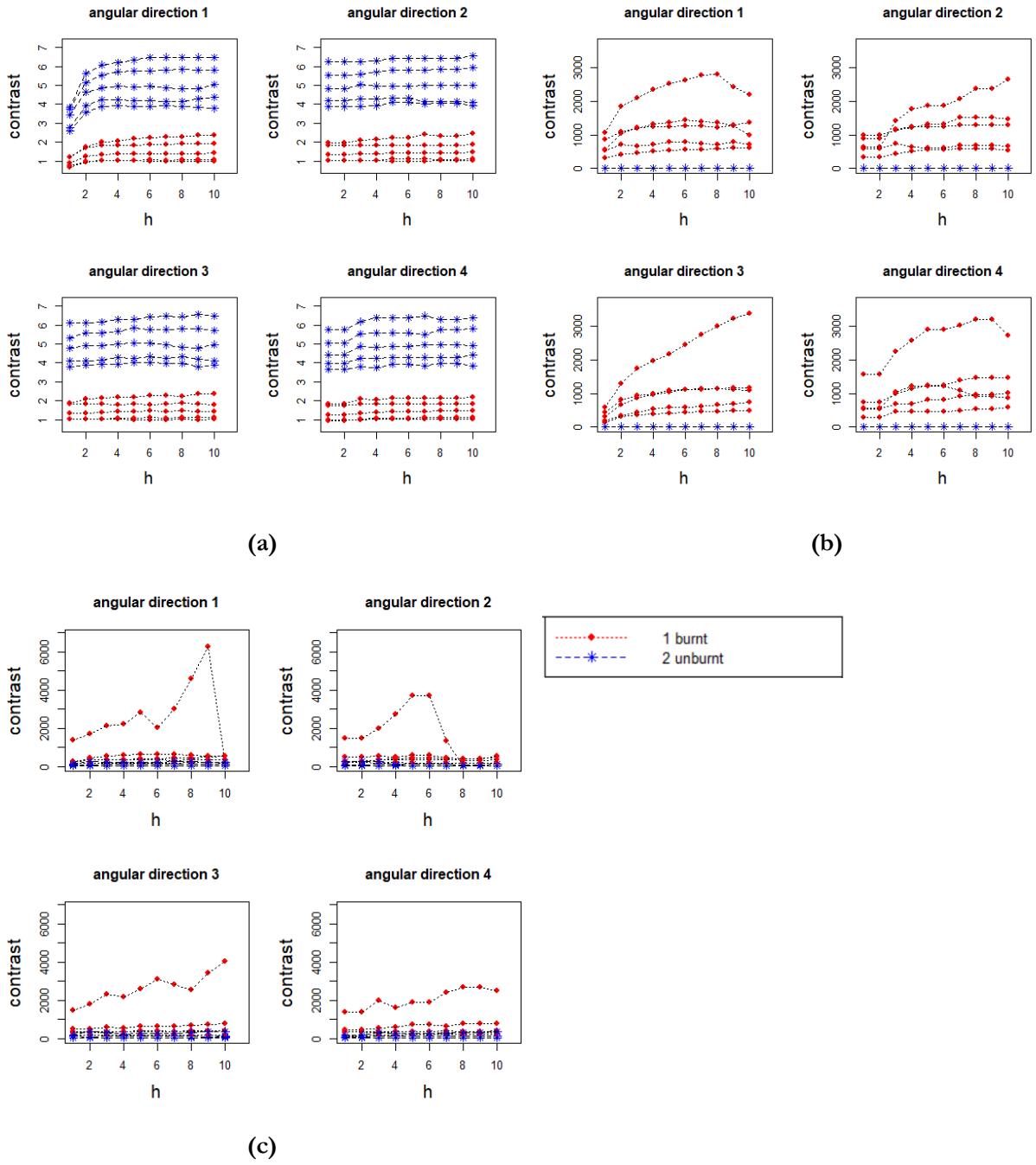

Figure 20: GLCM textural analysis showing the measure of contast values S1 VH backscatter intensity covering bushfire a) fire 1, b) fire 2 and c) fire 3 respectively in Victoria, Australia. Red color representing burnt areas and blue color representing unburnt areas.

The entropy results showed a measure of homogeneity and good visual differences between burnt and unburnt areas as shown in Figure 18. However, the range between the burnt and unburnt areas was minimal the pattern remained the same in all directions this shows that it is not affected by orientation variation rather as one changed the quantization levels the entropy increased. Similar results were depicted in all the fire 2 & 3. For steep terrain areas such as fire area 2 & 3 represented in Figure 18 (b) and (c) respectively the entropy values showed higher values compared to flat areas fire 1 Figure 18 (a). The order

changes also and the steep areas proved difficult to separate burnt and unburnt zones especially for fire 3 Figure 18 (c) as the backscatter intensity was highly affected by the incidence angle and presence of shadows. The homogeneity measure in Figure 19 (a) depicted higher values for burnt areas compared to unburnt areas. In Figure 19 (b) and (c), the unburnt areas depicted higher values while the burnt areas very low values that were varying. This shows much of the terrain area remained unburnt however due to the effect of incidence angle on steep areas and affecting backscatter intensity we cannot ascertain the results of both Figure 19 (b) and (c). For Figure 19 (c) the marginal difference between burnt and unburnt areas was very minimal depicting closeness in texture for both of two classes.

Contrast measures the degree of smoothness or roughness of the area. In Figure 20 (a) because the defined area was a flat area the contrast values were low (1-7) as compared to Figure 20 (b) and (c) whose values range (0-6000) and the area was terrain. This shows in flat areas homogeneity was high as compared to terrain areas. It was also noted in Figure 19 (a) the separation of burnt areas from unburnt areas had a marginal difference that could be visually seen while for Figure 20 (b) and (c) the marginal difference of separation between the burnt and unburnt areas was extremely minimal. The contrast values increased as the quantization levels increased. The large contrast reflects large intensity differences in GLCM analysis of defined classes.

In general, it was noted that homogeneity and entropy were least affected by the directional change as compared to the contrast measure. Also as one increased the quantization levels the homogeneity values increased leading to a higher marginal separation between the burnt and unburnt areas. In all the three bushfire zones they were least influenced by orientation parameter except for Figure 19 (c) which kept changing with directional change. Nevertheless, they all showed good results in separation of burnt and unburnt areas in both flat and steep areas of Victoria, Australia.

5.5. Summary of results

From our results, we can conclude that the use of S1 SAR sensor and S2 in the classification of burnt and unburnt areas was successful as it yielded good accuracy results that could relate to the fire perimeter shapefiles obtained from their respective database of Spain and Victoria, Australia. From our results, we could see remote sensing as an essential tool in wide coverage of wildfires and through the vegetation index dNBR we could relate the magnitude of change that has occurred after the fire in both areas. The vegetation index was a reference dataset in obtaining our training sets for classification of both S1 and S2. Through the classifier, we could see differences in spectral and polarimetric sensitivity of burnt and unburnt areas. This is especially in areas that were considered as regrowth in the dNBR index were unburnt in S2 classifier while in S1 they were burnt. Also through the analysis of polarimetric entropy and alpha decomposition, we could see the ability of S1 in showing changes in forest structure which is a key thing in the use of SAR. However, the use of backscatter intensity was limited to local incidence angle and steep slopes orientation thus integration of polarimetric decomposition enabled us to quantify the changes directly occurring after a bushfire. Also, the use of SAR was only successful in Victoria, Australia but in

Spain, it could not detect changes after the fire using backscatter intensity and a very minimal change in use of H- alpha decomposition. This was directly foreseen to be due to the intensity of the fire that was not severe to have caused changes in forest structure. Nevertheless, in the optical dataset, it gave similar results in both areas. Also, the use of GLCM to measure spatial variation in the texture of burnt and unburnt scars was successful as it showed discrimination, especially on steep slopes. The textural variation was highly influenced by parameter changes in quantization levels, lag distance and window size as they changed with different textural measures. Lastly, from the accuracy results we could note even though our classification accuracies were high for both SAR and optical and even the producer and user accuracy results it was not sufficient to ascertain our results. This is because of S1 classification in steep areas affected by large incidence angle there was no return of radar signal thus difficult to ascertain whether the areas were burnt or unburnt directing influencing overall accuracy. Also in S2 due to the spectral similarity of burnt pixels with unburnt pixels outside fire perimeter led to classification errors. Nevertheless, the results obtained from identification of burnt and unburnt scars using both SAR sensor and optical was successful and could relate to both datasets in our study areas.

6. DISCUSSION

This chapter further gives a detailed description of the understanding of our results. It mainly identifies what was well achieved at the end of our research, what was not well accomplished and what were the limitations experienced. The opened gateways the research avails in line with future studies together with the likely threats that are to be expected as research furthers. Lastly is the benefits the research brings onboard and the stakeholders that would also be directly or indirectly related to it.

6.1. Evaluation and discussion of results

This study analysed the use of satellite SAR sensor and optical data in the detection and classification of burnt and unburnt patches after a forest fire in Victoria, Australia, and Spain. We used satellite remote sensing images S1 and S2 to distinguish the two defined classes and also a contextual classifier in looking at the ability of spectral and backscatter intensity in separability of the two defined classes. We have made use of data available in the Victoria fire database and also Spain dataset. From these datasets, we were able to use the fire polygons as a guiding factor in our classification results showing us the extent of fire perimeter zones in relation to the spectral and polarimetric pattern of burnt areas.

In looking into the diverse use of forestry and forest resources management further studies could be done on advancement in sensor technology and also the use of drones. The drones carry a variety of sensing instruments including visible light, near-infrared (NIR), shortwave infrared (SWIR) and radar sensors could be helpful in terms of area coverage, time and also efficiency (Berni et al., 2009; Ojala et al., 2011). The benefits of a drone being flexible control of its spatial and temporal resolution, high intensity of data collection and low operating costs with less hazard to forest fire crews. This would be a key aspect when tracking forest wildfires, especially in support of near real-time fire control strategies at the infancy stages before it causes a hazard. A series of the experiment has been done in Spain and Portugal wildfires and allowed coverage of large areas and real-time view of fire and control strategy (Merino et al., 2012; Martínez de Dio, 2011). Numerous remote sensing studies have also been applied especially in assessing how severe wildfire is based on ecological changes in vegetation indices from spectral analysis measured by satellite sensors. Also, more focus could be enhanced on relating ecological measures to fire-induced physical changes on the land surface and how it influences forest regeneration fastly (Remmel & Perera, 2001; Allison et al., 2005; Benson, 2005; Hughes et al., 2015).

The resilience and impact of forest fires have been major focus worldly in recent past and is currently ongoing. This is in relation to joint research center (JRC) which supports services that are related to protection of forests against fires in European Union (EU) countries and also provide updated and reliable information on wildfires in Europe (JRC, 2014). Their reports confirm a trend in longer and intense wildfire seasons across Europe and neighboring regions. The 2016 report analyzed the frequent bushfires occurring together with burnt areas using best available data at the time mostly optical dataset in analyzing the impact of the fire and provided it to policymakers across the EU. In addition, the JRC reports aim at providing

important information like fire causes, impacts, dangers, responsive and prevention measures. However, this has been coupled by a number of challenges including the presence of smoke particles, cloud cover, and weather that hinder fire analysis. Additionally, satellites being used were missing in some areas, the time lag between acquisition of some satellites and also the image resolutions was inadequate and inefficient for detection of fires over large areas. There exists a gap in most JRC reports in analysing the influence of forest structure and its relation in the rate of fire spread and that has not been adequately researched upon. Therefore our research method and use of satellite SAR sensor with optical data would be of great benefit especially to the JRC. This is because it would foreshow the importance of radar in the analysis of forest structure and how it will minimize most of the challenges experienced beforehand taking consideration the weather independence, spatial and temporal resolution and revisit period that is key in monitoring changes in the forest over time.

In relation to the aim of our research as mentioned in the introduction is to characterize the difference in burnt and unburnt scars using remote sensing methods comparing S1 and S2. Firstly was to explore the extent of severity of the fire. This was done by use of vegetation indices dNBR in S2 resulted in the identification of burnt and unburnt patches in both Victoria, Australia, and Spain. The comparison of pre- and post-fire reflectance values showed spectral similarity as there was a decrease in the post-fire values indicating complete or partial loss of vegetation based on fire intensity section 5.1. The differences at burnt severity maps displayed in section 5.1 particularly at intermediate severity levels point out classification errors that eventually affect the overall accuracy result. The spectral confusion has been commonly reported by various authors (Sunderman & Weisberg, 2011; Stambaugh et al., 2015). These changes were highly influenced by the timely acquisition of the images as this is a key component in relation to the start of fire dates and sampling of the vegetation changes. More comparison should also be done on spectral indices after a wildfire in relation to fire behavior for risk assessment of fire-prone areas and implementation of prevention and risk assessment strategy (Sannier et al., 2002).

Secondly was to analyze the use of satellite SAR imagery in polarimetric aspect and backscatter intensity. This resulted in discrimination of burnt areas from the unburnt areas and provided distinct information that was related more to changes in the forest structure. The changes were mainly associated with backscatter intensity of the fire resulting in changes in vegetation structure and also topography similar results obtained from (Siegert & Ruecker, 2000). However, the influence of local incidence angle and topography was of greater effect resulting in shadows. Thus the backscatter could not penetrate in some areas making it difficult to discriminate whether the areas were burnt or unburnt lead to commission and omission errors (Sun & Ranson, 2015). We did not further expound on whether the limitation experienced in using satellite SAR could be minimized by integration of SAR and optical data using a similar method defined in method section 3 . Finally, the use of S1 was only sensitive to bushfires in Victoria, Australia but not in Spain this was based on an assumption on fire intensity did not cause much changes in Spain forest structure. However, an in-depth in time series analysis would be efficient in understanding the structural and behavioural changes caused by fire, despite the intensity of the fire. In relation to vegetation changes past and recent analysis of

wildfire behaviour relates it to the rate of fuel consumption, weather, and topography. A clear understanding should be brought forth on how fire ignition points influence the direction of fires based on wind pattern (Fischer et al., 2015; Yebra et al., 2013).

Thirdly was determining the degree of spectral contrast between the burnt and unburnt areas. This was done by assessing the use of kappa coefficient and f-score measurement. Both the producer's accuracy and users accuracy were taken into consideration as shown in table 9 and 10. The remote sensing indices that accessed burned versus unburned areas produced better overall accuracy, user and producer accuracy results as section 5.3. This showed the capability of the electromagnetic spectrum to correspond to changes in vegetation after fire. Nevertheless, it was important to note that overall accuracy obtained could not be relied upon as it could be biased on the sample size of one class in relation to the other (Benson, 2005; Stambaugh et al., 2015). This is clearly shown with the dNBR values whereby the bright areas within and outside fire perimeter zones were classified as burnt areas even though some of the were unburnt areas such as rocky areas and buildings outside fire perimeter zone shown in section 5.3. This drew forth a conclusion that it is not enough to rely on higher kappa coefficient or accuracy assessment to affirm the clear separation of defined classes. However, keen attention should be kept when relating to the accuracy assessment result and expected the outcome of defined classes. Also, validation maps or existing forms of information on the land use of the patches of holes that remain unburned would help in understanding its influence on fire regeneration. This at the moment was not within the scope of the study. However further research could be expounded on the influence of the threshold of vegetation indices which could help in the reduction of classification errors. One would relate the vector representing the fire perimeter wall to be an exact match of our classification results as the burned pixels would have similar spectral sensitivity. However, the task of accounting for precise boundary of the classified image that relates to vector shapefile representing fire perimeter zone becomes complex and difficult. It was noted in particular after classification with SVM_MRF the vector shapefile that represents fire perimeter zone was not exactly fitting the boundary edges of the burnt zones depicted in Figure 17. This could have been attributed to the disparity of fire perimeter based on the reference data and actual ground truth vector file may differ. Another problem could be related to the timing of digitization of vector fire perimeter which might have occurred at early stages of the fire especially for Victoria database while our spectral classification analysis was based on post-fire analysis of the image. This may lead difference of fire perimeter shapefile with the actual ground timing of fire timeout. Also the use of contextual classifiers SVM_MRF which cope up with the problem of intraclass spectral variation and spatial variability along the boundaries (Tarabalka et al., 2010; Li, 2011). The classifier is applied as a post-smoothing method which was developed using spectrally based classifiers that were not collected as ground truth data collected from the actual field (Magnussen et al., 2004). Our research did not go in depth to understanding the causes of boundary variation in relation to mixed pixels in cases of both burnt and unburnt scars. This could be further addressed by the use of soft classification techniques which involves sub-pixel classification or fuzzy classification and super-resolution mapping (Suresh & Jain, 2018). However, it was also not part of our objective within our scope of the study.

Fourthly was the evaluation of texture variation and separability of burnt and unburnt scars. This was done through GLCM textural analysis using backscatter intensity. The contrast, entropy and homogeneity measures performed well in texture separation of two defined classes shown in section 5.4. This could be linked to the GLCM parameters that were influential which include window size, lag distance, and quantization level. However, GLCM is a time-consuming process mainly due to the need to determine many orientations scales and window sizes to accurately capture the textural differentiation of the defined classes. The quantization level has an overall impact on texture feature values. In-depth research could be done to better understand the relationship that exists between forest structure and type and GLCM textural features when varying geographical and image resolution. Also, the algorithms that are computationally time-saving and efficient in textural analysis other than the GLCM algorithm.

Finally, it would be important to mention how our results would be helpful to various stakeholders based on their interests. The main stakeholders being state forest agencies including state government departments, community or landowners and finally, firefighters, risk emergency providers, and forest managers. We could see the state government departments who are keen on forest management use the spatial mapping of bushfire coverage and remote sensing analysis of fire severity act as a guide in providing emergency resources in most affected areas. Also, they would create restricted boundaries surrounding frequent bushfire zones that should not be inhabited as a measure of safety of human and ecological preparedness. Community and landowners that reside within and close to the fire forested zones could be educated on the factors that aggregate and influence the fast spread of bushfire, the particular zones that are highly susceptible to fire and should be avoided and the impact of fire to their physical health and economic wealth. Firefighters and risk emergency providers would benefit from the study by additional integration of fire ignition points in developing fire escape zones and setting up of fire emergency units. Forest managers would benefit in decision making on how to minimize adverse impacts caused by the bushfire in relation to unburnt areas that may act as reignition points of fire again. They would also use the information from radar to understand the influence of forest type and structure to fuel connectivity and use it to adequately allocate resources to manage fire risks in an effective and safe manner.

7. CONCLUSION AND RECOMMENDATION

This chapter concludes the research with some recommendation. Section 7.1 presents the conclusion drawn from this research and Section 7.2 presents some recommendations for future study.

7.1. Conclusion

This study explored the use of satellite SAR and optical dataset in the identification and classification of burnt and unburnt areas with the main focus being an analysis of unburnt areas. It was done through the classification of polarimetric and backscatter intensity in S1 and spectral aspect of S2. The result was also compared to the textural variation of the defined classes by use of GLCM statistical measure. From the results, it was concluded that the use of the SAR system in the mapping of burnt and unburnt scars has the potential for consistent estimation of wildfires as compared to reflectance based indices provided by the optical dataset. However, the effect of the local incidence angle has to be normalized especially for terrain tropical areas and also the backscatter variation that results from environmental conditions such as wet or dry needs to be considered. The field accessed vegetation indexes should also contain more information on forest structure which is the main factor causing variation in the SAR backscatter. The research also identified that for use of satellite SAR S1 in forest fire analysis is highly dependent on the level of wildfire severity. This is because of its influence in the use of SAR in monitoring the changes when comparing backscatter intensity before and after the fire to determine the extent of damage caused by fire. This was concluded as a result of variation in Spain data to Australian bushfires using the same methodology and dataset type. The following conclusion with respect to the research questions can be made on the basis of results achieved from the research objectives.

7.1.1. What is the suitable measure of burnt severity levels existing after the forest fire?

The use of optical reflectance based indices dNBR as depicted in Chapter 5 resulted in the good measure of burnt severity levels existing after the fire. This gave us the magnitude of five levels of burnt severity which includes the (1) highly burnt areas (2) medium burnt areas (3)low severity areas (4) unburnt areas and (5) post-fire regrowth shown in Section 5.1. The NIR reflectance declined due to loss of vegetation after the fire while the short-wavelength infrared (SWIR) increased this is due to the presence of charred remains of fuel and also minimal or hardly any vegetation and soil content. For the highly burnt areas and the unburnt areas, there was consistency in their result among all the bushfire zones however for the intermediate burn levels was difficult to ascertain the surety of results.

7.1.2. Is there a difference of target decomposition and backscatter intensity in the analysis of burnt and unburnt areas?

The results of this study confirmed there was a difference between the backscatter intensity and target decomposition in the analysis of burnt and unburnt areas, especially in Australian bushfires. Scattering from the tree crown was the most predominant of the backscatter for the forested areas at C-band. However, the backscatter intensity was highly dependent on environmental conditions such as terrain effect and also on the local incidence angle. This affected the separation of burnt and unburnt areas. The integration of target decomposition however improved the results and aided in the formation of pattern comparing pre- and post-fire images. This resulted in visual identification of the burnt perimeter zones shown in Section 5.2. The H-alpha dual decomposition showed the potential of burnt and unburnt area estimation without much hindrance from the topography. The scattering properties from burned areas related to the vegetation indices were obtained from entropy and alpha values. It was noted that the entropy and alpha values decreased with increase in burnt severity due to a decrease in volume scatter while for the unburnt areas the entropy and alpha values remained the same as similar to pre-fire images. Also looking into the physical scattering characteristics described H-alpha plane that contains nine zones all the bushfire zones were dominated by dihedral and volume scattering which lied between medium to high entropy values described in Section 3.2. This showed the ability of polarimetric decomposition to sensitivity in the interpretation of the scattering mechanism in bushfire areas using dual C-band. Although a different result was obtained in Spain data as there was very minimal changes between pre- and post-fire backscatter and polarimetric decomposition. This was assumed to be due to very low fire intensity that could hardly alter changes in canopy structure as compared to Australian fire showing how SAR sensitivity to fire varies from one area to another. Nevertheless, in high severity levels of fire satellite, SAR provides a good understanding of changes in forest structural properties of an area in relation to backscatter and target decomposition tool.

7.1.3. What are the effects of utilizing radar backscatter in retrieving the spectral and polarimetric aspect of the burnt and unburnt areas?

Both spectral and polarimetric aspect were able to distinguish the burnt and unburnt areas shown in figure Section 5.3 for Australian bushfire and Spain fire. The results were obtained through classification of both optical and SAR contextual classifier SVM_MRF classification. For Australia bushfires, the S1 burnt and unburnt areas backscatter related well to the burnt severity levels of vegetation indices of dNBR for S2. In both Australia and Spain fire zones, the dNBR vegetation indices produced similar and relatable results in relation to spectral analysis. Utilizing of polarimetric sensitivity of S1 was applicable in Australia but not Spain as its highly related to burn severity level. The optical and SAR gave us good accuracy classification results obtaining over 80% accuracy results from the classification of both S1 and S2 in all bushfire zones. The overlap of the classes could not be avoided although it was minimal when analyzing both the producer and user accuracies obtained for optical S2 and radar S1 shown in Table 9 and Table 10. In

Section 5.1 for Spain, the optical showed high sensitivity to burnt and unburnt areas in spectral analysis as compared to SAR polarimetric sensitivity. However, in Australian bushfire in S1 the regrowth areas were classified as burnt while for S2 they were classified as unburnt. This was due to the polarimetric and spectral differences respectively in both the radar and optical shown Section 5.3. The optical (S2) in Spain also depicted classification error between areas that were burnt within the fire perimeter zone and areas that were unburnt outside the fire perimeter zones. Relatively high determination accuracy and low estimation errors of the burnt and unburnt areas were obtained for both the SAR and the optical dataset in Australia and optical for Spain as shown in Table 9 and Table 10. Nevertheless, both spectral and polarimetric decomposition were successful in the delineation of burnt and unburnt areas in all the bushfire zone after the fire.

7.1.4. What are the effects of utilizing radar backscatter in retrieving the GLCM textural variation of the burnt and unburnt areas?

The GLCM co-occurrence texture analysis revealed a good descriptor in that the homogeneity statistics (homogeneity, entropy) provided a good result in the separation of burnt and unburnt. This is especially in steep areas compared to the smoothness statistics (contrast) shown in Section 5.4. The three features produced consistent texture measures at different orientation angles but increased higher as the quantization level increased. The variation of texture between the burnt and unburnt areas was noticeable at high quantization level (256 × 256). Similar results were obtained across all texture features when adjusting the quantization level, however, for the correlation feature, no much difference was obtained. Thus we concluded that the analysis of SAR backscatter using GLCM method can be successful in the retrieval of textural features of classes specified. Also when using GLCM features the window size, quantization level, and orientation parameters are key descriptors in texture analysis and must be chosen carefully. The GLCM analysis was faster in speed and computationally time-saving, however in choosing of parameters it was time-consuming. Nevertheless, the use of GLCM was a good descriptor in the separation of the two define classes.

7.2. Recommendations for Future Work

Further improvements in the research would include:

- The use of the proposed methodology to other SAR sensors such as ALOS 2, Radarsat - 2 which has additional polarizations and longer wavelength to be compared and analyzed.
- Explore other target decomposition theorems and compare its results to the Cloud and pottier decomposition theorem and see its effectiveness in burnt severity estimation compared to vegetation indices.
- The use of L-band or P-band which have a longer wavelength compared to C- band to understand the state of structural damage and its relation to the soil stability and rehabilitation of burned areas.

- Asses the benefits of using fully polarimetric data over dual backscatter channel acquisition mode.

8. REFERENCES

Akagi, S. K., Yokelson, R. J., Wiedinmyer, C., Alvarado, M. J., Reid, J. S., Karl, T., … Wennberg, P. O. (2011). Emission factors for open and domestic biomass burning for use in atmospheric models. *Atmospheric Chemistry and Physics*, *11*(9), 4039–4072. https://doi.org/10.5194/acp-11-4039-2011

Alan Genz , Frank Bretz , Tetsuhisa Miwa , Xuefei Mi , Friedrich Leisch , Fabian Scheipl , Bjoern Bornkamp , Martin Maechler, T. H. O. iD. (2018). Multivariate Normal and t Distributions [R package mvtnorm version 1.0-10]. Retrieved March 16, 2019, from https://cran.r-project.org/web/packages/mvtnorm/index.html

Allison E. Cocke, Peter Z. Fulé, J. E. C. (2005). Comparison of burn severity assessments using dNBR and ground data, 189–198.

Allison, R. S., Johnston, J. M., Craig, G., & Jennings, S. (2016). Airborne optical and thermal remote sensing for wildfire detection and monitoring. *Sensors (Switzerland)*, *16*(8). https://doi.org/10.3390/s16081310

Almeida-Filho, R., & Shimabukuro, Y. E. (2004). Monitoring biomass burning in the Brazilian Amazônia. *International Journal of Remote Sensing*, *25*(24), 5537–5542. https://doi.org/10.1080/0143116031000075143

Anderson, L. O., Shimabukuro, Y. E., Saatchi, S., Aragão, L. E. O. C., Malhi, Y., & Roman-Cuesta, R. M. (2007). Spatial patterns and fire response of recent Amazonian droughts. *Geophysical Research Letters*, *34*(7), 1–5. https://doi.org/10.1029/2006gl028946

Antropov, O., Rauste, Y., Vaananen, A., Mutanen, T., & Hame, T. (2016). Mapping forest disturbance using long time series of Sentinel-1 data: Case studies over boreal and tropical forests. *International Geoscience and Remote Sensing Symposium (IGARSS)*, *2016–Novem*, 3906–3909. https://doi.org/10.1109/IGARSS.2016.7730014

Arivazhagan, S., & Ganesan, L. (2003). Texture classification using wavelet transform. *Pattern Recognition Letters*, *24*(9–10), 1513–1521. https://doi.org/10.1016/S0167-8655(02)00390-2

Arnalds, O. (2015). *Vegetation and Ecosystems*. https://doi.org/10.1007/978-94-017-9621-7_4

Attiwill, P. M., & Adams, M. A. (2013). Mega-fires, inquiries and politics in the eucalypt forests of Victoria, south-eastern Australia. *Forest Ecology and Management*, *294*, 45–53. https://doi.org/10.1016/j.foreco.2012.09.015

B. D.Ripley & W. N. Venables. (2002). *Modern Applied Statistics with S* (Fourth). Newyork: Springer. Retrieved from http://www.stats.ox.ac.uk/pub/MASS4/

B.Rosich, P. M. (2004). Absolute Calibration of Asar Level 1 Products Generated With Pf- -Asaas R. *European Space Agency*, (1), 126. Retrieved from https://www.researchgate.net/publication/245149504_Absolute_Calibration_of_ASAR_Level_1_Products_Generated_with_PF-ASAR

Bassett, R., & Deride, J. (2018). Maximum a posteriori estimators as a limit of Bayes estimators. *Mathematical Programming*, 1–16. https://doi.org/10.1007/s10107-018-1241-0

Bastarrika, A., Alvarado, M., Artano, K., Martinez, M. P., Mesanza, A., Torre, L., … Chuvieco, E. (2014). BAMS: A tool for supervised burned area mapping using landsat data. *Remote Sensing*, *6*(12), 12360–12380. https://doi.org/10.3390/rs61212360

Bastarrika, A., Chuvieco, E., & Martín, M. P. (2011). Mapping burned areas from landsat TM/ETM+ data with a two-phase algorithm: Balancing omission and commission errors. *Remote Sensing of Environment*, *115*(4), 1003–1012. https://doi.org/10.1016/j.rse.2010.12.005

Benson, K. &. (2005). Landscape assessment: ground measure of severity, the composite burn index, and remote sensing of severity, the normalized burn index. In: Lutes, D., Keane, R., Caratti, J., Key, C., Benson, N., Sutherland, S., Gangi, L. (Eds.). *FIREMON: Fire Effects Monitoring and Inventory System, Rocky Mountains Research Station,USDA Forest Service: Fort Collins, CO, USA, Pp. 1– 51.*, 1–55. https://doi.org/10.1002/app.1994.070541203

Beyerer, J., León, F. P., & Frese, C. (2015). *Machine vision: Automated visual inspection: Theory, practice and applications*. *Machine Vision: Automated Visual Inspection: Theory, Practice and Applications*. https://doi.org/10.1007/978-3-662-47794-6

Boschetti, L., Roy, D. P., Justice, C. O., & Humber, M. L. (2015). MODIS-Landsat fusion for large area 30m burned area mapping. *Remote Sensing of Environment*, *161*, 27–42. https://doi.org/10.1016/j.rse.2015.01.022

Bourgeau-Chavez, Kasischke, A., & French. (1996). Using ERS-1 SAR Imagery to Monitor Variations in Burn Severity in an Alaskan Fire-Disturbed Boreal Forest Ecosystem. *International Journal of Remote Sensing*, (17), 3037–3053.

Cameron, W. L., Youssef, N. N., & Leung, L. K. (1996). Simulated polarimetric signatures of primitive geometrical shapes. *IEEE Transactions on Geoscience and Remote Sensing*, *34*(3), 793–803. https://doi.org/10.1109/36.499784

Chu, T., & Guo, X. (2013). Remote sensing techniques in monitoring post-fire effects and patterns of forest recovery in boreal forest regions: A review. *Remote Sensing*, *6*(1), 470–520. https://doi.org/10.3390/rs6010470

Chuvieco, E. (1999). Measuring changes in landscape pattern from satellite images: Short-term effects of fire on spatial diversity. *International Journal of Remote Sensing*, *20*(12), 2331–2346. https://doi.org/10.1080/014311699212056

Chuvieco, E., Martín, M. P., & Palacios, A. (2002a). Assessment of different spectral indices in the red-near-infrared spectral domain for burned land discrimination. *International Journal of Remote Sensing*, *23*(23), 5103–5110. https://doi.org/10.1080/01431160210153129

Chuvieco, E., Martín, M. P., & Palacios, A. (2002b). Assessment of different spectral indices in the red-near-infrared spectral domain for burned land discrimination. *International Journal of Remote Sensing*, *23*(23), 5103–5110. https://doi.org/10.1080/01431160210153129

Clarke, H., Lucas, C., & Smith, P. (2013). Changes in Australian fire weather between 1973 and 2010. *International Journal of Climatology*, *33*(4), 931–944. https://doi.org/10.1002/joc.3480

Clausi, D. A., & Yu, B. (2004). Comparing cooccurrence probabilities and Markov random fields for texture analysis of SAR sea ice imagery. *IEEE Transactions on Geoscience and Remote Sensing*, *42*(1), 215–228. https://doi.org/10.1109/TGRS.2003.817218

Cloude, Pottier, E., & Boerner, W. M. (2008). Unsupervised Image classification using the Entropy/Alpha/Anisotropy method in Radar Polarimetry., *44*(1334). Retrieved from http://scholar.google.com/scholar?hl=en&btnG=Search&q=intitle:Magnetically+Levitated+Trains+(+Maglev+)#8

Cloude, S., & Pottier, E. (1997). An entropy based classification scheme for land applications of polarimetric SAR. *IEEE Transactions on Geoscience and Remote Sensing*, *35*(1), 68–78. https://doi.org/10.1109/36.551935

Cloude, S. R., & Pettier, E. (1996). A review of target decomposition theorems in radar polarimetry. *IEEE Transactions on Geoscience and Remote Sensing*, *34*(2), 498–518. https://doi.org/10.1109/36.485127

Cortes, C., & Vapnik, V. (1995). Support-Vector Networks. *Assembly*, *44*(13), 97. https://doi.org/10.1111/j.1747-0285.2009.00840.x

David Meyer, Evgenia Dimitriadou, Kurt Hornik, A. W. & F. L. (2018). e1071: Misc Functions of the Department of Statistics, Probability Theory Group (Formerly: E1071), TU Wien. Retrieved February 16, 2019, from https://cran.r-project.org/web/packages/e1071/index.html

Dekker, R. J. (2003). Texture analysis and classification of SAR images of urban areas. *2nd GRSS/ISPRS Joint Workshop on Remote Sensing and Data Fusion over Urban Areas, URBAN 2003*, *41*(9), 258–262. https://doi.org/10.1109/DFUA.2003.1220000

Dinstein, I., Shanmugam, K., & Haralick, R. M. (1973). Textural Features for Image Classification. *IEEE*

Transactions on Systems, Man, and Cybernetics, *SMC-3*(6), 610–621. Retrieved from http://haralick.org/journals/TexturalFeatures.pdf

Dubois-Fernandez, P. C., Souyris, J. C., Angelliaume, S., & Garestier, F. (2008). The compact polarimetry alternative for spaceborne SAR at low frequency. *IEEE Transactions on Geoscience and Remote Sensing*, *46*(10), 3208–3222. https://doi.org/10.1109/TGRS.2008.919143

Eddelbuettel, D., & François, R. (2011). Seamless R and C++ intgration with Rcpp. *Journal of Statistical Software*, *40*(8), 1–18. https://doi.org/10.1007/978-1-4614-6868-4

ESA. (2015). SENTINEL-2 User Handbook Sentinel-2 User Handbook SENTINEL-2 User Handbook Title Sentinel -2 User Handbook SENTINEL-2 User Handbook, (1), 1–64. https://doi.org/10.13128/REA-22658

Escuin, S., Navarro, R., & Fernández, P. (2008). Fire severity assessment by using NBR (Normalized Burn Ratio) and NDVI (Normalized Difference Vegetation Index) derived from LANDSAT TM/ETM images. *International Journal of Remote Sensing*, *29*(4), 1053–1073. https://doi.org/10.1080/01431160701281072

Fairman, T. A., Nitschke, C. R., & Bennett, L. T. (2016). Too much, too soon? A review of the effects of increasing wildfire frequency on tree mortality and regeneration in temperate eucalypt forests. *International Journal of Wildland Fire*, *25*(8), 831–848. https://doi.org/10.1071/WF15010

Fernández-Manso, A., Fernández-Manso, O., & Quintano, C. (2016). SENTINEL-2A red-edge spectral indices suitability for discriminating burn severity. *International Journal of Applied Earth Observation and Geoinformation*, *50*, 170–175. https://doi.org/10.1016/j.jag.2016.03.005

Forshed, O., Brearley, F. Q., van Valkenburg, J. L. C. H., Nilus, R., Nagamasu, H., Sidiyasa, K., … Sheil, D. (2009). Environmental correlates of tree biomass, basal area, wood specific gravity and stem density gradients in Borneo's tropical forests. *Global Ecology and Biogeography*, *19*(1), 50–60. https://doi.org/10.1111/j.1466-8238.2009.00489.x

Franklin, S. E. (2001). *Remote sensing for sustainable forest management* (First). Boca Raton: CRC Press.

Freeman, A., & Durden, S. L. (1998). A three-component scattering model for polarimetric SAR data. *IEEE Transactions on Geoscience and Remote Sensing*, *36*(3), 963–973. https://doi.org/10.1109/36.673687

Gaglione, D., Clemente, C., Pallotta, L., Proudler, I., De Maio, A., & Soraghan, J. J. (2014). Krogager decomposition and Pseudo-Zernike moments for polarimetric distributed ATR. *2014 Sensor Signal Processing for Defence, SSPD 2014*, 1–5. https://doi.org/10.1109/SSPD.2014.6943309

Geospatial, H. (2016). Release Guide 5.0.0, 1–83. https://doi.org/10.6103/SHARE.w5.500

Giannakopoulos, C., Bindi, M., Moriondo, M., LeSager, P., & Tin, T. (2005). Climate change impacts in the Mediterranean resulting from a 2 C global temperature rise. *WWF Report*, (July), 67. https://doi.org/10.1067/mva.2001.111989

Giglio, L., van der Werf, G. R., Randerson, J. T., Collatz, G. J., & Kasibhatla, P. (2006). Global estimation of burned area using MODIS active fire observations. *Atmospheric Chemistry and Physics*, *6*(4), 957–974. https://doi.org/10.5194/acp-6-957-2006

Gimeno, M., San-Miguel-Ayanz, J., & Schmuck, G. (2004). Identification of burnt areas in Mediterranean forest environments from ERS-2 SAR time series. *International Journal of Remote Sensing*, *25*(22), 4873–4888. https://doi.org/10.1080/01431160412331269715

Gitas, I., Mitri, G., Veraverbeke, S., & Polychronaki, A. (2012). Advances in Remote Sensing of Post-Fire Vegetation Recovery Monitoring - A Review. *Remote Sensing of Biomass - Principles and Applications*, (March). https://doi.org/10.5772/20571

GmbH, T. V. D. (2015). S2Pad-Vega-Sum-0001-2.2, *49*(2), 1–51.

Gütlein, M., Helma, C., Karwath, A., & Kramer, S. (2013). A large-scale empirical evaluation of cross-validation and external test set validation in (Q)SAR. *Molecular Informatics*, *32*(5–6), 516–528. https://doi.org/10.1002/minf.201200134

Hoekman, D. H., Vissers, M. A., & Wielaard, N. (2010). PALSAR Wide-Area Mapping of Borneo: Methodology and Map Validation. *IEEE Journal of Selected Topics in Applied Earth Observations and Remote Sensing*, *3*(4), 605–617. https://doi.org/10.1109/JSTARS.2010.2070059

Huang, S., & Siegert, F. (2004). Envisat multisensor data for fire monitoring and impact assessment. *International Journal of Remote Sensing*, *1161*. https://doi.org/10.1080/01431160412331269670

J.S. Lee, E. P. (2009). *Polarimetric radar imaging: From basics to applications*. (P. Taylor, Ed.) (Second). London, New York: CRC Press.

Jackson, Q., Member, S., Landgrebe, D. A., & Fellow, L. (2002). Adaptive Bayesian Contextual Classification Basedon Markov Random Fields, *40*(11), 2454–2463.

Jagdhuber, T., Stockamp, J., Hajnsek, I., & Ludwig, R. (2014). Identification of soil freezing and thawing states using SAR polarimetry at C-band. *Remote Sensing*, *6*(3), 2008–2023. https://doi.org/10.3390/rs6032008

Jenkins, M., Collins, L., Price, O., Penman, T., Zylstra, P., Horsey, B., & Bradstock, R. (2016). Environmental values and fire hazard of eucalypt plantings. *Ecosphere*, *7*(11), 1–14. https://doi.org/10.1002/ecs2.1528

Jin, Q. & Xu, F. (2013). Inversions from Polarimetric, (1998).

kasischke. (1997). The Use of Imaging Radars for Applications A Review Ecological, *4257*(96), 141–156. https://doi.org/10.1016/S0034-4257(96)00148-4

Kasischke, E. S., Bourgeau-chavez, L. L., French, N. H. F., & Harrell, P. A. (2000). Monitoring Boreal Forests by Using Imaging Radars. In *Climate change and carbon cycling in the boreal forest* (pp. 331–332).

Kasischke, E. S., Brunzell, S., Mudd, J. P., Tukman, M., Kasischke, E. S., Brunzell, S., & Mudd, J. P. (2010). Mapping fire scars in global boreal forests using imaging radar data, *1161*. https://doi.org/10.1080/01431160110109589

Kavzoglu, T., & Colkesen, I. (2009). A kernel functions analysis for support vector machines for land cover classification. *International Journal of Applied Earth Observation and Geoinformation*, *11*(5), 352–359. https://doi.org/10.1016/j.jag.2009.06.002

Kontoes, C. C., Poilvé, H., Florsch, G., Keramitsoglou, I., & Paralikidis, S. (2009). A comparative analysis of a fixed thresholding vs. a classification tree approach for operational burn scar detection and mapping. *International Journal of Applied Earth Observation and Geoinformation*, *11*(5), 299–316. https://doi.org/10.1016/j.jag.2009.04.001

Koo, Y. K., & Chan, V. C. (2008). An Introduction To Synthetic Aperture Radar (SAR). *Progress In Electromagnetics Research B*, *2*(6), 27–60. https://doi.org/10.1037/008772

Koutsias, N., Karteris, M., & Chuvieco, E. (2000). The Use of Itensity-Hue-Saturation Transformation of Landsat-5 Thematic Mapper Data for Burned Land Mapping. *Photogrammetric Engineering & Remote Sensing*, *66*(7), 829–839.

Koutsias, N., Pleniou, M., Mallinis, G., Nioti, F., & Sifakis, N. I. (2013). A rule-based semi-automatic method to map burned areas: Exploring the USGS historical Landsat archives to reconstruct recent fire history. *International Journal of Remote Sensing*, *34*(20), 7049–7068. https://doi.org/10.1080/01431161.2013.816452

Kuenzer, C., & Dech, S. (2013). *Thermal Infrared Remote Sensing*. (S. D. Claudia Kuenzer, Ed.) (Vol. 17). Germany. https://doi.org/10.1007/978-94-007-6639-6

Kumar, S., Khati, U. G., Chandola, S., Agrawal, S., & Kushwaha, S. P. S. (2017). Polarimetric SAR Interferometry based modeling for tree height and aboveground biomass retrieval in a tropical deciduous forest. *Advances in Space Research*, *60*(3), 571–586. https://doi.org/10.1016/j.asr.2017.04.018

Lee, J.-S., & Pottier, E. (2009). *Polarimetric Radar Imaging: From Basics to Applications*. *Polarimetric Radar Imaging: From Basics to Applications*. https://doi.org/10.1201/9781420054989.fmatt

Lentile, L. B., Smith, F. W., & Shepperd, W. D. (2006). Influence of topography and forest structure on

patterns of mixed severity fire in ponderosa pine forests of the South Dakota Black Hills, USA. *International Journal of Wildland Fire*, *15*(4), 557–566. https://doi.org/10.1071/WF05096

Li, S. Z. (2010). *Markov Random Field Modeling in Image Analysis* (Vol. 6256, Fift). https://doi.org/10.1007/978-3-642-15992-3

Lucas, C., Hennessy, K., Mills, G., & Bathols, J. (2007). Bushfire weather in southeast Australia : recent trends and projected climate change impacts. *Bushfire Cooperative Research Centre Consultancy Report Prepared for The Climate Institute of Australia*, (September), 84 pp. https://doi.org/10.1109/CSIT.2013.6588776

Luckman, A. J. (1998). The effects of topography on mechanisms of radar backscatter from coniferous forest and upland pasture. *IEEE Transactions on Geoscience and Remote Sensing*, *36*(5 PART 2), 1830–1834. https://doi.org/10.1109/36.718651

Madoffe, S. S., Bakke, A., & Tarimo, J. A. (2000). The effect of fire on the diversity and abundance of wood-living beetles in a miombo woodland, Tanzania. *The Southern African Forestry Journal*, *187*(1), 51–57. https://doi.org/10.1080/10295925.2000.9631256

Maeda, E. E., Arcoverde, G. F. B., Pellikka, P. K. E., & Shimabukuro, Y. E. (2011). Fire risk assessment in the Brazilian Amazon using MODIS imagery and change vector analysis. *Applied Geography*, *31*(1), 76–84. https://doi.org/10.1016/j.apgeog.2010.02.004

Maeda, E. E., Formaggio, A. R., Shimabukuro, Y. E., Arcoverde, G. F. B., & Hansen, M. C. (2009). Predicting forest fire in the Brazilian Amazon using MODIS imagery and artificial neural networks. *International Journal of Applied Earth Observation and Geoinformation*, *11*(4), 265–272. https://doi.org/10.1016/j.jag.2009.03.003

Maître, H. (2008). *Processing of synthetic aperture radar images*. *Journal of the Electrochemical Society* (2nd editio, Vol. 129). London SW19 4EU: ISTE Ltd and John Wiley & Sons, Inc. Apart. https://doi.org/10.1002/9780470611111

Martin, P., & Topp, V. (2018). Drought impacts on broadacre and dairy farms in South-Eastern Australia, (December).

Masek, J. G., Vermote, E. F., Saleous, N. E., Wolfe, R., Hall, F. G., Huemmrich, K. F., … Lim, T. (2006). A landsat surface reflectance dataset, 1990-2000. *IEEE Geoscience and Remote Sensing Letters*, *3*(1), 68–72. https://doi.org/10.1109/LGRS.2005.857030

Massonnet, D., & Souyris, J.-C. (2008). *Imaging with Synthetic Aperture Radar*. Retrieved from https://books.google.com/books?hl=en&lr=&id=76cCM-y-d7cC&pgis=1

Mather, P., & Tso, B. (2013). *Classification Methods for Remotely Sensed Data.* (C. Press, Ed.), *Engineering &*

Technology, Environment & Agriculture (second, Vol. 84). Boca Raton. Retrieved from http://ir.obihiro.ac.jp/dspace/handle/10322/3933

Menges, C. H., Bartolo, R. E., Bell, D., & Hill, G. J. E. (2004). The effect of savanna fires on SAR backscatter in northern Australia. *International Journal of Remote Sensing*, *25*(22), 4857–4871. https://doi.org/10.1080/01431160410001712945

Menges, C. H., Bartolo, R. E., Bell, D., Hill, G. J. E., Bartolo, R. E., Bell, D., & The, G. J. E. H. (2004). The effect of savanna fires on SAR backscatter in northern Australia. *International Journal of Remote Sensing*, *1161*, 4857–4871. https://doi.org/10.1080/01431160410001712945

Metropolis, N., Rosenbluth, A. W., Rosenbluth, M. N., Teller, A. H., & Teller, E. (1953). Equation of state calculations by fast computing machines. *The Journal of Chemical Physics*, *21*(6), 1087–1092. https://doi.org/10.1063/1.1699114

Mitri, G. H., & Gitas, I. Z. (2004). A semi-automated object-oriented model for burned area mapping in the Mediterranean region using Landsat-TM imagery. *International Journal of Wildland Fire*, *13*(3), 367. https://doi.org/10.1071/wf03079

Moreira, A., Prats, P., Younis, M., Krieger, G., Hajnsek, I., & Papathanassiou, K. (2013). A tutorial on synthetic aperture radar. *IEEE Geoscience and Remote Sensing Magazine*, *1*(1), 6–43. https://doi.org/10.1109/MGRS.2013.2248301

Moreira, A., Prats-iraola, P., Younis, M., Krieger, G., Hajnsek, I., & Papathanassiou, K. P. (2013). *A tutorial on synthetic aperture radar*. Germany. https://doi.org/10.1109/MGRS.2013.2248301

Mouillot, F., Schultz, M. G., Yue, C., Cadule, P., Tansey, K., Ciais, P., & Chuvieco, E. (2014). Ten years of global burned area products from spaceborne remote sensing-A review: Analysis of user needs and recommendations for future developments. *International Journal of Applied Earth Observation and Geoinformation*, *26*(1), 64–79. https://doi.org/10.1016/j.jag.2013.05.014

Ojala, T., Pietikäinen, M., & Harwood, D. (1996). A comparative study of texture measures with classification based on feature distributions. *Pattern Recognition*, *29*(1), 51–59. https://doi.org/10.1016/0031-3203(95)00067-4

Pathak, B., & Barooah, D. (2013). Gray-Level Co-Occurrence Matrix Considering Possible. *Matrix*, 4206–4212.

Pau Costa Foundation (PAU). (2018). PAU COSTA FOUNDATION - Ecología del fuego y gestión de incendios - fire ecology & management. Retrieved February 24, 2019, from http://www.paucostafoundation.org/ing/publicacions.php

Pereira, M. C., Gre, J., Stroppiana, D., & Pinnock, S. (2002). Radiometric analysis of SPOT-

VEGETATION images for burnt area detection in Northern Australia. *Remote Sensing of Environment*, *82*, 21–37. https://doi.org/10.1016/S0034-4257(02)00021-4

Polychronaki, A., Gitas, I. Z., Veraverbeke, S., & Debien, A. (2013). Evaluation of ALOS PALSAR imagery for burned area mapping in greece using object-based classification. *Remote Sensing*, *5*(11), 5680–5701. https://doi.org/10.3390/rs5115680

Powers, D. M. W. (2007). *Evaluation: From Precision, Recall and F-Factor to ROC, Informedness, Markedness & Correlation*.

R Development Core Team, R. (2018). R: The R Project for Statistical Computing. Platform: x86_64-w64-mingw32/x64 (64-bit). Retrieved February 16, 2019, from https://www.r-project.org/

Randerson, J. T., Chen, Y., Van Der Werf, G. R., Rogers, B. M., & Morton, D. C. (2012). Global burned area and biomass burning emissions from small fires. *Journal of Geophysical Research G: Biogeosciences*, *117*(4). https://doi.org/10.1029/2012JG002128

Rao, P. V. N., Sesha Sai, M. V. R., Sreenivas, K., Rao, M. V. K., Rao, B. R. M., Dwivedi, R. S., & Venkataratnam, L. (2002). Textural analysis of IRS-1D panchromatic data for land cover classification. *International Journal of Remote Sensing*, *23*(17), 3327–3345. https://doi.org/10.1080/01431160110104665

Remmel, T. K., & Perera, A. H. (2001). Fire mapping in a northern boreal forest: Assessing AVDRR/NDVI methods of change detection. *Forest Ecology and Management*, *152*(1–3), 119–129. https://doi.org/10.1016/S0378-1127(00)00594-6

Richards, J. A., & Jia, X. (2006). *Remote sensing and digital image analysis* (fourth). Australia.

Richards, J. a, & Jia, X. (2006). *Remote Sensing Digital Image Analysis. Methods* (fifth). Australia: Springer Heidelberg New York Dordrecht London. https://doi.org/10.1007/3-540-29711-1

Riera Mora, S. (2006). Cambios vegetales holocenos en la región mediterránea de la Península Ibérica: ensayo de síntesis. *Ecosistemas: Revista Científica y Técnica de Ecología y Medio Ambiente*, *15*(1), 3. Retrieved from http://dialnet.unirioja.es/servlet/articulo?codigo=1388500&info=resumen&idioma=ENG

Roger, A., Stuetz, R., Ove, K., Giraudoux, P., Davis, M., & Santilli, S. (2018). *Package ' rgeos .'* Retrieved from https://cran.r-project.org/web/packages/rgeos/

Rowlingson, R. B. and T. K. and B. (2018). rgdal: Bindings for the "Geospatial" Data Abstraction Library. Comprehensive R Archive Network (CRAN). Retrieved from https://cran.r-project.org/web/packages/rgdal/index.html

Roy, D. P., Jin, Y., Lewis, P. E., & Justice, C. O. (2005). Prototyping a global algorithm for systematic fire-affected area mapping using MODIS time series data. *Remote Sensing of Environment*, *97*(2), 137–162.

https://doi.org/10.1016/j.rse.2005.04.007

Roy, D. P., Lewis, P. E., & Justice, C. O. (2002). Burned area mapping using multi-temporal moderate spatial resolution. *Remote Sensing Letters*, *83*, 263–286.

Ruecker, G., & Siegert, F. (2000). Burn Scar Mapping and Fire Damage Assessment Using Ers-2 Sar Images in East Kalimantan , Indonesia. *Iaprs*, *XXXIII*(2000), 1–8.

Salvador, R., Valeriano, J., Pons, X., & Diaz-Delgado, R. (2000). A semi-automatic methodology to detect fire scars in shrubs and evergreen forests with Landsat MSS time series. *International Journal of Remote Sensing*, *21*(4), 655–671. https://doi.org/10.1080/014311600210498

Sanders, J., Greene, R., Elffers, J., Hour, R., Pouch, C., Pouch, S., … Dao, N. L. (2016). Sentinel-1 Toolbox TOPS Interferometry Tutorial. *Remote Sensing of Environment*, *2017*(1), 1–13. https://doi.org/10.1007/BF01167858

Schepers, L., Haest, B., Veraverbeke, S., Spanhove, T., Borre, J. Vanden, & Goossens, R. (2014). Burned area detection and burn severity assessment of a heathland fire in belgium using airborne imaging spectroscopy (APEX). *Remote Sensing*, *6*(3), 1803–1826. https://doi.org/10.3390/rs6031803

Schroeder, W., Oliva, P., Giglio, L., Quayle, B., Lorenz, E., & Morelli, F. (2016). Active fire detection using Landsat-8/OLI data. *Remote Sensing of Environment*, *185*, 210–220. https://doi.org/10.1016/j.rse.2015.08.032

Schubert, A., & Small, D. (2008). Guide to ASAR Geocoding. *Remote Sensing Laboratories*, (1.01), 1–36.

Schubert, A., Small, D., Meier, E., Miranda, N., & Geudtner, D. (2014). Spaceborne SAR product geolocation accuracy: A Sentinel-1 update. *International Geoscience and Remote Sensing Symposium (IGARSS)*, (July), 2675–2678. https://doi.org/10.1109/IGARSS.2014.6947025

Shoshany, M., & Sternberg, M. (2001). Aboveground biomass allocation and water content relationships in Mediterranean trees and shrubs in two climatological regions in Israel. *Plant Ecology*, *157*, 171–179. Retrieved from file:///D:/inga/dissertation/literatur/sternberg_2001a.pdf

Silva, J. M. N., Sá, A. C. L., & Pereira, J. M. C. (2005). Comparison of burned area estimates derived from SPOT-VEGETATION and Landsat ETM+ data in Africa: Influence of spatial pattern and vegetation type. *Remote Sensing of Environment*, *96*(2), 188–201. https://doi.org/10.1016/j.rse.2005.02.004

Sinha, S., Jeganathan, C., Sharma, L. K., & Nathawat, M. S. (2015). A review of radar remote sensing for biomass estimation. *International Journal of Environmental Science and Technology*, *12*(5), 1779–1792. https://doi.org/10.1007/s13762-015-0750-0

Sivasankar, T., Srivastava, H., Sharma, P., Kumar, D., & Patel, P. (2015). Study of Hybrid Polarimetric

Parameters generated from RISAT-1 SAR data for various Land Cover targets. *International Journal of Advancement in Remote Sensing, GIS and Geography*, *3*(January), 32–42.

Small, D. (2011). Flattening Gamma: Radiometric Terrain Correction for SAR Imagery. *IEEE Geoscience and Remote Sensing Environment*, *49*(8), 407–417. https://doi.org/10.1006/jtbi.1994.1036

Small, D., Holecz, F., Meier, E., & Nüesch, D. (1998). Radiometric Normalization for Multimode Image Comparison. *Proc. of EUSAR '98 - European Conference on Synthetic Aperture Radar*, (January 1998), 191–194. Retrieved from http://www.geo.uzh.ch/publications/daves/1998/Small_EUSAR_1998.pdf

Soh, L., Tsatsoulis, C., & Member, S. (1999). *Texture Analysis of SAR Sea Ice Imagery*. *IEEE Transactions on Geoscience and Remote Sensing* (Vol. 37). https://doi.org/10.1109/36.752194

Sowter, A., Bin, M., Amat, C., Cigna, F., Marsh, S., Athab, A., & Alshammari, L. (2016). Mexico City land subsidence in 2014–2015 with Sentinel-1 IW TOPS: Results using the Intermittent SBAS (ISBAS) technique. *International Journal of Applied Earth Observation and Geoinformation*, *52*, 230–242. https://doi.org/10.1016/j.jag.2016.06.015

Stretton, A. J. (2016). *Radiation heat transfer*. *SFPE Handbook of Fire Protection Engineering, Fifth Edition*. https://doi.org/10.1007/978-1-4939-2565-0_4

Stroppiana, D., Azar, R., Calò, F., Pepe, A., Imperatore, P., Boschetti, M., … Lanari, R. (2015). Integration of optical and SAR data for burned area mapping in Mediterranean regions. *Remote Sensing*, *7*(2), 1320–1345. https://doi.org/10.3390/rs70201320

Stroppiana, D., Bordogna, G., Carrara, P., Boschetti, M., Boschetti, L., & Brivio, P. A. (2012). A method for extracting burned areas from Landsat TM/ETM+ images by soft aggregation of multiple Spectral Indices and a region growing algorithm. *ISPRS Journal of Photogrammetry and Remote Sensing*, *69*, 88–102. https://doi.org/10.1016/j.isprsjprs.2012.03.001

Stroppiana, D., Tansey, K., Grégoire, J. M., & Pereira, J. M. C. (2003). An algorithm for mapping burnt areas in Australia using SPOT-VEGETATION data. *IEEE Transactions on Geoscience and Remote Sensing*, *41*(4 PART II), 907–909. https://doi.org/10.1109/TGRS.2003.808898

Tanase., Santoro, M., De La Riva, J., Pérez-Cabello, F., & Le Toan, T. (2010). Sensitivity of X-, C-, and L-band SAR backscatter to burn severity in Mediterranean pine forests. *IEEE Transactions on Geoscience and Remote Sensing*, *48*(10), 3663–3675. https://doi.org/10.1109/TGRS.2010.2049653

Tanase, M. A., Santoro, M., Aponte, C., & De La Riva, J. (2014). Polarimetric properties of burned forest areas at C- and L-band. *IEEE Journal of Selected Topics in Applied Earth Observations and Remote Sensing*, *7*(1), 267–276. https://doi.org/10.1109/JSTARS.2013.2261053

Tanase, Santoro, M., De La Riva, J., Pérez-Cabello, F., & Le Toan, T. (2010). Sensitivity of X-, C-, and L-

band SAR backscatter to burn severity in Mediterranean pine forests. *IEEE Transactions on Geoscience and Remote Sensing*, *48*(10), 3663–3675. https://doi.org/10.1109/TGRS.2010.2049653

Tansey, K., Grégoire, J. M., Stroppiana, D., Sousa, A., Silva, J., Pereira, J. M. C., … Peduzzi, P. (2004). Vegetation burning in the year 2000: Global burned area estimates from SPOT VEGETATION data. *Journal of Geophysical Research D: Atmospheres*, *109*(14), 1–22. https://doi.org/10.1029/2003JD003598

Toan, A. Beaudoin, J. R. & D. G. (1992). Relating Forest Biomass to SAR Data. *IEEE Geoscience and Remote Sensing Environment*, *30*(2), 403–411.

USDA, U. states department of A. U. (2003). Influence of Forest Structure on Wildfire Behavior and the Severity of Its Effects. *Agriculture*, (May).

Vallejo, R. (1999). Remote Sensing of Large Wildfires, (June). https://doi.org/10.1007/978-3-642-60164-4

van Zyl, J. J. (1989). Unsupervised classification of scattering behavior using radar polarimetry data. *IEEE Transactions on Geoscience and Remote Sensing*, *27*(1), 36–45. https://doi.org/10.1109/36.20273

Veci, L. (2015). *SENTINEL-1 Toolbox Polarimetric Tutorial*. Retrieved from http://sentinel1.s3.amazonaws.com/docs/S1TBX Polarimetry Tutorial.pdf

Vito Alberga, Ernst Krogager, Madhu Chandra, & Gerd Wanielik. (2004). Potential of coherent decompositions in SAR polarimetry and interferometry. *IGARSS 2004. 2004 IEEE International Geoscience and Remote Sensing Symposium*, *3*(C), 1792–1795. https://doi.org/10.1109/igarss.2004.1370682

Vladimir Vapnik. (2006). *Estimation of Dependencies Based on Empirical Data*. (M. J. K. Schölkop, Ed.). Springer NewYork.

Westerling, A. L., Hidalgo, H. G., Cayan, D. R., & Swetnam, T. W. (2006). Warming and earlier spring increase Western U.S. forest wildfire activity. *Science*, *313*(5789), 940–943. https://doi.org/10.1126/science.1128834

Whittaker, J., & Mercer, D. (2004). The Victorian bushfires of 2002-03 and the politics of blame: A discourse analysis. *Australian Geographer*, *35*(3), 259–287. https://doi.org/10.1080/0004918042000311313

Xaud, H. A. M., Martins, F. da S. R. V., & Dos Santos, J. R. (2013). Tropical forest degradation by mega-fires in the northern Brazilian Amazon. *Forest Ecology and Management*, *294*, 97–106. https://doi.org/10.1016/j.foreco.2012.11.036

Zhang, L., Zhang, J., Zou, B., & Street, W. D. (2008). Comparison of Methods for Target Detection and

Applications Using Polarimetric SAR Image. *Progress In Electromagnetics Research Symposium Proceedings*, *4*, 140–145.

Zhu, G., & Blumberg, D. G. (2002). Classification using ASTER data and SVM algorithms; *Remote Sensing of Environment*, *80*(2), 233–240. https://doi.org/10.1016/s0034-4257(01)00305-4

APPENDIX A

Simulated annealing parameter tuning

Simulated annealing was performed by tuning of parameters to find the optimal values for the Updating Temperature T_{upd}, Initial Temperature T_0 and Smoothing parameter λ. Each parameter was varied within a defined range while keeping the other two parameters constant at different times while looking at its behaviour of the curves. Table 12-14 shows the range of values used in each parameter and the values that were kept constant. The optimal values are shown in table 5 for all fire zones.

Parameter	Value
Updating Temperature T_{upd}	(0.7,0.8,0.85,0.9,0.95,1.00)
Initial Temperature T_0	4
Smoothing parameter λ	0.80

Table 12: Variation of updating temperature experiments: while monitoring the parameter values

Parameter	Value
Updating Temperature T_{upd}	0.90
Initial Temperature T_0	(1,3,4,5,7,8.5,10)
Smoothing parameter λ	0.80

Table 13: Variation of initial temperature experiments: while monitoring the parameter values.

Parameter	Value
Updating Temperature T_{upd}	0.90
Initial Temperature T_0	4
Smoothing parameter λ	(0.20,0.50,0.75,0.80,0.9,0.99)

Table 14: Variation of smoothing parameter experiments: while monitoring the parameter values.

APPENDIX B

GLCM parameter tuning

GLCM textural variation of parameters to determine optimal values that show the variation of burnt and unburnt areas. The parameter values included were Quantization level (Ql), Lag distance (L), Angular direction (θ). While one parameter was varied the others were kept constant. The optimal value was chosen in accordance to the output result that foreshowed clear description of the defined classes. We shall present for contrast and sa imilar method was done for all features.

Parameter	Value
Quantization level Ql	(16,64,128,256)
Lag distance L	1:10
Angular direction θ	4

Table 15: Variation of Quantization level experiments: while monitoring the parameter values.

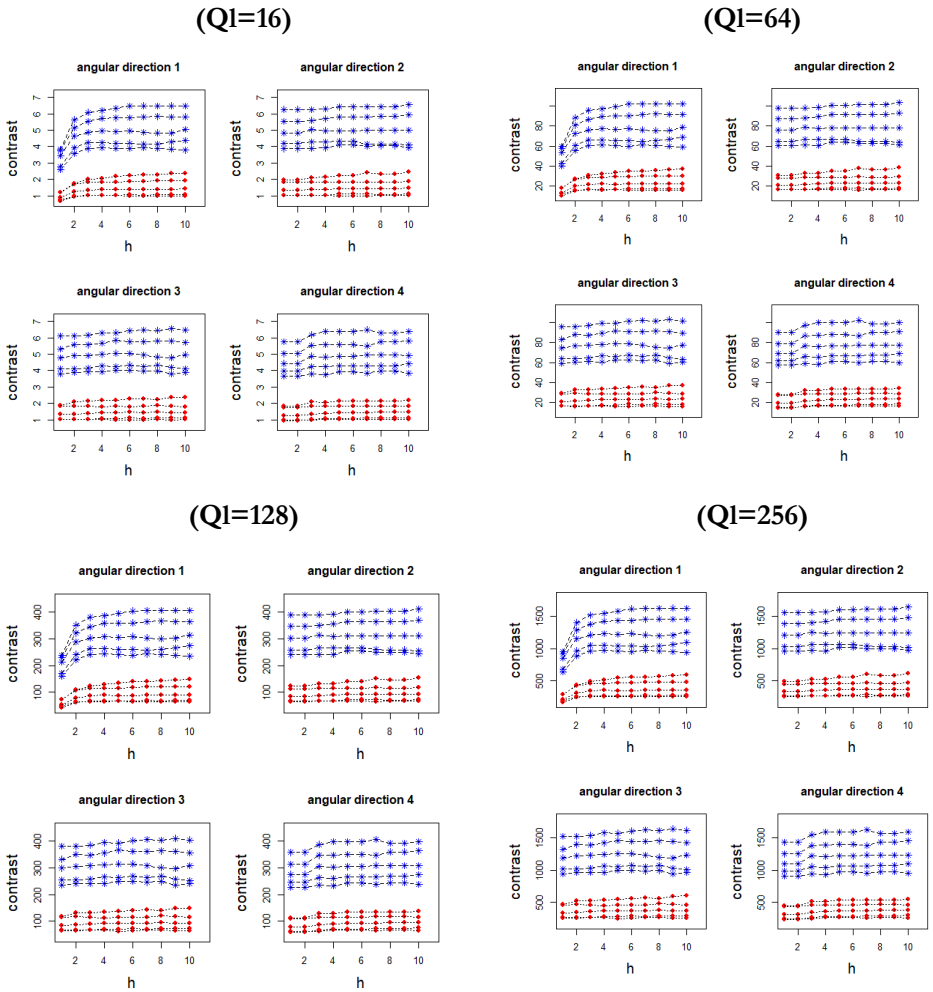

Figure 21: GLCM measure of contrast feature while varying quantization level representing fire 1 in Australia, Victoria.

APPENDIX C

Parameter	Value
Quantization level Ql	256
Lag distance L	(1:10,20,40,70)
Angular direction θ	4

Table 16: Variation of GLCM lag distance: while monitoring the parameter values.

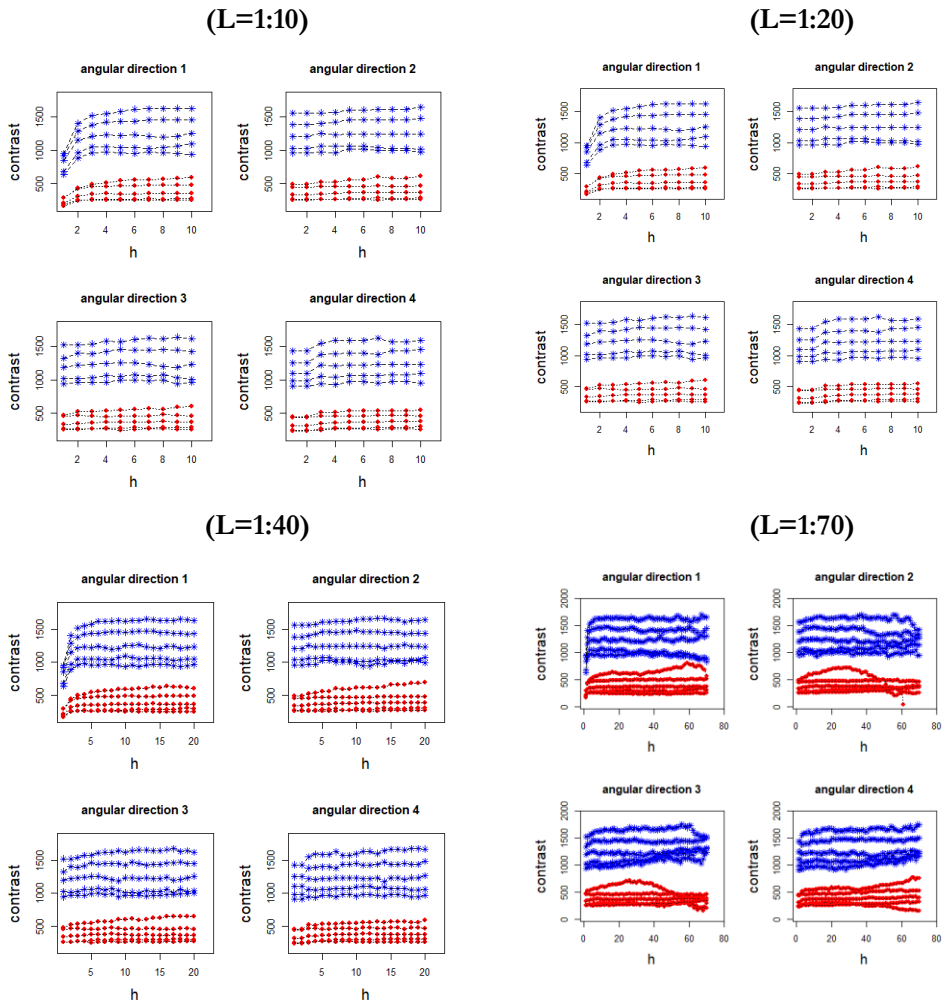

Figure 22: GLCM measure of contrast feature while varying lag distance representing fire 1 in Australia, Victoria.

APPENDIX D

Parameter	Value
Quantization level Ql	256
Lag distance L	1:10
Angular direction θ	(1,2,3,4)

Table 17: Variation of GLCM Angular direction: while monitoring the parameter values.

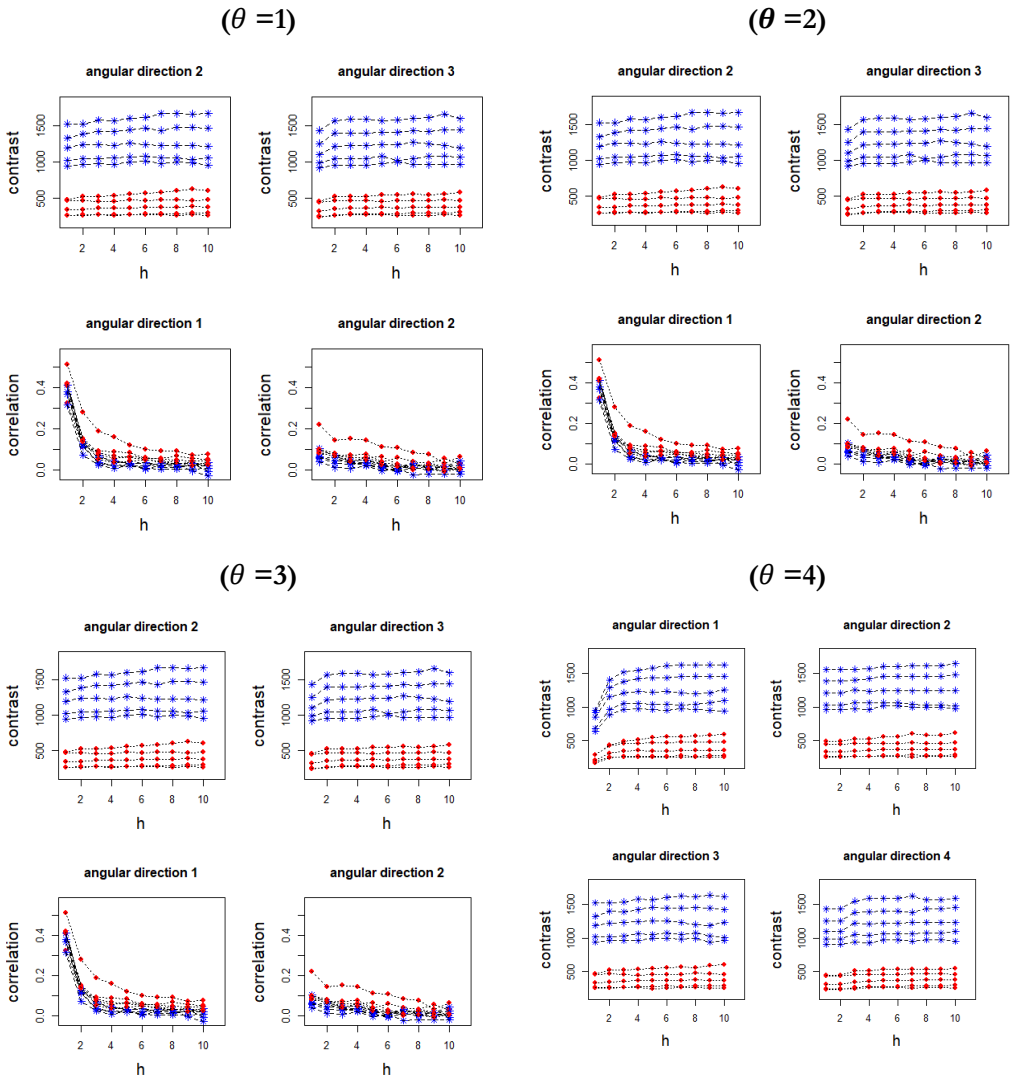

Table 18: GLCM measure of contrast feature while varying angular direction representing fire 1 in Australia, Victoria.